Scale and Boundary Condition Effects on Elastic Moduli of Trabecular Bone

Cong Yu Wang

A Thesis

in

the Department

of

Mechanical and Industrial Engineering

Presented in Partial Fulfillment of the Requirements
for the Degree of Master of Applied Science (Mechanical Engineering) at
Concordia University
Montreal, Quebec, Canada

February 2006

ABSTRACT

Scale and Boundary Condition Effects on Elastic Moduli of Trabecular Bone

Cong Yu Wang

We study elastic moduli of trabecular bone. Trabecular bone structure is very complex due to its randomness and spatial heterogeneity. To simplify the analysis one can choose to represent bone as having an idealized periodic structure. In this thesis we model bone as having a periodic prismatic structure, either two- or three-dimensional. More specifically, we are interested in predicting the apparent elastic moduli of such an idealized model of trabecular bone. If the "region of observation" is smaller than the Representative Volume Element then the moduli calculated for that region depend on size of that region and boundary conditions applied computationally or experimentally; these moduli are referred to as the apparent moduli. In order to investigate the effect of scale and boundary conditions on elastic moduli we apply displacement, traction, periodic or mixed boundary conditions. The results calculated using periodic boundary conditions give effective response while the remaining three boundary conditions give apparent moduli. The apparent moduli calculated using displacement boundary conditions bound effective moduli from above while the moduli obtained using traction boundary condition bound the effective moduli from below. The larger is the size of the "region of observation," the closer are the bounds. Since our geometric models of trabecular bone are effectively orthotropic with symmetry we apply only three loadings: unidirectional, hydrostatic and shear loadings. We conduct our analysis using a finite element method (ANSYS). We investigate the effect of mesh size, the mismatch in moduli (elastic modulus of bone versus bone marrow), the size of "region of observation", the effects of

bone structures geometries, and boundary conditions on the elastic moduli of the idealized models of trabecular bone. This research can give guidance in determining the sufficient size of bone samples used in experiments or computations so the effect of boundary conditions is minimized. These results are also applicable to other porous/cellular materials.

ACKNOWLEDGEMENTS

I would like to thank everyone whose assistance has made this work possible. First, I would like to thank Dr. I. Jasiuk, my supervisor who offered me an opportunity to be a graduate student at Concordia University, and conduct research under her guidance. Her advice and encouragement have been invaluable, as is the environment she provided to make this research possible.

I would also like to thank the members of Dr. Jasiuk's research group, particularly Mr. Smadi for his kind help and cooperation. In addition, the author would like to acknowledge the financial assistance provided by the Startup Funds and NSERC that made this research possible.

TABLE OF CONTENTS

LIST OF FIGURES

LIST OF TABLES

NOMENCLATURE

Abbreviations

FEM	Finite element method
RVE	Representative Volume Element

Symbols

D	Displacement
δ	Mesoscale window scale parameter
δ_0	Periodic unit cell; smallest mesoscale window
ε	Strain tensor
ε°	Applied uniform strain tensor
ν	Poisson's ratio
σ	Stress tensor
σ°	Applied uniform stress tensor
C_{1111}	Coefficient in the 1,1,1,1 position of the fourth-order stiffness tensor
C'	Instantaneous modulus relating average stress and average strain
C_d^{app}	Apparent stiffness tensor derived from displacement boundary conditions
C_t^{app}	Apparent stiffness tensor derived from traction boundary conditions
C^{eff}	Effective stiffness tensor
C^R	Reuss bound on effective stiffness tensor

C^V	Voigt bound on effective stiffness tensor
E	Young's modulus
G	Shear modulus
h	Interphase thickness
L	Mesoscale window edge length
M	Mixed boundary conditions
n	Outward normal unit vector
P	Periodic boundary conditions
r	Radial component of polar position vector
S_d^{app}	Apparent compliance tensor derived from displacement boundary conditions
S_t^{app}	Apparent compliance tensor derived from traction boundary conditions
S^{eff}	Effective compliance tensor
T	Traction
t	Traction vector
u	Displacement vector
V_f	Volume fraction of inclusions
w^C	Constituent bound width parameter
w^V	Variational bound width parameter
W	Strain energy

CHAPTER 1

INTRODUCTION

This thesis addresses the modeling of trabecular (also called cancellous) bone, more specifically the prediction of the elastic moduli of trabecular bone. Bone is a structural material that supports all tissues in a living body. In this chapter we discuss the hierarchical structure of bone, the motivation of this research, and the organization of this thesis.

1.1 Structure of bone

Bone is composed of periosteum, cortical bone, cancellous bone and bone marrow. The outer surface of most bone is covered by the periosteum, a sheet of fibrous connective tissue and an inner cellular or cambium layer of undifferentiated cells. Cortical bone is a dense, solid mass with only microscopic channels. Approximately 80% of the skeletal mass is cortical bone, which forms the outer wall of all bones and is largely responsible for the supportive and protective function of the skeleton. The remaining 20% of the bone mass is cancellous bone, a lattice of plates and rods known as the trabecula, found in the inner parts of bones.

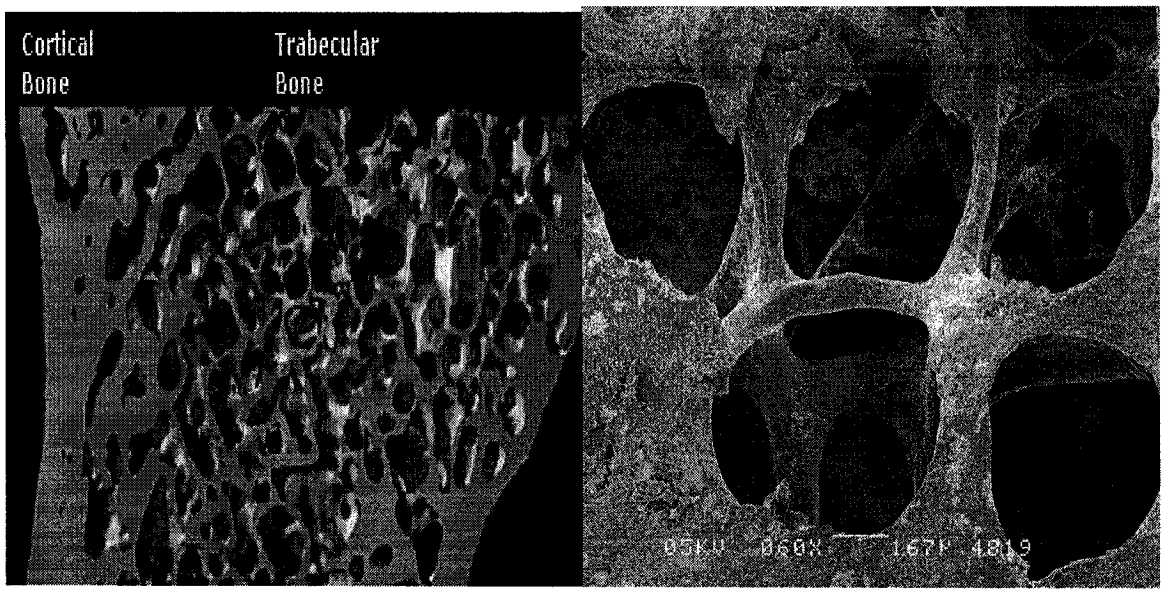

Figure 1. 1 Structure of trabecular bone [ASBMR, 2001] and [Bouyge, 2000]

1.2 Hierarchical modeling of trabecular bone

In order to understand the mechanical properties of bone, it is necessary to understand the response of bone at many length scales because bone's structure is hierarchical. These levels and structures are as follows: (1) the macrostructure: whole bone; (2) the mesostructure: trabecular and cortical bone; (3) the microstructure: Haversian systems, osteons, single trabeculae; (4) the sub-microstructure: lamellae; (5) the nanostructure: fibrillar collagen and embedded minerals; and (6) the sub-nanostructure: molecular structure of constituent elements, such as mineral, collagen, and non-collagenous organic proteins. This hierarchically organized structure has an irregular, yet optimized, arrangement and orientation of the components, resulting in bone's heterogeneous and anisotropic structure.

In this thesis, we focus on the trabecular bone at the mesostructure level, and study its elastic properties. More specifically, we focus on scale and boundary conditions effects on elastic moduli of trabecular bone.

1.3 Motivation of research

Bone fractures are major problems for osteoporotic patients. Osteoporosis is a disease in which bones become more porous, more fragile, and are more likely to break. If not prevented or if left untreated, osteoporosis can progress painlessly until a bone breaks. As a public health issue, osteoporosis is now considered the main disease for the elders. This is due to the fact that bone remodeling is affected and the bone formation rate is lower than the bone resorption rate. This causes low bone mass, which results in changes in geometric structure, accumulated microdamage, and differences in tissue properties. Osteoporosis affects trabecular bone more than cortical bone because trabecular bone is more porous to start with. Thus, much of the research in this area has focused on trabecular bone.

Secondly, biomaterials are becoming increasingly more important in biomedical practice. One such application is the use of biomaterials for bone implants. As a result, it is important to understand the bone structure and its mechanical behavior so that biomaterials can be correctly designed for orthopedic applications.

Thirdly, it is important to understand scale and boundary conditions effects in bone because when the sample size is too small the mechanical properties (measured or calculated) will be influenced by boundary conditions. This is an important issue for trabecular bone analysis because bone samples need to be small due to spatially varying porosity. Also, the amount of trabecular bone tissue in bone is limited

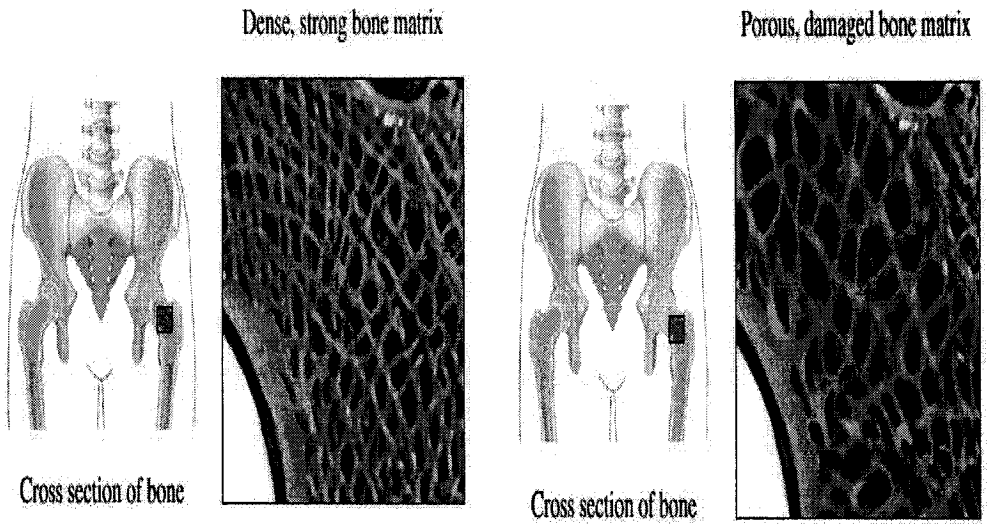

Figure 1. 2 Normal bone structure versus osteoporotic bone structure (Najarian,1995)

From an engineering point of view, bone can be considered as a natural composite material. Thus, the mechanical behavior of bone can be analyzed by the methods of mechanics of composite materials and micromechanics. The random and complex structure of trabecular bone can be characterized experimentally using Micro-CT. This technique can provide us with the details of the trabecular bone structure, the degree of its anisotropy, and its volume fraction. One can also predict the rate of bone mass loss by measuring the changes of its bone tissue volume fraction. In addition to analytical method, Finite Element Method (FEM) has been used extensively to compute mechanical properties of bone.

The theoretical concepts that will be used in this study will include the Hooke law to represent elastic stress-strain response of bone, the Hill condition to guarantee that direct and energy approaches give the same results, and the average stress and strain theorems. The trabecular bone structure will be represented as an idealized periodic structure. First,

the stiffness and compliance tensors will be found directly by applying uniform displacement and traction boundary conditions. Secondly, the effective properties of trabecular bone will be obtained by applying the periodic boundary condition to periodic models. In this study we will be interested in understanding the size of the Representative Volume Element (RVE). The RVE theory gives us the window size rule to determine the effective properties of trabecular bone.

Although bone properties can be measured experimentally, the main drawback of the experiments on bone is that not enough bone tissue may be available for testing. Therefore, the modeling of trabecular bone can complement experimental results and can be used to predict and better understand the mechanical response of trabecular bone.

It is known that the mechanical response of trabecular bone is dependent on a number of factors: the size of the sample material, the mechanical properties of constituents, the microstructure geometry of bone, the boundary conditions applied, the geometry of sample, and the relative amounts of the bone structure. All of the above factors will be addressed in this thesis. In summary, we will study the elastic moduli of trabecular bone numerically and focus on the effects of boundary conditions and the size of the region (scale effects) used for calculations or experiments.

1.4 Thesis organization

This thesis focuses on the modeling of the elastic response of trabecular bone using two-dimensional (2D) and three-dimensional (3D) geometric models. The analysis of scale effects is presented, along with the investigation of the effects of boundary conditions. Numerical modeling using the FEM software package ANSYS 8.1 is used to obtain the numerical examples to illustrate the topics addressed in this thesis.

The Introduction (present chapter) briefly outlines the motivation for this research and the hierarchical structure of trabecular bone.

Chapter 2 demonstrates the mechanics background. In this chapter, the concepts of effective properties, apparent properties, representative volume element, scale effects and boundary conditions effects are presented.

Chapter 3 outlines the key past research works on different models of trabecular bone, and the methodologies of the numerical analyses used.

The problem statement of our model with periodic structure is provided in Chapter 4. First, the discussions in boundary conditions for the two-dimensional elastic model are given. Then, two unit cells are examined in more detail. Also, the elastic material inputs and model geometry inputs are described in this chapter.

Chapter 5 shows the results and discussion. To begin with, the procedures of loading the boundary conditions in ANSYS are discussed. Then, it discusses the numerical results and their relationships obtained from ANSYS under different loads. Also, the results of uniform displacement and traction boundary conditions are compared with those of periodic and mixed boundary conditions. Furthermore, the bone structure-corner effect and volume fraction are considered. Finally, results from 2D and 3D models are compared, and the Hill condition, average stress, and average strain are investigated as well.

The thesis ends with Chapter 6, which provides the conclusions of this work, contribution to the current knowledge and the suggestions for the future work.

CHAPTER 2

MECHANICS BACKGROUND

2.1 Representative volume element

Composite materials consist of many inclusions (pores, fibers, particles). To account for all these micro-structural features would require very large computational efforts. To simplify the analysis, the concept of the representative volume element (RVE) was introduced (Biot, 1941, Hill, 1963). RVE is a region much smaller than the size of composite structure but much larger than the size of micro-structural features (diameter of pore, or of fiber, for example), and it has same properties as a whole composite. The representative volume element (RVE) plays an important role in the mechanics and physics of random heterogeneous materials with a view to predicting their effective properties. The application of a representative volume element was investigated by Hashin (1964), Huet (1990), Aboudi (1991), Christensen (1991), Drugan and Willis (1996), and Jiang, Ostoja-Starzewski, and Jasiuk (2001), among others.

In his 1941 paper, M. A. Biot defined a representative volume element (RVE) as follows: "Consider a small cubic element of soil, its sides being parallel with the coordinate axes. This element is taken to be large enough compared to the size of the pores so that it may be treated as homogenous, and at the same time small enough, compared to the scale of the macroscopic phenomena in which we are interested, so that it may be considered as infinitestimal in the mathematical treatment."

In general, the RVE has a sufficient number of phases and it is structurally typical of the entire composite material. More specifically, the RVE represents the properties of the whole composite, and these properties are not influenced by the values of boundary

conditions (uniform traction and displacement) (Hill, 1963, Aboudi, 1991). Thus, effective properties can be calculated using RVE which it is much smaller than the structure to be analyzed.

Another definition of the RVE was proposed by Drugan and Willis (1996): ''It is the smallest material volume element of the composite for which the usual spatially constant (overall modulus) macroscopic constitutive representation is a sufficiently accurate model to represent mean constitutive response''. This approach uses the solution of homogenization, assuming periodicity of an infinite sample.

In summary, the RVE is an element that is small enough compared to the scale of the macroscopic phenomena and large enough compared to the size of the inclusions (pores, fibers, particles) so that the overall properties are independent of the external boundary conditions.

2.2 Average stress, average strain theorems

The strain energy is described as the volume integral of the inner tensor product of the material stress and strain tensors.

$$W = \frac{1}{2}\int_V \sigma_{ij}\varepsilon_{ij}dV = \frac{1}{2}\cdot\overline{\sigma_{ij}\varepsilon_{ij}}\cdot V \tag{2.1}$$

The bar denotes volume average as shown and V is the volume of the representative volume element.

The average stress and strain are noted by the over bar.

$$\overline{\sigma}_{ij} = \frac{1}{V}\int \sigma_{ij}dV \tag{2.2}$$

$$\overline{\varepsilon}_{ij} = \frac{1}{V}\int \varepsilon_{ij}dV \tag{2.3}$$

When applying a displacement at the boundary surface, the boundary condition is given in the form

$$u_i = \varepsilon_{ij}^0 \cdot x_j \tag{2.4}$$

where ε_{ij}^0 is a uniform strain.

Alternatively, the traction is applied at the boundary surface, the boundary condition is given in the form

$$t_i = \sigma_{ij}^0 \cdot n_j \tag{2.5}$$

where σ_{ij}^0 is a uniform stress.

The average stress theorem states when we apply a traction boundary condition $t_i = \sigma_{ij}^0 \cdot n_j$, where σ_{ij}^0 is uniform, then the average stress $\overline{\sigma_{ij}}$ in the composite is equal to the applied stress σ_{ij}^0,

$$\overline{\sigma}_{ij} = \sigma_{ij}^o \tag{2.6}$$

The superscript (°) indicates "applied".

Similarly, the average strain theorem states when we apply a displacement boundary condition $u_i = \varepsilon_{ij}^{\circ} \cdot x_j$, where ε_{ij}° is uniform, then the average strain $\overline{\varepsilon_{ij}}$ is equal to the applied strain ε_{ij}°,

$$\overline{\varepsilon}_{ij} = \varepsilon_{ij}^o \tag{2.7}$$

The average strain theorem is valid for materials that have the perfectly bonded interfaces (inclusion-matrix) while average stress theorem does not have this requirement.

2.3 Direct & energy approaches

2.3.1 Relations between averages - Direct approach

Consider the homogeneous boundary conditions with uniform σ_{ij}° or ε_{ij}° applied on the surface of an RVE. Then, the average stress and strain are related by Hooke's law as,

$$\overline{\sigma}_{ij} = C_{ijkl}^{eff} \overline{\varepsilon}_{kl} \tag{2.8}$$

$$\overline{\varepsilon}_{ij} = S_{ijkl}^{eff} \overline{\sigma}_{kl} \tag{2.9}$$

where C_{ijkl}^{eff} are the effective elastic moduli and S_{ijkl}^{eff} are the effective elastic compliances.

Eqn. (2.8) is used when ε_{ij}° is applied. We evaluate the average stress $\overline{\sigma}_{ij}$ and use the average strain theorem (2.7). This allows us to evaluate C_{ijkl}^{eff}. Similarly, Eqn. (2.9) is used when σ_{ij}° is applied. The average strain $\overline{\varepsilon}_{ij}$ is calculated and the average stress is found by using the average stress theorem (2.6). This gives S_{ijkl}^{eff}.

When the size of the window of observation is smaller than the RVE, the average stress and strain are related to Hooke's law as,

$$\overline{\sigma}_{ij} = C_{ijkl}^{app} \overline{\varepsilon}_{ij} \tag{2.10}$$

$$\overline{\varepsilon}_{ij} = S_{ijkl}^{app} \overline{\sigma}_{kl} \tag{2.11}$$

where C_{ijkl}^{app} and S_{ijkl}^{app} are apparent stiffness and compliance, respectively. Following the same procedure as above, the apparent moduli C_{ijkl}^{app} and S_{ijkl}^{app} can be evaluated

2.3.2 Relations between averages - Energy approach

Consider an elastic sample material, when ε_{ij}° or σ_{ij}° are applied on the surface of an RVE element. When the uniform strain ε_{ij}° is applied, the elastic strain energy is

$$W = \frac{V}{2}\varepsilon_{ij}^{o} C_{ijkl}^{eff} \varepsilon_{kl}^{o} \tag{2.12}$$

where the average strain theorem was used. W is calculated and the C_{ijkl}^{eff} can be found. Similarly, when uniform stress σ_{ij}° is applied, the elastic strain energy is

$$W = \frac{V}{2}\sigma_{ij}^{o} S_{ijkl}^{eff} \sigma_{kl}^{o} \tag{2.13}$$

using the average stress theorem. W is calculated and S_{ijkl}^{eff} can be found.

When the size of the window of observation is smaller than the RVE, the W is

$$W = \frac{V}{2}\varepsilon_{ij}^{o} C_{ijkl}^{app} \varepsilon_{kl}^{o} \tag{2.14}$$

$$W = \frac{V}{2}\sigma_{ij}^{o} S_{ijkl}^{app} \sigma_{kl}^{o} \tag{2.15}$$

Following the same procedure as for the case of an RVE, C_{ijkl}^{app} and S_{ijkl}^{app} can be found.

The discussion of the average stress, strain theorems, and direct and energy approaches can be found in (e.g., Aboudi, 1991; and Christensen, 1991).

2.4 Hill's condition

Consider a two phase composite material subjected to displacement or traction boundary conditions (2.4) and (2.5)

The strain energy is given by

$$W = \frac{1}{2}\int_S t_i u_i dS = \frac{1}{2}\int_S t_i \varepsilon_{ij}^{0} x_j dS (or \frac{1}{2}\int_S \sigma_{ij}^{0} n_j u_i dS) = \frac{1}{2}\bar{\sigma}_{ij}\bar{\varepsilon}_{ij} V \tag{2.16}$$

Since,

$$W = \frac{1}{2}\int_S t_i u_i dS = \frac{1}{2}\int_V \sigma_{ij}\varepsilon_{ij} dV \tag{2.17}$$

So,

$$\overline{\sigma}_{ij}\overline{\varepsilon}_{ij} = \frac{1}{V}\int_V \sigma_{ij}\varepsilon_{ij}dV \tag{2.18}$$

Hill's condition states that the volume averages of the product of stress and strain are equal to the product of the volume average of stress and the volume average of strain (Hill, 1963). It is given as,

$$\overline{\sigma_{ij}\varepsilon_{ij}} = \overline{\sigma}_{ij}\overline{\varepsilon}_{ij} \tag{2.19}$$

where σ_{ij} and ε_{ij} are the stress and strain tensors, respectively and an over bar denotes a volume average.

2.5 Boundary conditions

From the Hill condition (2.19), we can obtain by integrating by parts

$$\int_s (t_i - \overline{\sigma}_{ij}n_j)\cdot(u_i - \overline{\varepsilon}_{ij}x_j)\cdot dS = 0 \tag{2.20}$$

where S is the boundary surface. This equation is satisfied for the following boundary conditions: displacement, traction, mixed, and periodic boundary conditions, which are discussed below.

2.5.1 Displacement boundary conditions

Equation (2.20) is satisfied when $u_i - \overline{\varepsilon}_{ij}x_j = 0$. If we use the average strain theorem (2.7), the displacement boundary condition can be written as

$$u_i = \varepsilon_{ij}^{\circ}\cdot x_j \qquad \text{on} \quad S \tag{2.21}$$

2.5.2 Traction boundary conditions

Equation (2.20) is satisfied when $t_i - \overline{\sigma}_{ij}n_j = 0$. If we use the average stress theorem (2.6), the traction boundary condition can be written as

$$t_i = \sigma_{ij}^{\circ}\cdot n_j \qquad \text{on} \quad S \tag{2.22}$$

2.5.3 Mixed boundary conditions

The mixed boundary conditions are including both traction and displacement boundary conditions applied along the boundary of the sample material. However, they can't be applied at the same time on a given surface. More specifically, traction and displacement components in the same direction cannot be both specified on the same boundary. The mixed boundary conditions are written in the following form

$$\left(t_i - \sigma^{\circ}_{ij} \cdot n_j\right) \cdot \left(u_i - \varepsilon^{\circ}_{ij} \cdot x_j\right) = 0 \tag{2.23}$$

2.5.4 Periodic boundary conditions

The periodic boundary condition can also be used to predict the effective properties of sample material on the RVE. However, it can only be applied to the sample with the periodic microstructure. They can be written as:

$$u_i(x+L) = u_i(x) + \varepsilon^{\circ}_{ij} \cdot L_j \qquad t_i(x+L) = -t_i(x) \tag{2.24}$$

2.6 The hierarchy of bounds

The effective properties are calculated by using the material sample size equal to an RVE. When the material sample size is smaller than the RVE, it gives the apparent properties. It has been shown by Huet (1990) that apparent properties under displacement and traction boundary conditions bound effective properties:

$$(S_t^{app})^{-1} \leq C^{eff} \leq C_d^{app} \tag{2.25}$$

where the subscripts t (traction) and d (displacement) denote the type of applied boundary condition. The use of the superscript ($^{-1}$) designates the inverse of a tensor.

When the window size is getting close to the RVE, the bounds are approaching the effective properties. Therefore, it means that there are the scale effects. They can be shown as the complete hierarchy of bounds (Huet, 1990)

$$C^R \le (S_t^{app})_\delta^{-1} \le (S_t^{app})_\Delta^{-1} \le C^{eff} \le (C_d^{app})_\Delta \le (C_d^{app})_\delta \le C^V \tag{2.26}$$

where the subscript δ is a finite material size and Δ is a larger finite material size, and C^R and C^V denote Reuss and Voigt bounds (Voigt, 1910; Reuss, 1929).

2.7 Scale effects

As has been discussed in section 2.6, there are scale effects and boundary conditions effects on composite material's elastic properties when the sample is smaller than the RVE. This is the subject studied in this thesis.

2.7.1 Mesoscale window

The finite-sized domain is called a window, and the relative size of this window is described by the parameter:

$$\delta = L/d \ge 1 \tag{2.27}$$

where L is an edge-length, d is diameter of the inclusions within the window, assuming a square geometry.

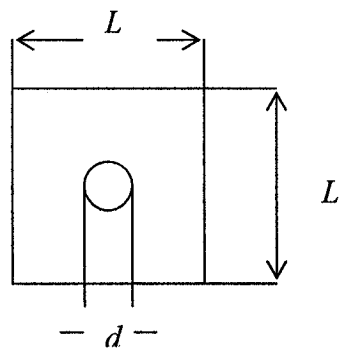

2.7.2 Volume fraction

The volume fraction of a phase of a composite is defined as the total volume of that phase divided by the total volume of the composite. In general, the term volume fraction will be assigned to be the volume fraction of the inclusion phase

$$v_f = \frac{V_{inclusion}}{V_{composite}} \tag{2.28}$$

2.7.3 Microstructures of the mesoscale window

Generally, there are three choices of microstructures, periodic, random-periodic, or purely random, for choosing up a mesoscale window to describe the local geometry of a composite.

1. Periodic structures

A periodic microstructure can be described as a structure with repeating geometry. In this case, the smallest domain of a composite, representing the repeating unit, gives all of the morphological characteristics of the composite. Two examples of unit cells for periodic microstructure, effectively orthotropic and isotropic, can be seen in Figure 2.1 for a composite with the inclusion microstructures.

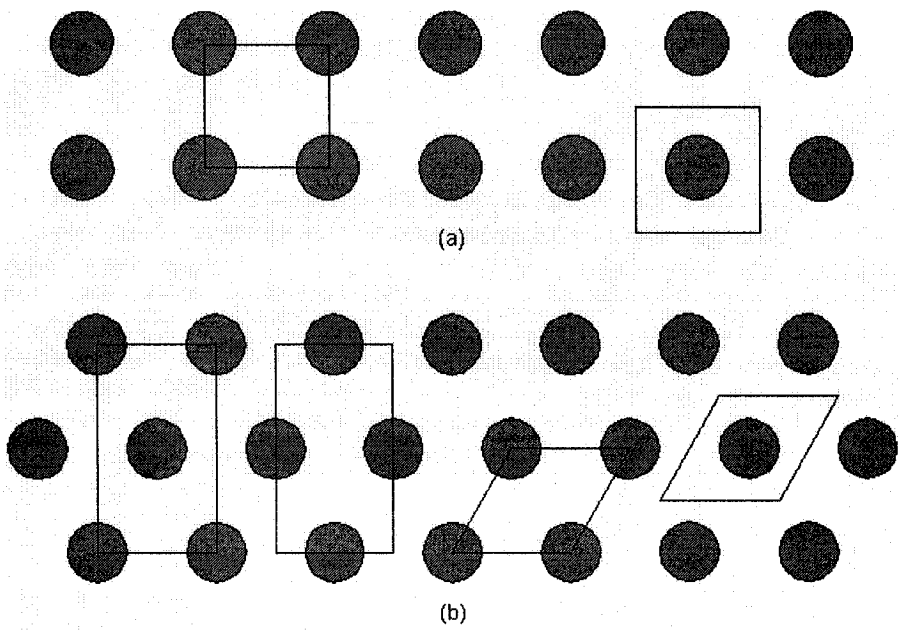

Figure 2. 1 Periodic microstructures with sample unit cells (Jiang, 2000b)
(a) orthotropic, with square array, and (b) isotropic, with triangular array of inclusions

When a composite has a periodic structure, periodic boundary conditions can be used on a unit cell to evaluate its effective properties.

Periodic composites can also be used to study scale and boundary conditions effects and this is the subject of this dissertation research. More specifically, we will be applying displacement and traction boundary conditions on window sizes consisting of increasing number of unit cells to study the convergence in apparent moduli to effective ones. This will give us guidance on the response of random composites.

2. Random-periodic microstructure

The analysis of a random composite is more difficult than the analysis of a periodic composite. Although most composites as manufactured are indeed not periodic, a specific microstructure can be taken so that the analysis of the random composite can follow the methods of periodic analysis. This type of microstructure is called random-periodic.

A random-periodic composite has a random distribution of inclusions in a unit cell, but the cell itself is repeated throughout the composite domain. Figure 2.2 shows the random-periodic composites microstructure.

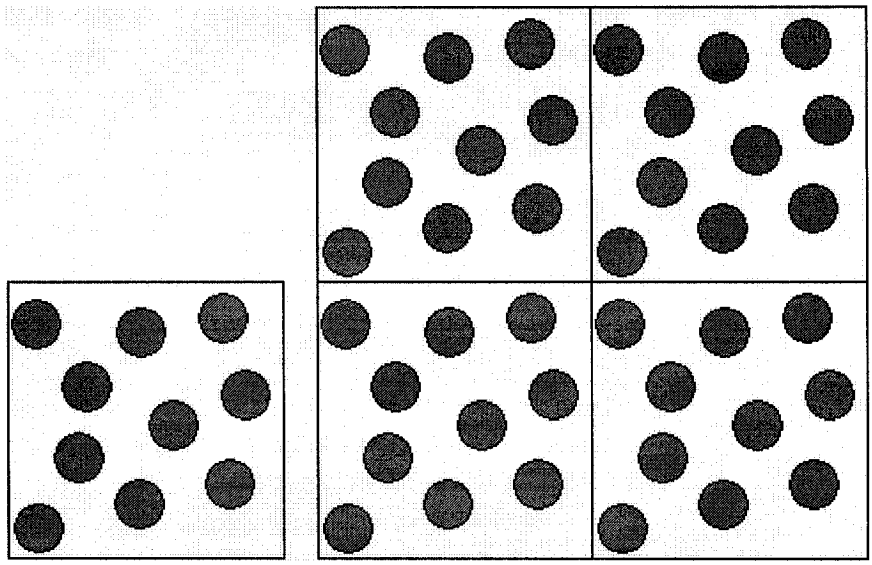

Figure 2. 2 Random-periodic composites (Jiang, 2000b)

So, the periodic conditions can be applied to a random-periodic unit cell, and effective properties of a random-periodic composite can be calculated.

3. Purely random composite microstructure

Comparing with periodic and random-periodic microstructures, a purely random microstructure has no repeated unit cells and a mesoscale window will have a random arrangement of inclusions. No periodic boundary conditions can be used for that case. Many different realizations need to be considered. Also, windows taken from different sections of the composite may have the different volume fraction and represent different properties. (See Figure 2.3.)

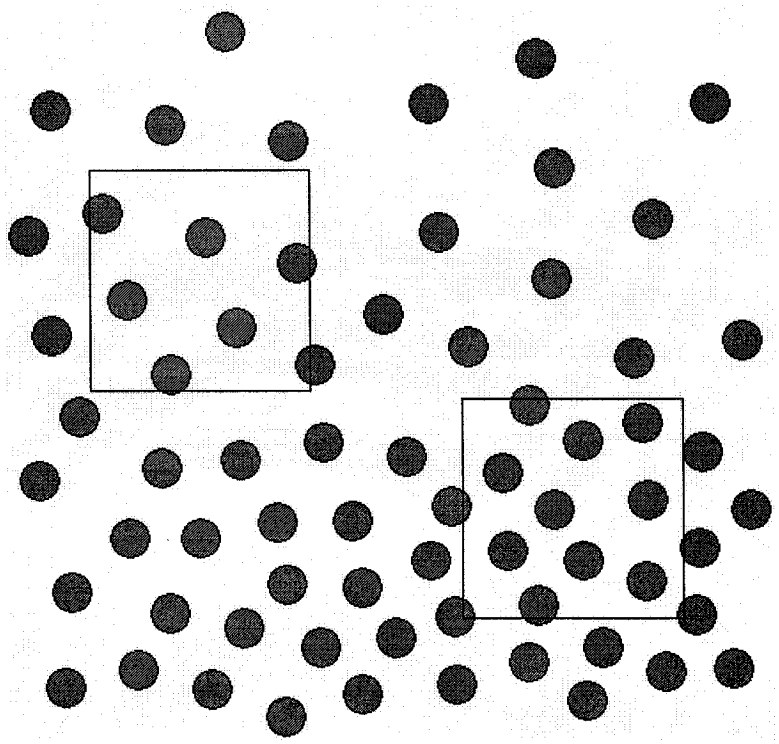

Figure 2. 3 Mesoscale windows taken from different locations in a random composite (Jiang, 2000b)

2.7.4 Scale effects for periodic composites

1. Choice of window

The unit cell size is denoted by δ_0. Larger windows, which are multiples of the δ_0 window, are chosen in order to study the effects of scale by increasing the window size. (Figure 2.4.)

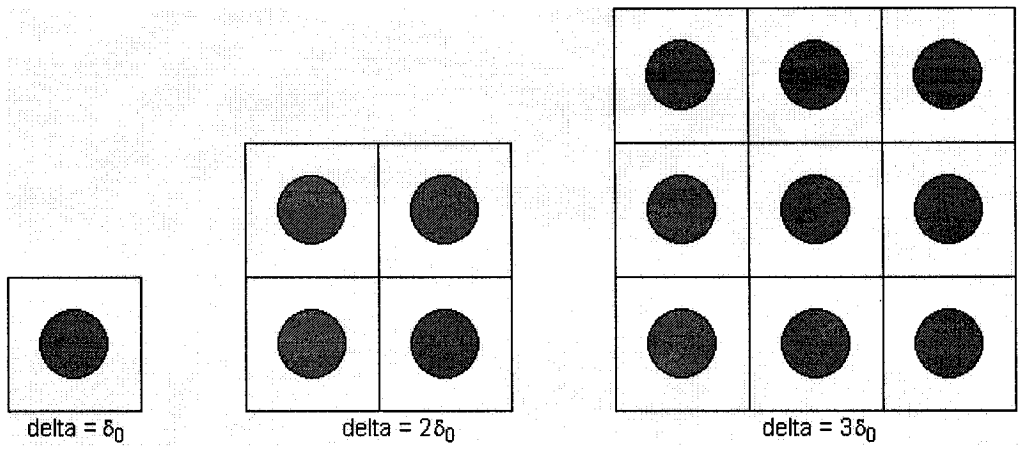

Figure 2. 4 δ_0 and larger scales (Jiang, 2000b)

2. Scale effects for periodic composites

The understanding of scale effects for periodic composites can help the understanding of scale effects for random composites.

There are two bound width parameters introduced in thesis (Jiang, 2000b) to discuss bounds on effective properties. The first parameter will be called the variational bound width parameter and is defined:

$$w^V = \frac{\left|C_d^{app} - C_t^{app}\right|}{\left|C^V - C^R\right|} \tag{2.29}$$

where w^V is the variational bound width parameter; $\left(C^V\right)$ and $\left(C^R\right)$ are Voigt and Reuss bounds.

The other parameter is called the constituent bound width parameter and is defined:

$$w^C = \frac{\left|C_d^{app} - C_t^{app}\right|}{\left|C^i - C^m\right|} \tag{2.30}$$

where w^C is the constituent bound width parameter; $\left(C^i\right)$ and $\left(C^m\right)$ are the material parameters of the constituent phases (inclusion and matrix, respectively).

Bounds are influenced by the stiffness mismatch $\left(E^i/E^m\right)$, edge of unit cell, and even mesh size of models.

Several researchers have focused on scale effects for periodic composites (Pecullan, Gibiansky, and Torquato, 1999; and Jiang, Ostoja-Starzewski, and Jasiuk, 2001).

CHAPTER 3

REVIEW of TRABECULAR BONE MODELS

In this thesis we study the elastic moduli of the trabecular bone at the microstructure level. In this chapter we present a review of the literature on the modeling approaches and the 2D and 3D geometric models of trabecular bone at this structural level.

More specifically, this chapter outlines some past research work on the mechanical properties of trabecular bone. The parameters of bone structure (bone volume fraction), the inputs for mechanical properties of bone tissue and soft tissue (bone marrow), the models of bone geometry, and the analysis methodologies are addressed.

3.1 Mechanical properties of trabecular bone

3.1.1 Axial structural properties

Trabecular bone has a porous structure. Often more than half the bone volume is associated with the pore volume. The theoretical models predicting the elastic moduli and strength of high porosity materials are generally classified as to whether the pores of the materials are connected (open cell) or not (closed cell) and as to whether the loads applied to the cell walls deform them primarily in simple axial loading (tension compression) or in bending. These classifications are used to represent idealized mechanical models. An open cell high porosity material has the solid structure made of struts. A closed cell high porosity material has none of its voids interconnected with each other. There are four kinds of models for three-dimensional high porosity materials: open

cell axially loaded models, open cell bending models (Christensen, 1986), closed axially loaded models, and closed cell bending models (Gibson and Ashby, 1988).

Gibson (1985) proposed to model cancellous bone by a periodic network of cubic or hexagonal cells. This model was used to estimate compressive behavior of cancellous bone as a function of mechanical properties of the cell material and dimensions of the cell (thickness t, length l). For cubic cells, the buckling is the dominant form of deformation. The relations for Young's moduli were obtained as follows:

$$\text{For open cubic cells, } \frac{E}{E_W} \propto \left(\frac{t}{l}\right)^4 \tag{3.1}$$

$$\text{For closed cubic cells, } \frac{E}{E_W} \propto \left(\frac{t}{l}\right)^3 \tag{3.2}$$

where the subscript W stands for bone wall (bone tissue).

At higher loads, the cubic cells began to collapse. The elastic collapse stress σ^*_{el} and the plastic collapse stress σ^*_{pl} can be expressed in term of cell wall properties as follows:

$$\text{For open cubic cells, } \frac{\sigma^*_{el}}{E_W} \propto \left(\frac{t}{l}\right)^4, \frac{\sigma^*_{pl}}{\sigma_{yw}} \propto \left(\frac{t}{l}\right)^3 \tag{3.3}$$

$$\text{For closed cubic cells, } \frac{\sigma^*_{el}}{E_W} \propto \left(\frac{t}{l}\right)^3, \frac{\sigma^*_{pl}}{\sigma_{yw}} \propto \left(\frac{t}{l}\right)^2 \tag{3.4}$$

Similar relations are derived for hexagonal cells considering similar deformation modes and axial deformation. The transverse behavior of hexagonal cells is similar to cubic cells under axial compression.

Mech. Properties	Open cell	Closed cell
$\frac{E}{E_W}$	$\left(\frac{t}{l}\right)^2$	$\frac{t}{l}$
$\frac{\sigma^*_{el}}{E_W}$	$\left(\frac{t}{l}\right)^4$	$\left(\frac{t}{l}\right)^3$
$\frac{\sigma^*_{pl}}{E_{yw}}$	$\left(\frac{t}{l}\right)^2$	$\frac{t}{l}$

Table 3. 1 Mechanical properties of hexagonal cellular material (Gibson, 1985)

These results fit experimental data quite well except for the hexagonal model loaded in transverse direction. Ashby (1993) used the same type of modeling to formulate creeping and tensile behavior of cellular materials.

A separate analysis for very low density materials was done by Christensen (1986) where exact expressions were derived for effective moduli of 3D open cell and closed cell geometric models in isotropic or transversely isotropic media. The results were independent of the cell geometry provided that the orientation of the cell walls was sufficiently random to yield isotropy. The results showed that tensile Young's moduli of closed cells material (plates) were higher than open cells (rods) properties. On the other hand, the compressive Young's moduli of cellular materials with plate-like walls were lower than the moduli of materials with rod-like connections. The plane stress assumption reduced the strut stress-strain relationship to two-dimensions.

$$\frac{E}{E_m} = \frac{2(7-5\nu_m)}{3(1-\nu_m)(9+5\nu_m)}c \tag{3.5}$$

$$\nu = \frac{1+5\nu_m}{9+5\nu_m} \tag{3.6}$$

Where c is the volume fraction of the material, and ν_m and E_m are Poisson's ratio and Young's modulus of the constituent material.

Christensen compared the values to the bounds for the composite spheres model introduced by Hashin (1962), where for very low density materials the bounds coincide giving an exact result which was the same as the above elastic constants written in the form of effective bulk and shear moduli. This result shows that the Christensen formulation of effective properties of low density foams is independent of the cell geometry as long as the material behaves such that the cell walls transmit the load according to the two dimensional form appropriate for the elastic plane stress condition (Christensen, 1986).

3.1.2 Volume fraction of trabecular bone

Measurement of volume fraction is of primary importance in the evaluation of trabecular microstructure. Volume fraction can be obtained from three-dimensional reconstructions of micro-CT images.

Those measurements have been based on Archimedes' principle or on using stereological techniques on histological sections. For quantifying the accuracy of this measurement, one hundred and sixty human trabecular bone specimens which covered a large range of volume fraction (9.8-39.8%) were studied (Ding, 1999).

Method I is such that all micro-CT data were segmented using individual thresholds determined by the scanner supplied algorithm while in method II the individual thresholds were determined based on a calibration of volume fraction to the Archimedes-based volume fractions.

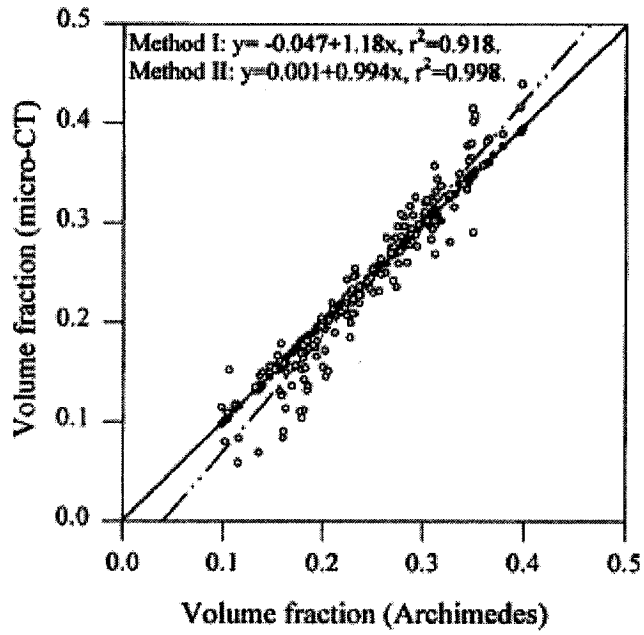

Figure 3. 1 Bone volume fractions obtained by Micro-CT (Ding, 1999)

3.1.3 Material properties of trabecular bone

Several references addressed the trabecular tissue material properties. In these studies a wide range of values was reported, with many studies suggesting that the actual tissue modulus is much less than generally accepted for cortical bone (16-20 GPa). Methods reported include traditional tensile and bending tests applied to single trabeculae or similar sized specimens. Ryan and Williams (1989) used tensile testing experiments on single trabeculae, and found a trabecular tissue modulus of 0.4-3.6 GPa. Other studies, using three or four point bending experiments, have resulted in tissue values of 3.81-5.72 GPa (Kuhn *et al.*, 1989). Recently, Rho *et al.* (1993) determined the Young's tissue modulus of single trabeculae, using microtensile testing and ultrasonic techniques, finding a tissue modulus of 10.4-14.8 GPa. An indirect way to determine the tissue properties uses a numerical or analytical model representing a typical piece of trabecular bone, in combination with apparent experimental data. These models can also be used to

determine the stresses and strains in the trabeculae. Williams and Lewis (1982) used a two-dimensional FE model of a trabecular cross-section in combination with experimental results. They found a trabecular tissue modulus of 13 GPa. (Van Rietbergen, B., 1995)

3.2 Trabecular bone models

The simplest way to model trabecular bone is to represent it as a material with a periodic structure. For example, some geometric models were introduced by Gibson (1985) and Ashby (Gibson and Ashby, 1988). Because trabecular bone structure varies spatially and with the type of in-situ loading, four different idealized periodic unit cell assemblages that take advantage of similar mechanisms of deformation were developed.

1) An equiaxed cubic open model of rod-like structure (Fig. 3.2)

2) A higher density equiaxed cubic cell composed of plates

3) The stress oriented prismatic composed of plates

4) The stress oriented parallel plate structure.

These four different model geometries for trabecular bone are illustrated in Gibson and Ashby (1988).

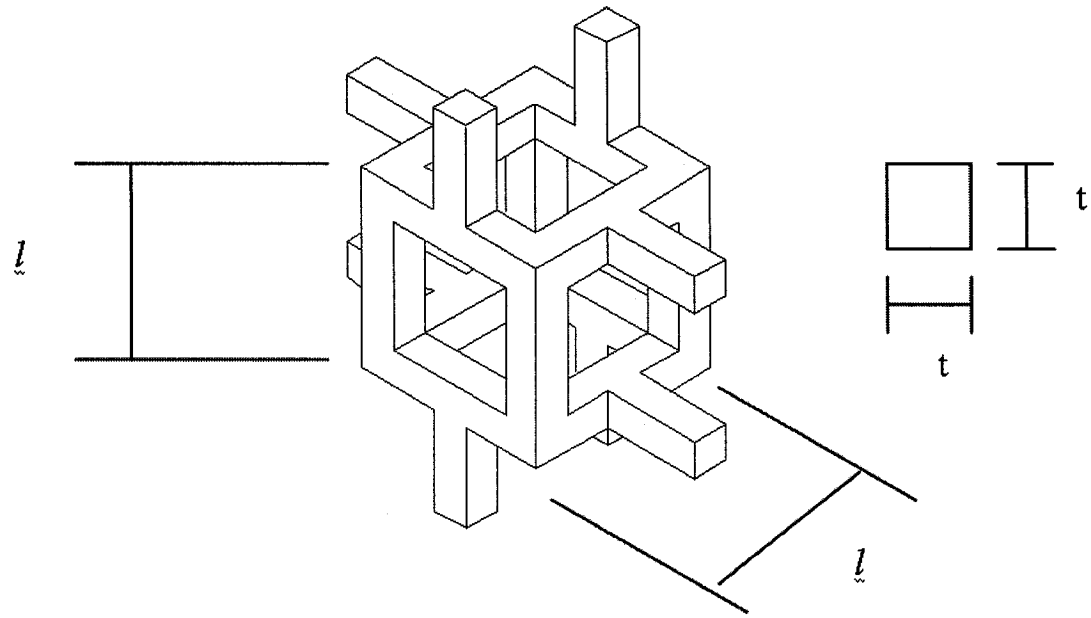

Figure 3. 2 Cubic equiaxed unit cell trabecular bone (Gibson and Ashby, 1988)

Beaupre and Hayes (1985) modeled trabecular bone and investigated its linear elastic constants by using an open cellular idealized geometry containing a body centered spherical void. They applied uniaxial compressive strain and shear strain. The unit cell, as shown in Figure 3.3, assumed a porous shape of a spherical void placed in the center of the cell producing a body centered cubic structure. The numerical results utilized finite element methods.

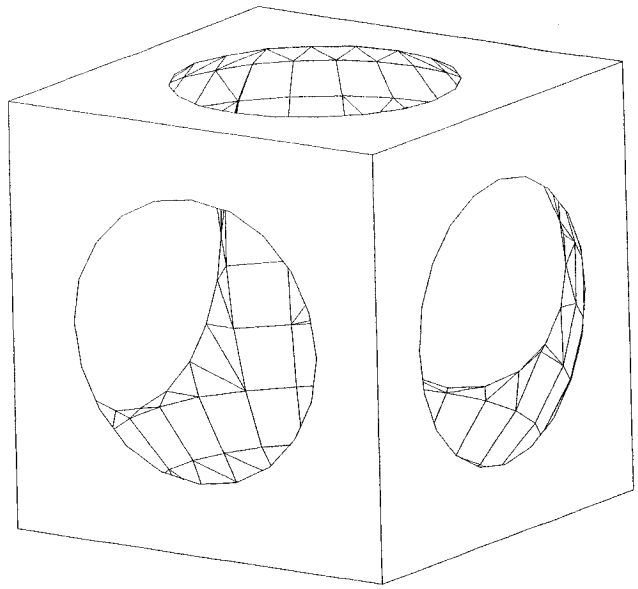

Figure 3. 3 Body centered cubic unit cell (Beaupre and Hayes, 1985)

Hollister et al. (1991) compared the strain energy distribution within two simple periodic models: one consists of parallelepipedic struts forming cubic cells and a body centered spherical model. The strain energy distribution within two models had been computed based on homogenization theory.

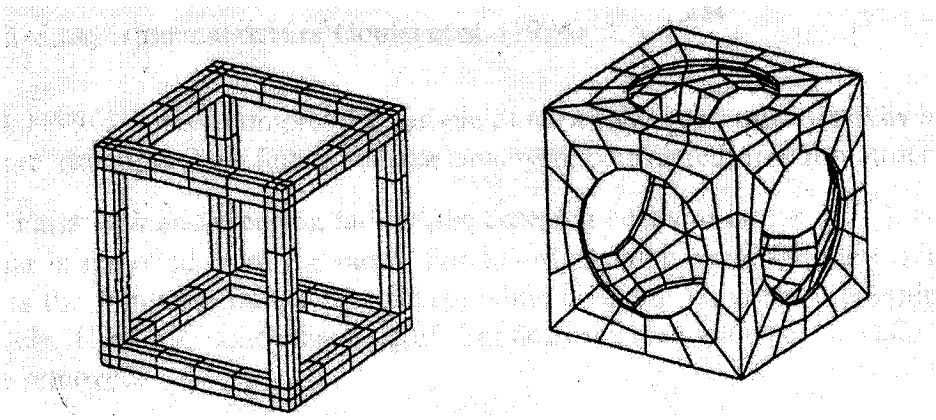

Figure 3. 4 Finite element models for strut and spherical void cells (Hollister et al., 1991)

Werner et al. (1996) introduced orthotropy in an idealized periodic model of trabecular bone and developed a more complex cell unit. They were able to vary trabecular length, thickness and length of trabecular connection to be close to real bone geometric features. They also introduced a degree of deviation from a perfectly rectangular lattice by removing trabecular units so they could model bone loss. They found that compressive Young's modulus and shear modulus are proportional to bone volume fraction to the 1.2th and 1.5th power respectively.

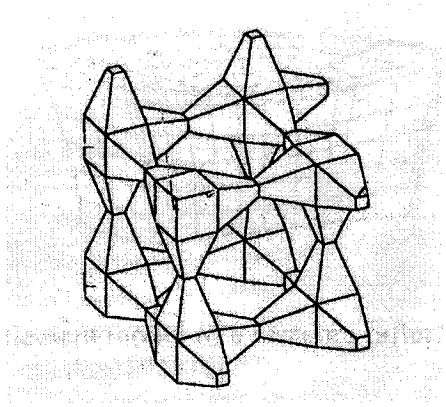

Figure 3. 5 Finite element model of trabecular structure (Werner et. al., 1996)

Guo et al. (1994) studied the compressive fatigue of trabecular bone modeled by a 2-D hexagonal honeycomb structure. Silva et al. (1997) quantified the influence of defects on both periodic and non periodic 2-D honeycomb microstructure. They used Voronoi structures and showed that results are close to periodic arrangements of cell walls in low-density honeycombs. Silva et al.(1997) also showed that the variability in the arrangement of cell walls creates a small amount of variability in the elastic constants of honeycombs, but that overall the relationship between the microstructure and the elastic properties for isotropic and anisotropic non-periodic honeycombs are no different

from periodic honeycombs. This result lends some evidence in utilizing periodic unit cells in modeling the random geometry of trabecular bone.

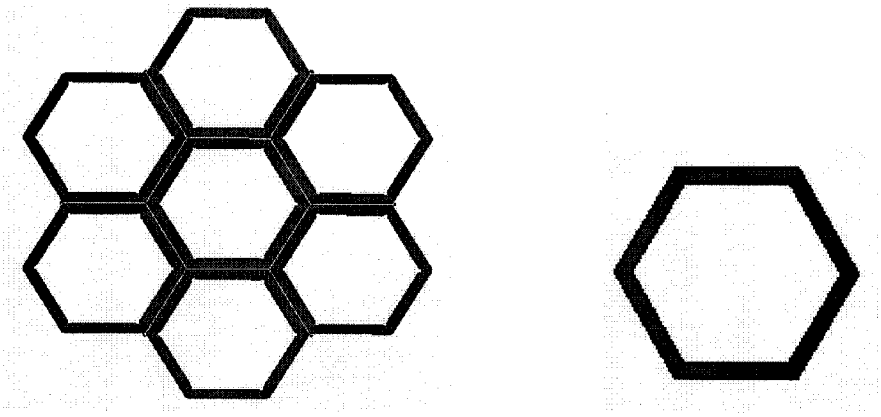

a. Honeycomb Structure b.Unit Cell

Figure 3. 6 2-D honeycomb microstructure of trabecular bone

Analytical model was also developed to investigate the strength asymmetry observed in trabecular bone. This has been observed experimentally in trabecular bone (Keaveny, *et al*, 1994; Stone *et al*, 1983; and Kaplan *et al*, 1985). The geometry formulations included a two dimensional honeycomb (Figure 3.6a) and a three dimensional tetrahedral open cell foam (Figure 3.6b). The models were loaded under a remote uniaxial stress and the unit cells were aligned with the direction of loading (Ford and Gibson, 1998).

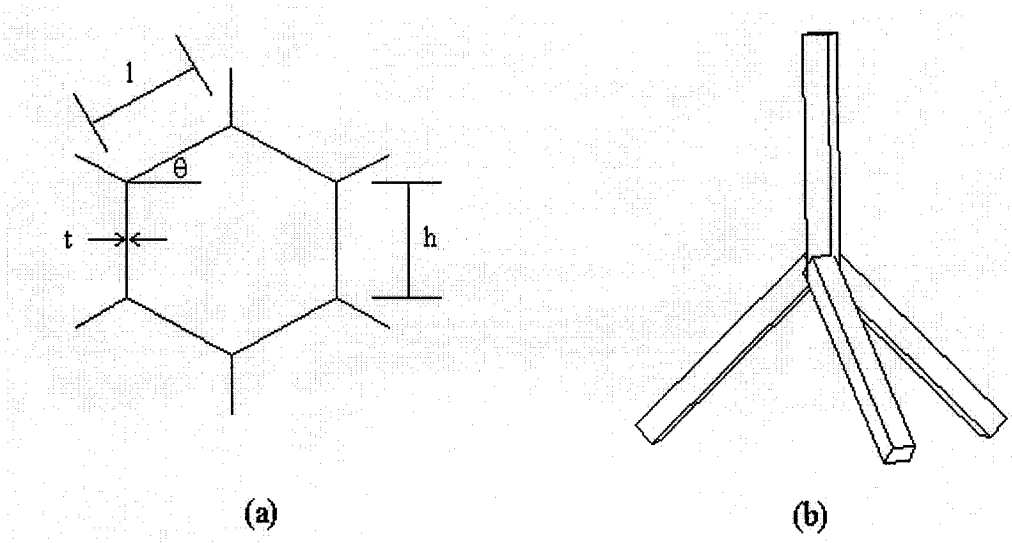

Figure 3. 7 Two-dimensional honeycomb and three-dimensional tetrahedral elements used to model asymmetric trabecular bone (Ford and Gibson, 1998)

Periodic models have also been used to model the osteoporotic bone density loss. The effects of this bone loss have been implemented as either uniform thinning of trabecular struts or reduction in trabecular connections. A three dimensional array of tetrakaidecahedral cells composed of elastic material was used to model the effect of osteoporosis on the elastic modulus. The importance of trabecular bone microstructure was underscored by the large reduction in modulus produced with a removal of a small number of trabeculae (Guo and Kim, 1999).

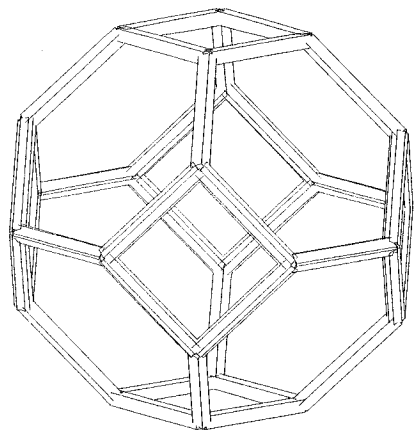

Figure 3. 8 Tetrakaidecahedral unit cell (Guo and Kim, 1999)

Adachi et. al. (1998) studied bone as a lattice continuum which was modeled as a continuum consisting of rigidly interconnected elastic rod / beam elements and they used the couple stress theory to represent elastic constants. They considered a two-dimensional orthogonal lattice with unit cell thickness as shown in Fig. 3.9(a), where the coordinate axes x_i were chosen to be parallel to the principal axes of the lattice.

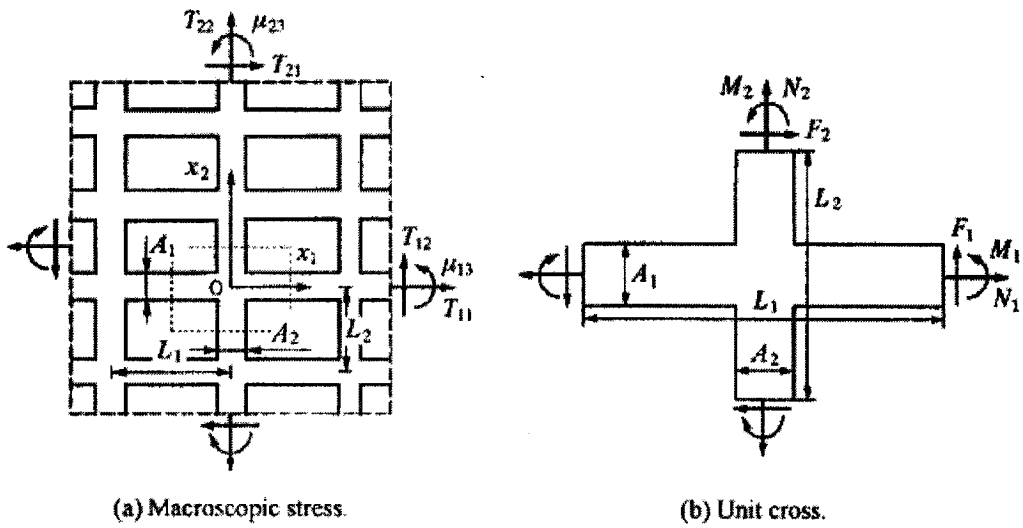

(a) Macroscopic stress. (b) Unit cross.

Figure 3. 9 Lattice continuum model (Adachi et. al., 1998)

Bouyge et al. (2001) used a 2D model to replace the periodic cellular structure with triangular arrangement of pores by a higher order continuum (couple stress theory). They used a periodic unit cell as a rhombus shaped domain of edge length L and volume $V=bL^2\sqrt{\frac{2}{3}}$. The rhombus' height in the x_2 direction is $H=2h=L\sqrt{\frac{2}{3}}$, and its thickness is b. This geometry gives a composite material which is effectively isotropic.

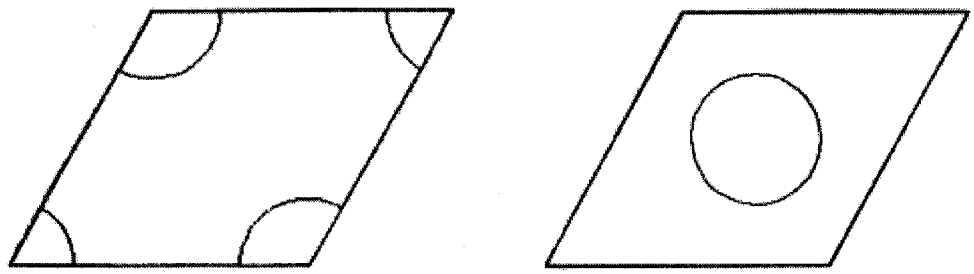

Figure 3. 10 Periodic unit cell with the inclusion(s) at the corner and the center (Bouyge et. al., 2001)

Mathematical models are very useful tools for predicting of material properties and they need to be compared with the experimental results. Through reviewing the models in literatures described above, we found that the overall behavior depends on three parameters: the type of cell structure; the volume fraction of solids; and the properties of the cell wall material. In this thesis we focus on the additional factors: scale and boundary conditions effects on elastic properties of trabecular bone. We use a two-dimensional finite element model of an idealized trabecular bone. More specifically, the trabecular bone is modeled as a two-dimensional periodic structure, square shaped with thickness, consisting of hard tissue (bone) and soft tissue (bone marrow). The

understanding of scale and boundary conditions effects is important in computational and experimental studies of bone's mechanical response.

CHAPTER 4

PERIODIC FEM MODEL

4.1 Periodic model

4.1.1 Finite element model

In this chapter we use a computational approach to predict material properties of trabecular bone. Trabecular bone is generally characterized as a cellular solid, consisting of an interconnected network of rods and plates. The overall behavior depends on three parameters: the type of cell structure (open- or closed-celled); the volume fraction of solid phase; and the properties of the cell wall material. Trabecular bone is usually represented as an open-celled material, since it has a very low relative density (the volume fraction of bone tissue). Thus, the open-celled regular network is chosen as the unit cell in this thesis.

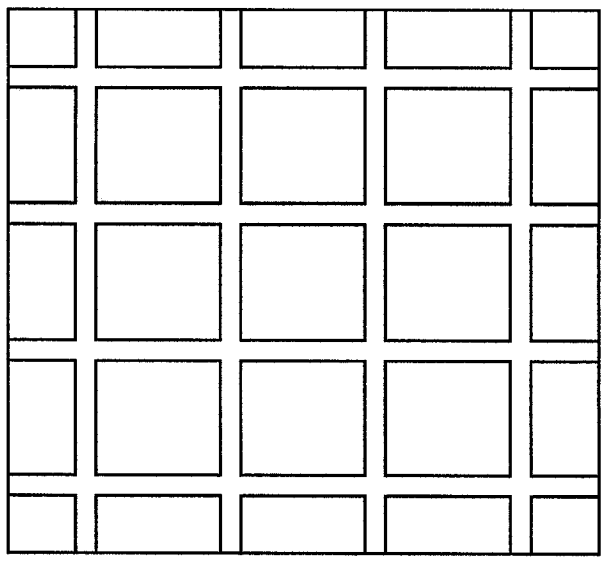

Figure 4. 1 Two-dimensional finite element model of trabecular bone

In this thesis we represent trabecular bone as having idealized 2D or 3D periodic structures, square shaped with thickness in 2D or cubic in 3D, consisting of hard tissue (bone) and soft tissue (bone marrow) (Fig. 4.1).

Two choices of unit cells are studied for this model (Fig. 4.2 and Fig. 4.3). Three volume fractions are examined: 10%, 15%, and 20%. These volume fractions were chosen from the ranges of trabecular bone obtained by the micro-CT measurements (10~40%) (Ding et al, 1999). The geometric parameters are the length of sample material (L), the thickness of sample material (t), and the thickness of bone strut (l) as shown in Figure 4.4. The material region window sizes are also shown in Figure 4.1. The finite element method is implemented using ANSYS 8.1 software.

1. Unit Cell 1

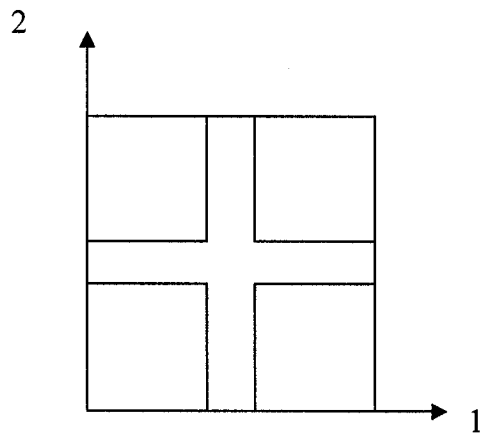

Figure 4. 2 Unit Cell 1

Unit Cell 1 involves the structure of bone sample which has stiff phase in the center of unit cell. (Fig. 4.2)

2. Unit Cell 2

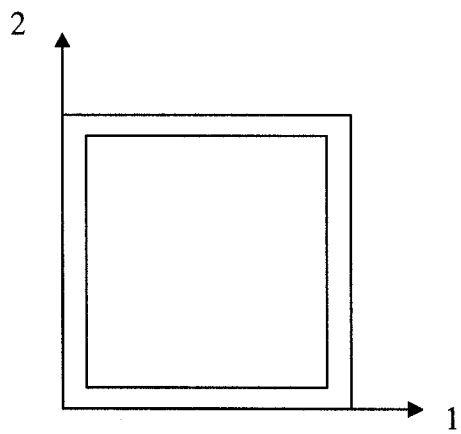

Figure 4. 3 Unit Cell 2

The alternate choice of unit cell is shown in Fig. 4.3, in which stiff (bone) phase is on outer edges of unit cell.

4.1.2 Elastic material inputs

In our analysis we model trabecular bone as a two phase material consisting of bone tissue (hard phase) forming a trabecular network and soft tissue, which we refer to as bone marrow (soft phase) present in pores. We assume that both phases are linear elastic and isotropic. Bone tissue is assigned a Young's modulus of 13.0 GPa and Poisson's ratio of 0.3 while the Young's modulus of bone marrow is given a range from 1.3 Pa to 13.0 GPa with same Poisson's ratio of 0.3. The Young's modulus was chosen from a variety of values given in literature. However, since the problem is linear elastic, it is scalable so the actual value is of no importance.

4.1.3 Model geometry inputs

We give every unit cell size 5 x 5 x 0.1 to dimension of sample material (L x L x *t*); the thickness of bone strut (*l*) is 0.528 according to volume fraction (20%). When

considering mesh sizes, we always take it as ¼, 1/3, and ½ of the thickness of bone strut (l), namely 0.132, 0.176, and 0.264.

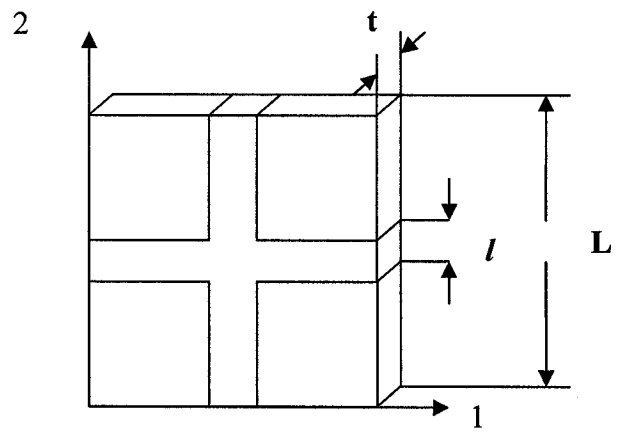

Figure 4. 4 Unit cell and its geometric parameters

4.2 Boundary conditions

The evaluation of elastic moduli of composite materials involves a solution of a boundary value problem. When the window size of region used for calculations or experiment is smaller than RVE, then the elastic moduli are dependent on boundary conditions, uniform strain or uniform stress, which give upper or lower bounds, respectively; such moduli are called the apparent moduli. On the contrary, when the sample material window size is of the RVE, it gives the effective properties. Periodic boundary conditions give the effective properties. In order to determine the components of either the stiffness matrix C_{ijkl}, or the compliance matrix S_{ijkl} for our geometric models, three types of loads: uniaxial extension/tension, biaxial tension/tension, and simple shear, are applied. We apply displacement, traction and mixed boundary conditions to study

scale effects. In addition, periodic boundary conditions are also studied here so that the effective properties of trabecular bone can be obtained.

4.2.1 Displacement boundary conditions

Applying the displacement boundary conditions, the stiffness tensor (C_{ijkl}^{app}) can be directly calculated, which gives the upper bound on effective moduli. The stiffness tensor (C_{ijkl}^{app}) is denoted as $(C_{ijkl}^{app})_d$ with the subscript (d) indicating the applied displacement boundary condition. For the 2D orthotropic model that we consider we need to evaluate $C_{1111}=C_{2222}$, $C_{1122}=C_{2211}$, and $C_{1212}=C_{2121}$.

1) Uniaxial extension

When a uniform ε_{11}^o is applied on the sample material boundary, the displacement boundary condition can be written as

$$u_1(x) = \varepsilon_{11}^o x_1; \qquad u_2(x) = 0; \qquad \text{on} \quad S \tag{4.1}$$

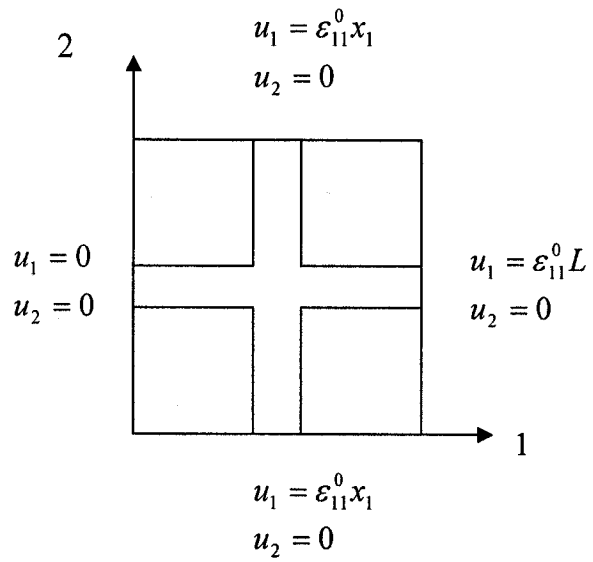

which gives $C_{1111} = \dfrac{2W^{cell}}{V}$ when ε_{11}^o=1.

2) Biaxial extension

When the uniform strain $\varepsilon_{11}^{o} = \varepsilon_{22}^{o}$ are applied on the sample material boundaries, the displacement boundary condition can be written as

$$u_1(x) = \varepsilon_{11}^{o} x_1; \qquad u_2(x) = \varepsilon_{22}^{o} x_2; \tag{4.2}$$

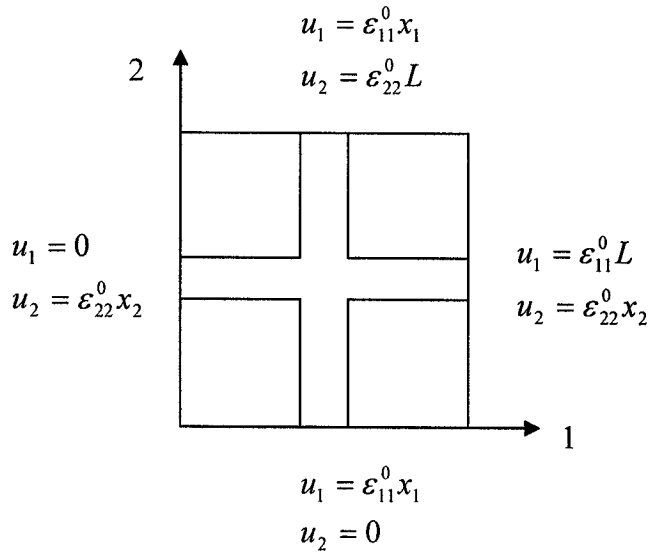

which gives $C_{1122} = \dfrac{2W^{cell}}{V} - C_{1111}$ when $\varepsilon_{11}^{o} = \varepsilon_{22}^{o} = 1$.

Note that the C_{1111} test must be done first to calculate C_{1122}.

3) Simple shear strain

When a uniform strain ε_{12}^{o} is applied on the sample material boundary, the displacement boundary condition can be written as

$$u_1(x) = \varepsilon_{12}^{o} x_2; \qquad u_2(x) = \varepsilon_{12}^{o} x_1; \tag{4.3}$$

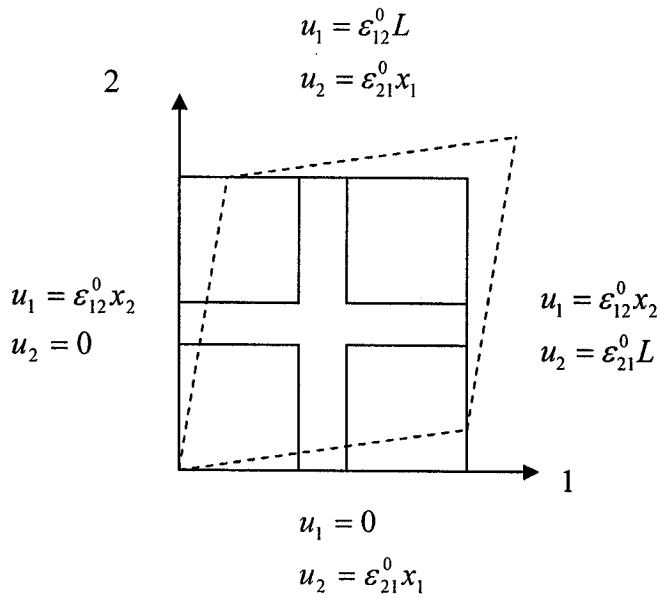

which gives $C_{1212} = \dfrac{2W^{cell}}{V}$ when $\varepsilon_{12}^o = 1$.

4.2.2 Traction boundary conditions

Applying the traction boundary conditions, we can directly obtain the compliance tensor $(S_{ijkl}^{app})_t$. Then inverting $(S_{ijkl}^{app})_t$, the stiffness tensor $(C_{ijkl}^{app})_t$, which gives the lower bound on the effective mechanical properties, can then be found. The stiffness tensor $(C_{ijkl}^{app})_t$ also equals to $(S_{ijkl}^{app})_t^{-1}$ with the subscript (t) indicating the applied traction boundary condition. For the orthotropic model that we consider we need to evaluate $S_{1111} = S_{2222}$, $S_{1122} = S_{2211}$, and $S_{1212} = S_{2121}$.

1) Uniaxial tension

When a uniform stress σ_{11}^o is applied on the sample material boundary, the traction boundary condition can be written as

$$t_1(x) = \sigma_{11}^o n_1; \quad t_2(x) = 0; \tag{4.4}$$

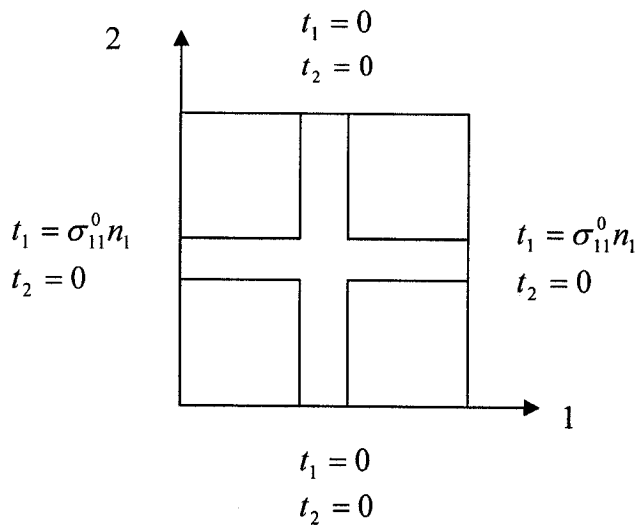

which gives $S_{1111} = \dfrac{2W^{cell}}{V}$ when $\sigma_{11}^o = 1$.

2) Biaxial tension

When the uniform stress $\sigma_{11}^o = \sigma_{22}^o$ are applied on the sample material boundaries, the traction boundary condition can be written as

$$t_1(x) = \sigma_{11}^o n_1; \quad t_2(x) = \sigma_{22}^o n_2; \tag{4.5}$$

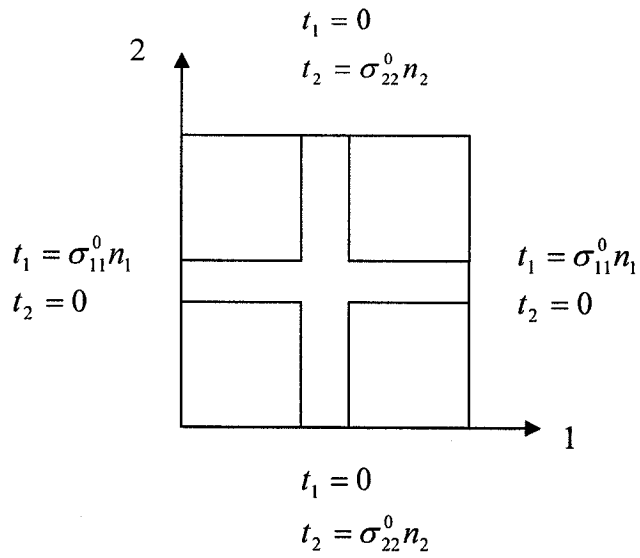

which gives $S_{1122} = \dfrac{2W^{cell}}{V} - S_{1111}$ when $\sigma^o_{11} = \sigma^o_{22} = 1$.

Note that the S_{1111} test must be done first to calculate S_{1122}.

3) Simple shear traction

When a uniform stress σ^o_{12} is applied on the sample material boundary, the traction boundary condition can be written as

$$t_1(x) = \sigma^o_{12} n_2 ; \quad t_2(x) = \sigma^o_{21} n_1 ; \tag{4.6}$$

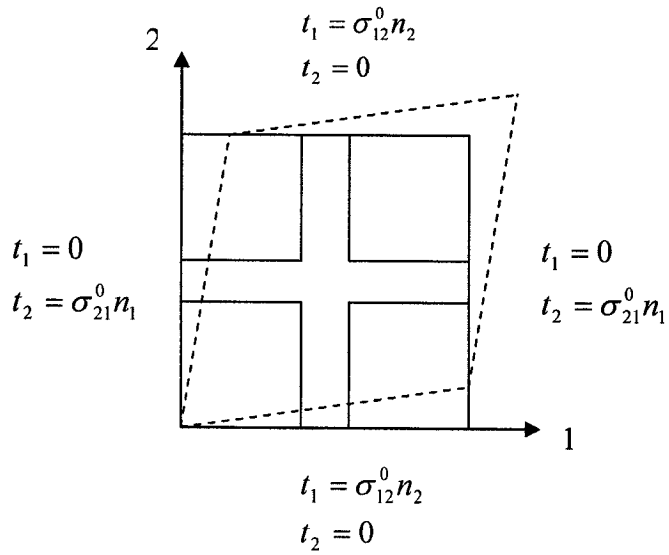

which gives $S_{1212} = \dfrac{2W^{cell}}{V}$ when $\sigma_{12}^o = \sigma_{21}^o = 1$.

4.2.3 Periodic boundary conditions

To predict the effective properties of trabecular bone, the periodic boundary conditions are used. The use of periodic boundary conditions eliminates surface effects from computations. Uniaxial extension, biaxial extension, and simple shear involving periodic deformations are used in to predict the effective properties of idealized models of trabecular bone.

1) Uniaxial extension

When a uniform strain ε_{11}^o is applied on the sample material boundary, the periodic boundary conditions can be written as

$$u_1(\underline{x} + \underline{L}) = u_1(\underline{x}) + \varepsilon_{11}^o L \underline{e_1} \qquad t_1(\underline{x} + \underline{L}) = -t_1(\underline{x}); \tag{4.7}$$

$$u_2(\underline{x} + \underline{L}) = u_2(\underline{x}) \qquad t_2(\underline{x} + \underline{L}) = t_2(\underline{x}); \tag{4.8}$$

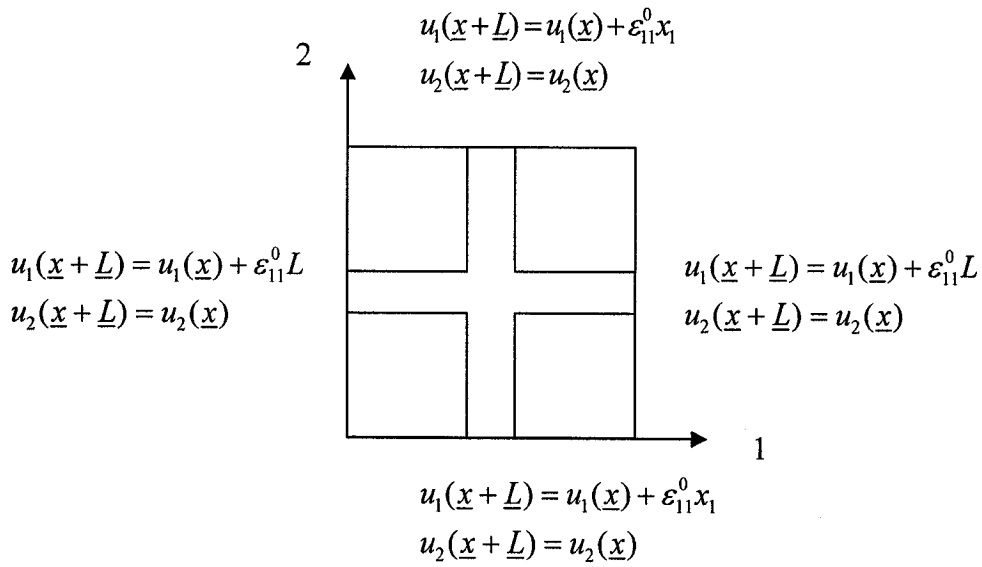

which gives $C_{1111}^{eff} = 2U^{cell} / V$ when $\varepsilon_{11}^o = 1$; where e_1 is the unit vector and L is the length of the unit cell.

2) Biaxial extension

The periodic boundary conditions with $\varepsilon_{11}^o = \varepsilon_{22}^o$ can be written as

$$u_1(\underline{x}+\underline{L}) = u_1(\underline{x}) + \varepsilon_{11}^o L\underline{e_1}\,; \quad t_1(\underline{x}+L) = -t_1(\underline{x}) \tag{4.9}$$

$$u_2(\underline{x}+\underline{L}) = u_2(\underline{x}) + \varepsilon_{22}^o L\underline{e_2}\,; \quad t_2(\underline{x}+L) = -t_2(\underline{x}) \tag{4.10}$$

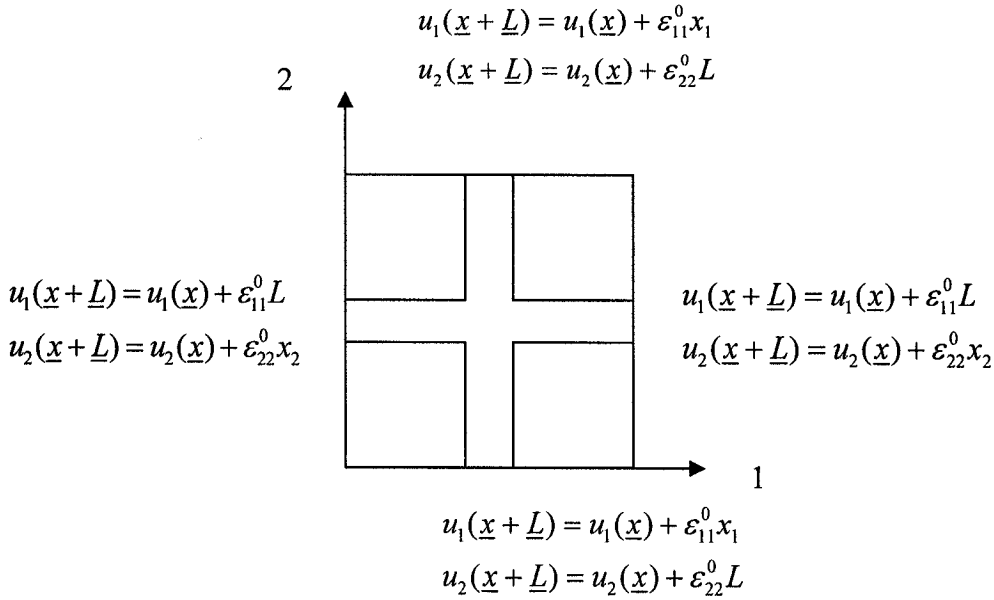

which gives $C_{1122}^{eff} = \frac{2W^{cell}}{V} - C_{1111}^{eff}$ when $\varepsilon_{11}^o = \varepsilon_{22}^o = 1$; where e_i is the unit vector and L is the length of the unit cell.

3) Simple shear

When a uniform strain ε_{12}^o is applied on the sample material boundary, the periodic boundary conditions can be written as

$$u_1(\underline{x}+\underline{L}) = u_1(\underline{x}) + \varepsilon_{12}^o L\underline{e_2}\ ;\quad t_1(\underline{x}+\underline{L}) = -t_1(\underline{x}) \tag{4.11}$$

$$u_2(\underline{x}+\underline{L}) = u_2(\underline{x}) + \varepsilon_{21}^0 Le_1\ ;\quad t_2(\underline{x}+\underline{L}) = -t_2(\underline{x}) \tag{4.12}$$

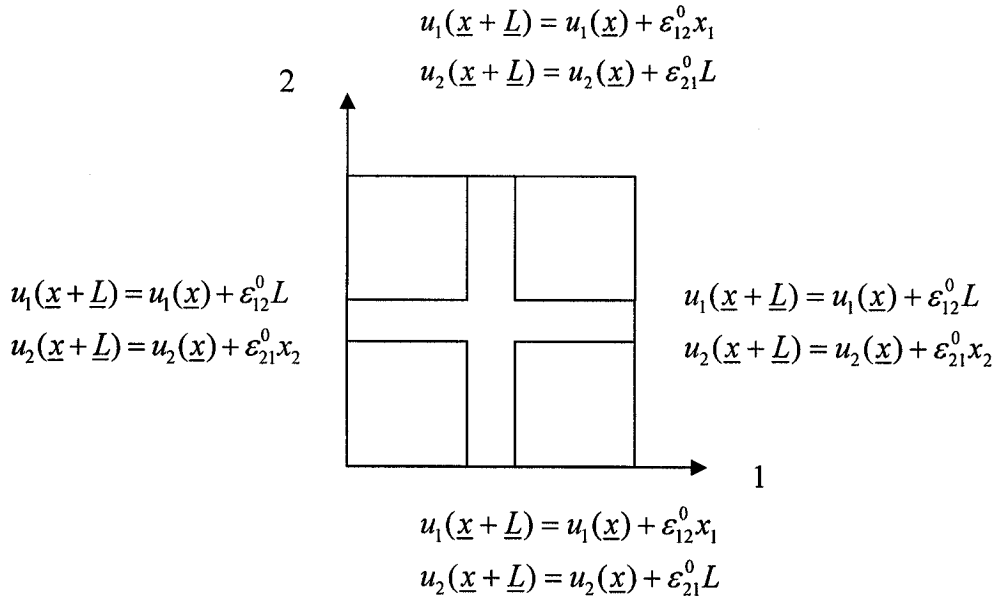

which gives $C_{1212}^{eff} = \frac{2W^{cell}}{V}$ when $\varepsilon_{12}^o = 1$; where e_2 is the unit vector and L is the length of the unit cell.

4.2.4 Mixed boundary conditions

Mixed boundary conditions are including both traction and displacement boundary conditions applied along the outer boundaries of the sample material in Eqn. (2.23). The mixed boundary condition is very important because it is the loading used in experiments to obtain Young's modulus of the bone samples.

1) Mixed uniaxial extension

When a uniform strain ε_{11}^o is only applied on the sample's boundary n_1 face with shear traction $\sigma_{12}^0 = 0$, the mixed boundary conditions can be written as

$u_i = \varepsilon_{ij} x_j$; $\varepsilon_{11}^0 \neq 0$

$$i=1 \quad u_1=\varepsilon_{11}x_1+\varepsilon_{12}x_2 \Rightarrow u_1=\varepsilon_{11}^0 x_1 \tag{4.13}$$

$$i=2 \quad u_2=\varepsilon_{21}x_1+\varepsilon_{22}x_2 \Rightarrow u_2=0 \tag{4.14}$$

$t_i=\sigma_{ij}n_j;\ \sigma_{12}^0=0;\ \sigma_{12}^0=\sigma_{21}^0$

$$i=1 \quad t_1=\sigma_{11}n_1+\sigma_{12}n_2 \Rightarrow t_1=0 \tag{4.15}$$

$$i=2 \quad t_2=\sigma_{21}n_1+\sigma_{22}n_2 \Rightarrow t_2=0 \tag{4.16}$$

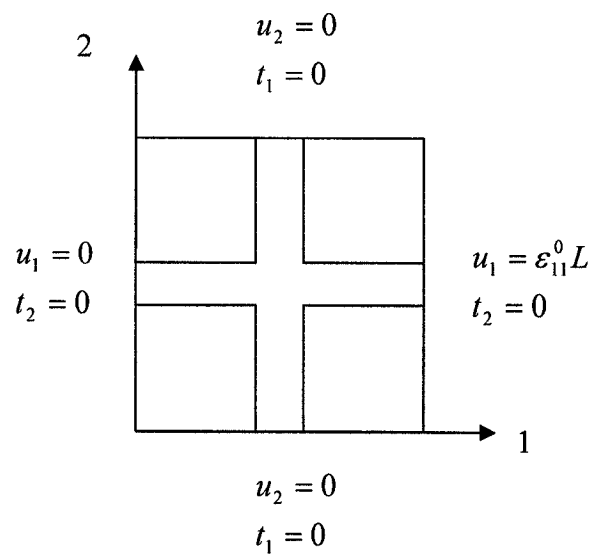

which give $C_{1111}^{eff}=2U^{cell}/V$ when $\varepsilon_{11}^o=1$.

2) Mixed biaxial extension

When the uniform strain $\varepsilon_{11}^o=\varepsilon_{22}^o$ are applied on the n_1 and n_2 faces with shear traction $\sigma_{12}^0=0$, the mixed boundary conditions can be written as

$$u_1=\varepsilon_{11}^o x_1; \quad t_2=\sigma_{12}n_1=0 \qquad \text{on } n_1 \text{ face} \tag{4.17}$$

$$u_2=\varepsilon_{22}^o x_2; \quad t_1=\sigma_{12}n_2=0 \qquad \text{on } n_2 \text{ face} \tag{4.18}$$

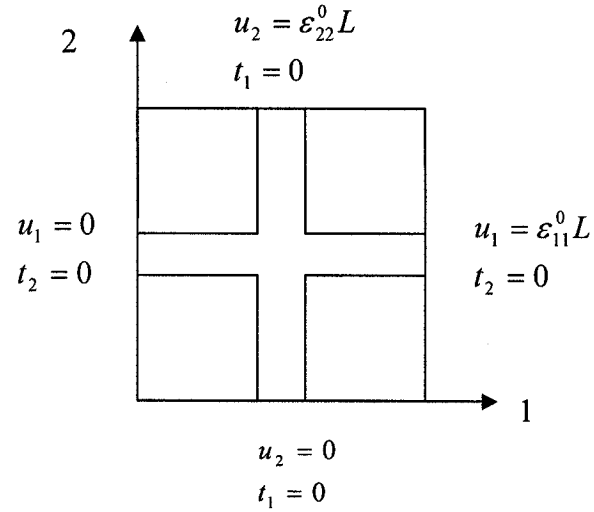

which gives $C_{1122}^{eff} = \dfrac{2W^{cell}}{V} - C_{1111}^{eff}$ when $\varepsilon_{11}^o = \varepsilon_{22}^o = 1$.

3) Simple shear

When a uniform strain ε_{12}^o is only applied with shear tractions, the mixed boundary conditions can be written as

$$u_1 = \varepsilon_{12}^o x_2; \quad t_2 = \sigma_{12} n_2 = 0 \qquad \text{on } n_1 \text{ face} \qquad (4.19)$$

$$u_2 = \varepsilon_{21}^o x_1; \quad t_1 = \sigma_{12} n_1 = 0 \qquad \text{on } n_2 \text{ face} \qquad (4.20)$$

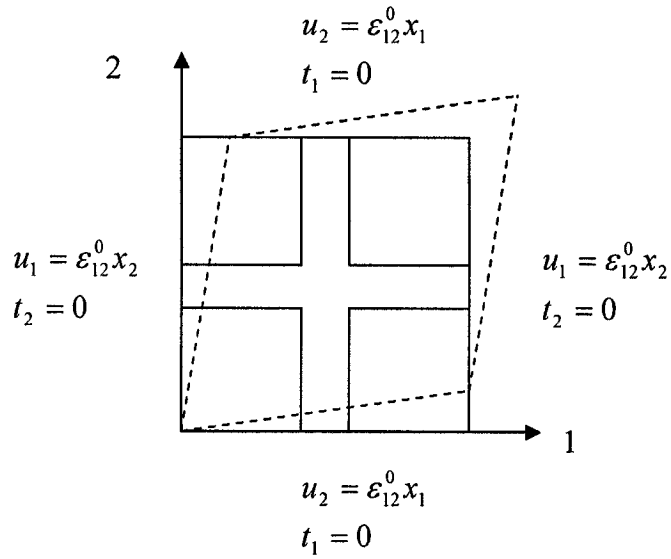

which gives $C_{1212}^{eff} = \frac{2W^{cell}}{V}$ when $\varepsilon_{12}^{o} = 1$.

The three boundary condition tests give a system of three simultaneous equations with the unknowns being C_{1111}, C_{1122}, and C_{1212} and the average stress $\bar{\sigma}_{ij}$, average strains ($\bar{\varepsilon}_{ij}$) and elastic strain energy (W) calculated by the finite element method.

CHAPTER 5

RESULTS

In this dissertation, we study elastic moduli of trabecular bone computationally, focusing on effects of scale and boundary conditions on elastic moduli. In this chapter, FEM, the finite element software package ANSYS Version 8.1, was used to determine the effective and apparent elastic moduli of trabecular bone. Two unit cells were studied under different boundary conditions. The effects of mesh size, the ratio of bone tissue and soft tissue (bone marrow), the sample window size, the sharp corners versus rounded corners of bone structure, bone volume fractions, and the boundary conditions are discussed. Hill's condition, average stress, and average strain are also investigated. The comparisons of 2D and 3D models are also presented in this chapter.

Several geometric models studied in this thesis are as follows. (Bf stands for bone volume fraction in Fig. 5.1)

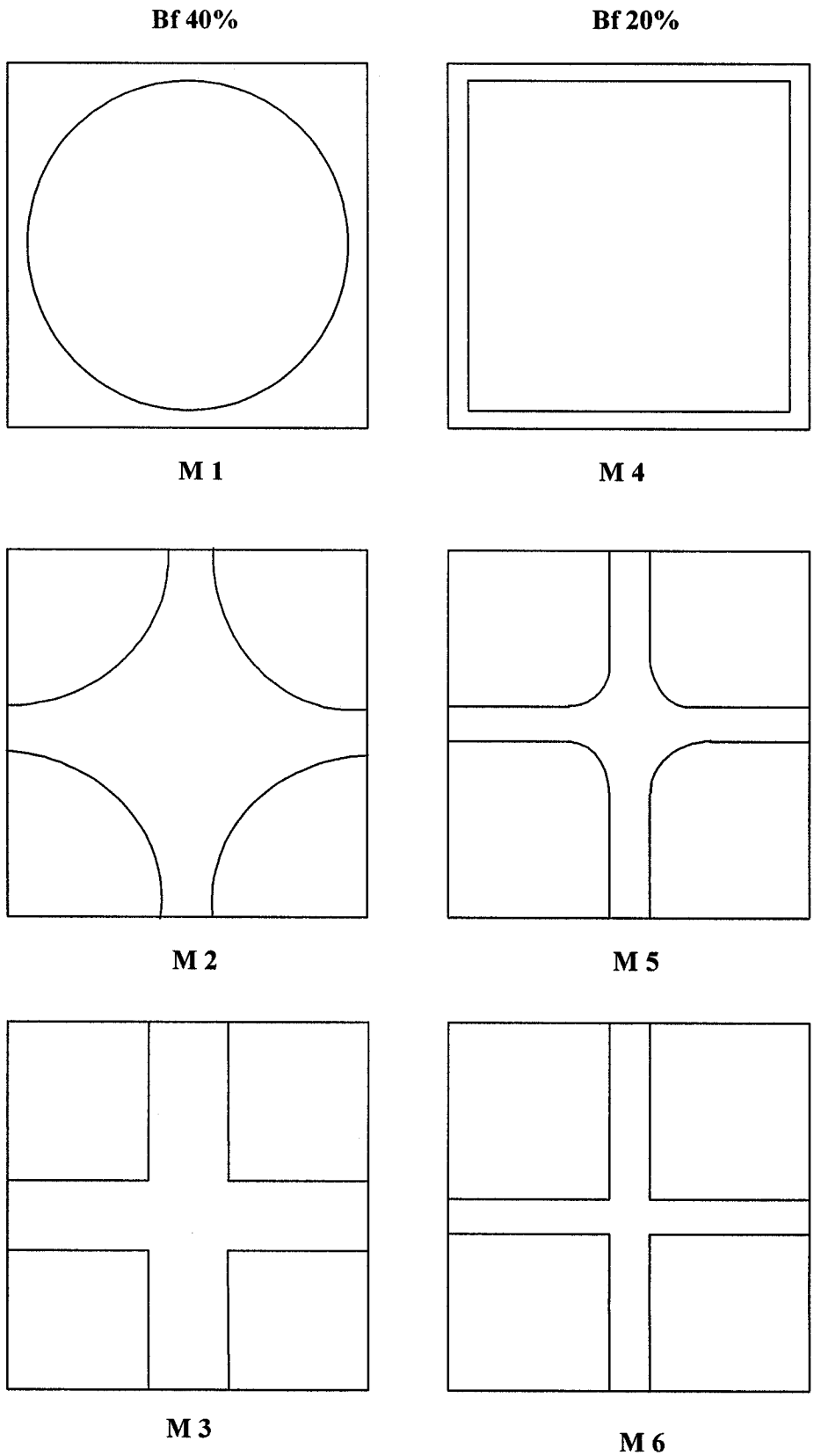

Figure 5. 1 Models of higher and lower bone volume fractions

5.1 Effects of mesh size

In this section, the effects of mesh sizes on properties of trabecular bone are investigated. To solve the elastic moduli of trabecular bone with FEM efficiently, the optimum mesh size for our calculations is our first concern. As a result, the same and different mesh sizes for bone tissue and bone marrow (soft tissue) are investigated, and the effects of different loads with varying of mesh sizes are discussed as well. Finally, the conclusions and recommendations about the mesh sizes are given.

5.1.1 Same mesh size used for bone and bone marrow

1. Uniaxial tension (σ_{11}^0 applied)

We take $E_b/E_m = 10^6$ where E_b and E_m are Young's moduli of bone tissue and bone marrow, respectively.

Mesh Size of Bone/Bone Marrow	Ratio of Bone/Bone Marrow Mesh Size	No. of Elements	Elastic Strain Energy (W)	ΔW (%) $(W_c - W_f / W_c)*100$
0.044/0.044	1	12960	22.5	0
0.066/0.066	1	5776	22.5	0
0.088/0.088	1	4128	22.5	0
0.132/0.132	1	1722	22.5	0
0.176/0.176	1	1018	22.5	0
0.264/0.264	1	486	22.4	0.4
0.528/0.528	1	150	22.3	0.9

Note: W_c is the elastic strain energy obtained using cruder mesh size; W_f is the elastic strain energy obtained using the finest mesh size.

Table 5. 1 Uniaxial tension results using same mesh sizes for bone tissue and soft tissue (bone marrow).

2. Uniaxial extension (ε_{11}^0 applied)

Results are given for $E_b/E_m = 10^6$.

Mesh Size of Bone/Bone Marrow	Ratio of Bone/Bone Marrow Mesh Size	No. of Elements	Elastic Strain Energy(W)	ΔW (%) $(W_c - W_f / W_c)*100$
0.044/0.044	1	12960	7.21×10^{-2}	0
0.066/0.066	1	5776	7.21×10^{-2}	0
0.088/0.088	1	4128	7.21×10^{-2}	0
0.132/0.132	1	1722	7.23×10^{-2}	0.28
0.176/0.176	1	1018	7.24×10^{-2}	0.42
0.264/0.264	1	486	7.26×10^{-2}	0.69
0.528/0.528	1	150	7.36×10^{-2}	2.08

Table 5. 2 Uniaxial extension results using same mesh sizes for bone tissue and bone marrow

When the mesh size is varied from cruder (0.528) to finer (0.044), the elastic strain energy error (ΔW) reduces from 0.9 to 0% for Uniaxial Tension Case and from 2.1 to 0% same trend in Uniaxial Extension Case. Note that the results do not change after certain mesh size, 0.176 for Uniaxial Tension Case and 0.088 for Uniaxial Extension Case while the results for larger mesh sizes are still very close (within 2%) of those obtained using the finest mesh size (0.044/0.044). Recall that the length of the side of the unit cell is 5 so the finest mesh corresponds to 114 elements along the width of the unit cell.

5.1.2 Fixed mesh size for bone tissue with varied mesh size for bone marrow

1. Uniaxial tension (σ_{11}^0 applied)

Results are given for $E_b/E_m = 10^6$.

Mesh Size of Bone/Bone Marrow	Ratio of Bone/Bone Marrow Mesh Size	No. of Elements	Elastic Strain Energy(W)	ΔW (%) $(W_c - W_f / W_c)*100$
0.264/0.044	6	11338	22.5	0
0.264/0.066	4	5176	22.5	0
0.264/0.088	3	3128	22.5	0
0.264/0.132	2	1382	22.5	0
0.264/0.264	1	486	22.4	0.4
0.264/0.4472	0.5903	268	22.3	0.9
0.264/1.118	0.2361	100	21.8	3.1
0.264/2.236	0.1181	40	20.2	10.2

Table 5. 3 Uniaxial tension results using fixed bone tissue mesh size

2. Uniaxial extension (ε_{11}^0 applied)

Results are given for $E_b/E_m = 10^6$.

Mesh Size of Bone/Bone Marrow	Ratio of Bone/Bone Marrow Mesh Size	No. of Elements	Elastic Strain Energy(W)	ΔW (%) $(W_c - W_f / W_c)*100$
0.264/0.044	6	11338	7.22×10^{-2}	0.14
0.264/0.066	4	5176	7.23×10^{-2}	0.28
0.264/0.088	3	3128	7.23×10^{-2}	0.28
0.264/0.132	2	1382	7.25×10^{-2}	0.55
0.264/0.264	1	486	7.26×10^{-2}	0.69
0.264/0.4472	0.5903	268	7.30×10^{-2}	1.25
0.264/1.118	0.2361	100	7.56×10^{-2}	4.85
0.264/2.236	0.1181	40	7.92×10^{-2}	9.85

Table 5. 4 Uniaxial extension results for fixed bone mesh size

When we change the mesh size of bone marrow from 2.236 to 0.044, the elastic strain energy errors are decreased. The results do not change much when we use mesh size 0.264 or finer (error is less than 1%). The elastic strain energy error is calculated by

comparing present results with those obtained using the finest mesh size (0.044/0.044). This approach is followed in this section.

5.1.3 One mesh size for bone marrow with varied mesh size for bone tissue

1. Uniaxial tension (σ_{11}^0 applied)

Results are given for $E_b/E_m = 10^6$.

Mesh Size of Bone/Bone Marrow	Ratio of Bone/Bone Marrow Mesh Sizes	No. of Elements	Elastic Strain Energy(W)	ΔW (%) $(W_c - W_f / W_c)*100$
0.088/1.118	0.0787	876	21.8	3.2
0.132/1.118	0.1181	414	21.8	3.2
0.176/1.118	0.1574	190	21.8	3.2
0.264/1.118	0.2361	100	21.8	3.2
0.528/1.118	0.4723	42	21.8	3.2

Table 5. 5 Uniaxial tension results for fixed bone marrow mesh size

2. Uniaxial extension (ε_{11}^0 applied)

Results are given for $E_b/E_m = 10^6$.

Mesh Size of Bone/Bone Marrow	Ratio of Bone/Bone Marrow Mesh Sizes	No. of Elements	Elastic Strain Energy(W)	ΔW (%) $(W_c - W_f / W_c)*100$
0.088/1.118	0.0787	876	7.52×10^{-2}	4.29
0.132/1.118	0.1181	414	7.52×10^{-2}	4.29
0.176/1.118	0.1574	190	7.53×10^{-2}	4.43
0.264/1.118	0.2361	100	7.56×10^{-2}	4.85
0.528/1.118	0.4723	42	7.64×10^{-2}	5.96

Table 5. 6 Uniaxial extension results for fixed bone marrow mesh size

The elastic strain energy error almost doesn't change even though the mesh sizes of bone are changed from 0.088 to 0.528 because bone marrow is the majority of sample.

5.1.4 Effects of mesh sizes versus different applied loads

Results are given for $E_b/E_m = 10^6$.

Mesh Size of Sample Material	No. of Element	Uniaxial Tension		Uniaxial Extension		Biaxial Tension		Biaxial Extension		Simple Shear Traction		Simple Shear Strain	
		W	ΔW	W	ΔW	W	ΔW	W	ΔW	W	ΔW	W	ΔW
0.044	12960	22.5	0	7.21×10^{-2}	0								
0.066	5776	22.5	0	7.21×10^{-2}	0	32.3	0	0.150	0	37.2	0	3.60×10^{-3}	0
0.088	4128	22.5	0	7.21×10^{-2}	0								
0.132	1722	22.5	0	7.23×10^{-2}	0.28	32.3	0	0.150	0	37.2	0	3.65×10^{-3}	1.4
0.176	1018	22.5	0	7.24×10^{-2}	0.42								
0.264	486	22.4	0.4	7.26×10^{-2}	0.69	31.9	1.2	0.152	1.3	37.1	0.3	3.9×10^{-3}	8.3
0.528	150	22.3	0.9	7.36×10^{-2}	2.08								

Table 5. 7 Effects of mesh size under different loads (mesh sizes of bone tissue and bone marrow are taken as equal)

Note that the displacement boundary conditions are more sensitive to the changes of mesh size as shown in Table 5.7.

5.1.5 Discussion

After reviewing the effects of mesh sizes, the conclusions are given as follows.

1. Results obtained using same mesh size used for bone tissue and bone marrow converge faster than corresponding cases with different mesh sizes for bone tissue and bone marrow.
2. Elastic strain energy is more sensitive to the change of mesh size of bone marrow. On the contrary, the elastic strain energy does not change when mesh size of bone tissue is varied.

3. Energy change as a function of different mesh sizes has the same trend under different boundary conditions. However, it is more sensitive under displacement boundary conditions, especially in simple shear strain.
4. The optimum mesh for our calculations is chosen as 0.264/0.264 due to its accuracy with less elements.

5.2 Effects of ratio of moduli of bone and bone marrow

In this thesis, the bone and bone marrow follow classical elasticity (linear elastic, isotropic) and they have Young's moduli E_b and E_m, Poisson's ratio $\nu_b = \nu_m = 0.3$. We set E_b= 13GPa and vary E_m= 1.3E-09 ~13GPa to model a range of materials with stiff bone and varying properties of bone marrow. The effects of the moduli ratio E_b / E_m are studied to determine how the elastic properties of trabecular bone are changing by varying the Young's modulus of bone marrow. To conduct this parametric study we apply displacement and traction boundary conditions.

5.2.1 Displacement boundary conditions (ε_{ij}^0 applied)

E_b/E_m	C_{1111}^d	C_{1122}^d	C_{1212}^d
10^{10}	1.53×10^3	50	78
10^8	1.53×10^3	50	78
10^6	1.53×10^3	50	78
10^4	1.53×10^3	50	78.6
10^2	1.67×10^3	1.00×10^2	1.43×10^2
10	2.96×10^3	5.40×10^2	6.98×10^2
5	4.34×10^3	1.03×10^3	1.27×10^3
1	1.43×10^4	4.30×10^3	5.00×10^3

Table 5. 8 Displacement boundary conditions results as functions of E_b/E_m

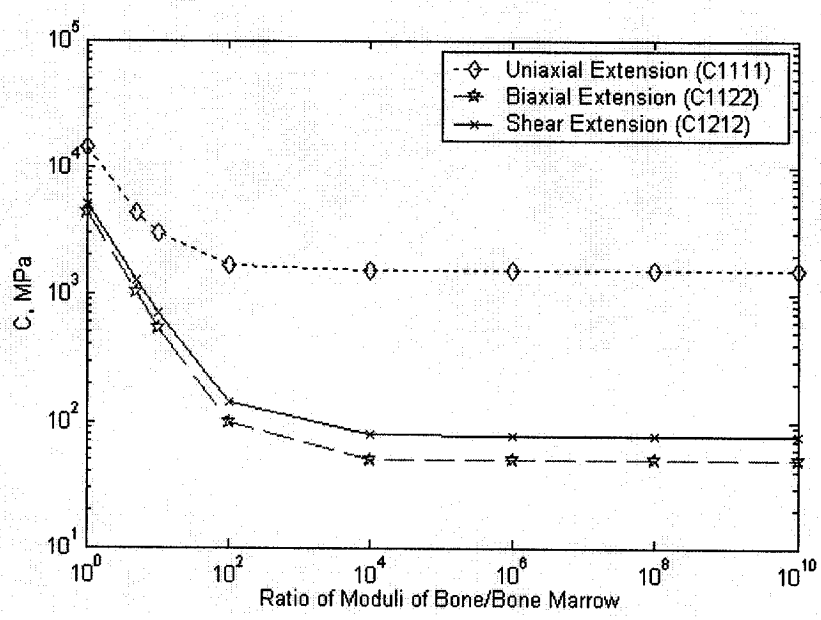

Figure 5. 2 Displacement boundary conditions results as functions of E_b/E_m

For displacement boundary conditions the elastic moduli results asymptote very quickly to those with lower mismatches and they are independent after the ratio of $E_b/E_m = 10^4$ (Fig. 5.2).

5.2.2 Traction boundary conditions (σ_{ij}^0 applied)

E_b/E_m	C'_{1111}	C'_{1122}	C'_{1212}
10^{10}	2.42×10^{-6}	6.75×10^{-7}	1.35×10^{-6}
10^8	2.42×10^{-4}	6.75×10^{-5}	1.35×10^{-4}
10^6	2.42×10^{-2}	6.75×10^{-3}	1.35×10^{-2}
10^4	2.42	0.675	1.35
10^2	2.36×10^{2}	66.2	1.04×10^{2}
10	2.05×10^{3}	5.72×10^{2}	6.17×10^{2}
5	3.75×10^{3}	1.06×10^{3}	1.20×10^{3}
1	1.43×10^{4}	4.29×10^{3}	5.00×10^{3}

Table 5. 9 Traction boundary conditions results as functions of E_b/E_m

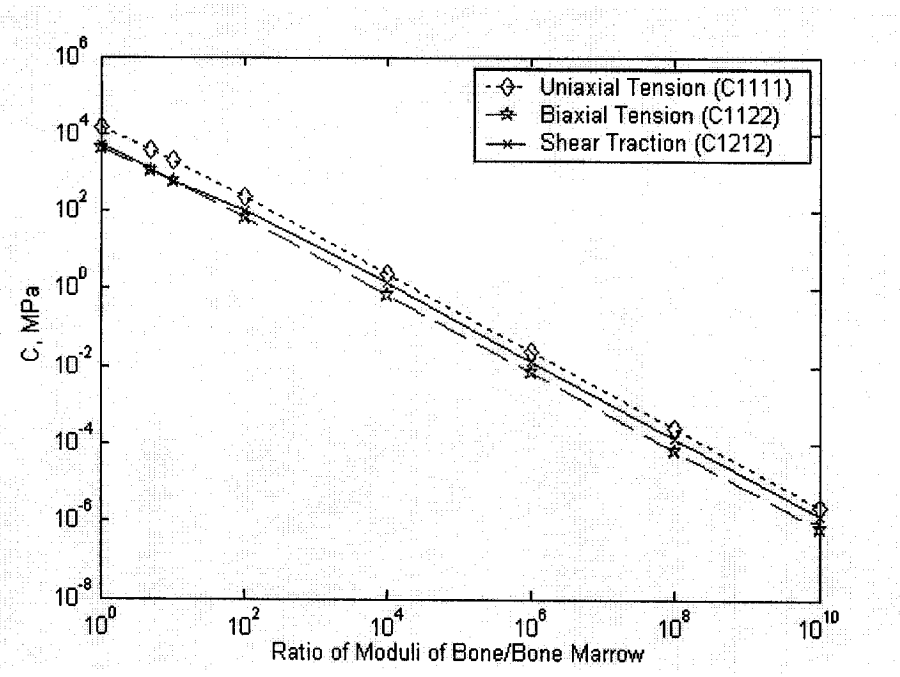

Figure 5. 3 Traction boundary conditions results as functions of E_b/E_m

The moduli under traction boundary condition are dependent on the changes of the ratio of Young's moduli of bone tissue and marrow in the linear way (Fig. 5.3).

5.3 Effects of sample window size

As it has been described in Section 4.1.1, a periodic model of trabecular bone can be represented by repeating unit cells (Figure 4.1) and each unit cell (unit cell 1 or 2) is the smallest part that contains same material properties and geometry (isotropic, linear) as the whole system. In this section we are exploring how the apparent moduli, obtained using displacement, traction or mixed boundary conditions, change when we increase a window size. Since we will be dealing with a periodic structure we will compare these results with effective properties obtained using periodic boundary conditions. This study should help us in understanding a response of random composites and give us guidance on the size of RVE for such materials.

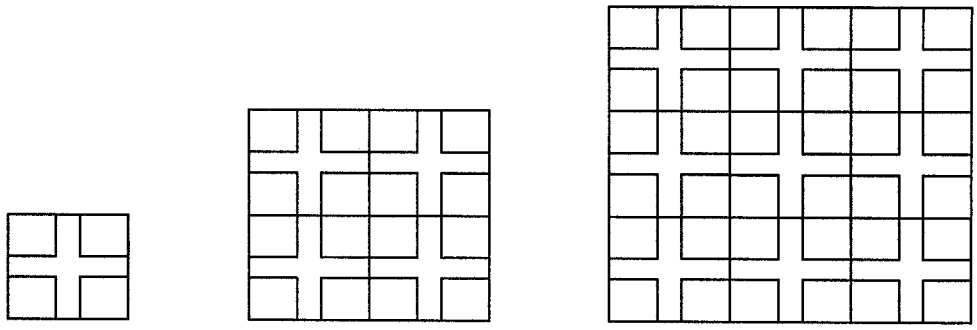

Figure 5. 4 δ_0 and larger scales of trabecular bone

5.3.1 C^d_{1111} under displacement boundary conditions (ε^0_{11} applied)

No. of δ_0	1	2	3	4	6
E_b/E_m	C^d_{1111}	C^d_{1111}	C^d_{1111}	C^d_{1111}	C^d_{1111}
10^{10}	1.53×10^3	1.52×10^3	1.50×10^3		1.49×10^3
10^8	1.53×10^3	1.52×10^3	1.50×10^3		1.49×10^3
10^6	1.53×10^3	1.52×10^3	1.50×10^3		1.49×10^3
10^4	1.53×10^3	1.52×10^3	1.50×10^3		1.50×10^3
10^2	1.67×10^3	1.66×10^3	1.64×10^3		1.64×10^3
10	2.96×10^3	2.94×10^3	2.92×10^3		2.92×10^3
5	4.34×10^3	4.32×10^3	4.30×10^3		4.30×10^3
1	1.43×10^4	1.43×10^4	1.43×10^4		1.43×10^4

Table 5. 10 Displacement boundary conditions results (C^d_{1111})

5.3.2 C^t_{1111} under traction boundary conditions (σ^0_{11} applied)

No. of δ_0	1	2	3	4	6
E_b/E_m	C^t_{1111}	C^t_{1111}	C^t_{1111}	C^t_{1111}	C^t_{1111}
10^{10}	2.45×10^{-6}	4.86×10^{-6}	7.26×10^{-6}		1.47×10^{-5}
10^{8}	2.45×10^{-4}	4.86×10^{-4}	7.26×10^{-4}		1.47×10^{-3}
10^{6}	2.45×10^{-2}	4.86×10^{-2}	7.26×10^{-2}		0.147
10^{4}	2.45	4.82	7.04		14.5
10^{2}	2.37×10^{2}				
10	2.06×10^{3}				
5	3.76×10^{3}				
1	1.43×10^{4}				

Table 5. 11 Traction boundary conditions results (C^t_{1111})

5.3.3 Bounds(C^{app}_{1111})

Data is given for $E_b/E_m=10^6$.

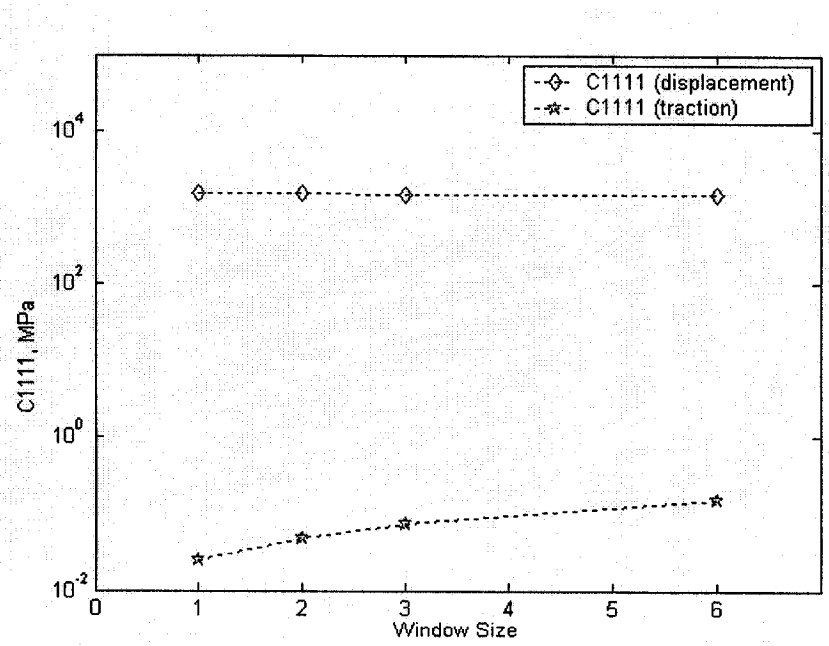

Figure 5. 5 Bounds(C^{app}_{1111})

Fig. 5.5 shows that C_{1111}^{app} are far apart but they become closer as the window size increases.

5.3.4 C_{1122}^{d} under displacement boundary conditions ($\varepsilon_{11}^{0} = \varepsilon_{22}^{0}$ applied)

No. of δ_0	1	2	3	4	6
E_b/E_m	C_{1122}^{d}	C_{1122}^{d}	C_{1122}^{d}	C_{1122}^{d}	C_{1122}^{d}
10^{10}	50	70	70		70
10^{8}	50	70	70		70
10^{6}	50	70	70		70
10^{4}	50	70	70		60
10^{2}	1.00×10^{2}	1.13×10^{2}	1.20×10^{2}		1.10×10^{2}
10	5.40×10^{2}	5.70×10^{2}	5.70×10^{2}		5.60×10^{2}
5	1.03×10^{3}	1.06×10^{3}	1.06×10^{3}		1.05×10^{3}
1	4.30×10^{3}	4.30×10^{3}	4.30×10^{3}		4.30×10^{3}

Table 5. 12 Displacement boundary conditions results (C_{1122}^{d})

5.3.5 C_{1122}^{t} under traction boundary conditions ($\sigma_{11}^{0} = \sigma_{22}^{0}$ applied)

No. of δ_0	1	2	3	4	6
E_b/E_m	C_{1122}^{t}	C_{1122}^{t}	C_{1122}^{t}	C_{1122}^{t}	C_{1122}^{t}
10^{10}	6.89×10^{-7}	6.94×10^{-7}	7.16×10^{-7}		7.55×10^{-7}
10^{8}	6.89×10^{-5}	6.94×10^{-5}	7.16×10^{-5}		7.54×10^{-5}
10^{6}	6.89×10^{-3}	6.94×10^{-3}	7.16×10^{-3}		7.54×10^{-3}
10^{4}	0.689	0.714	0.731		0.758
10^{2}	67.4				
10	5.76×10^{2}				
5	1.08×10^{3}				
1	4.30×10^{3}				

Table 5. 13 Traction boundary conditions results (C_{1122}^{t})

5.3.6 C^{d}_{1212} under displacement boundary conditions (ε^{0}_{12} applied)

No. of δ_0	1	2	3	4	6
E_b/E_m	C^{d}_{1212}	C^{d}_{1212}	C^{d}_{1212}	C^{d}_{1212}	C^{d}_{1212}
10^{10}	78	44.4	32		19.4
10^{8}	78	44.4	32		19.4
10^{6}	78	44.4	32		19.4
10^{4}	78.6	45	32		20
10^{2}	1.4×10^{2}	1.09×10^{2}	94.2		83
10	6.98×10^{2}	6.58×10^{2}	6.42×10^{2}		6.29×10^{2}
5	1.27×10^{3}	1.23×10^{3}	1.21×10^{3}		1.20×10^{3}
1	5.00×10^{3}	5.00×10^{3}	5.00×10^{3}		5.00×10^{3}

Table 5. 14 Displacement boundary conditions results (C^{d}_{1212})

5.3.7 C^{t}_{1212} under traction boundary conditions (σ^{0}_{12} applied)

No. of δ_0	1	2	3	4	6
E_b/E_m	C^{t}_{1212}	C^{t}_{1212}	C^{t}_{1212}	C^{t}_{1212}	C^{t}_{1212}
10^{10}	1.35×10^{-6}	2.22×10^{-6}	3.14×10^{-6}		5.95×10^{-6}
10^{8}	1.35×10^{-4}	2.22×10^{-4}	3.14×10^{-4}		5.95×10^{-4}
10^{6}	1.35×10^{-2}	2.22×10^{-2}	3.14×10^{-2}		5.95×10^{-2}
10^{4}	1.30	1.98	2.58×10^{-6}		3.92
10^{2}	1.03×10^{2}				
10	6.25×10^{2}				
5	1.21×10^{3}				
1	5.00×10^{3}				

Table 5. 15 Traction boundary conditions results (C^{t}_{1212})

5.3.8 Bounds (C^{app}_{1212})

Data is given for $E_b/E_m=10^{6}$.

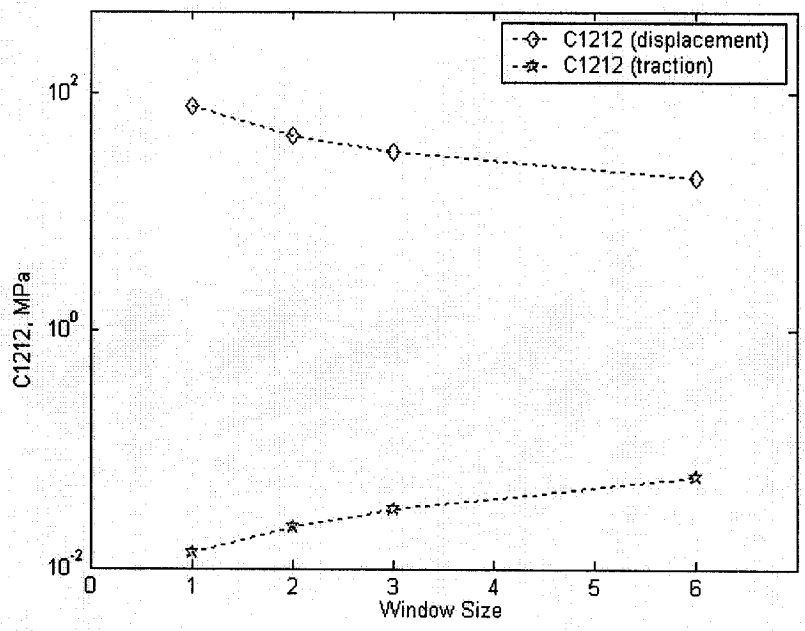

Figure 5. 6 Bounds (C_{1212}^{app})

Fig. 5.6 showed that C_{1212}^{app} are far apart but become as window size increases. However, the convergence is slow.

5.3.9 Discussion

1. The apparent stiffness components C_{1111} and C_{1212} are becoming more close to each other by increasing the sample window sizes.

2. The stiffness component C_{1122} is not as sensitive as C_{1111} and C_{1212} to the increase of window size.

3. According to the trend of each stiffness component above, we can conclude that the bounds are still wide for window sizes of 6 when the ratio of the modulus of bone and bone marrow is large (10^6).

5.4 Periodic boundary conditions results

Although the apparent stiffness components are coming closer to each other by increasing the widow sizes, the bounds are still wide when window size of 6 is taken and this is a computational limit for the available version of ANSYS. In this section the periodic boundary conditions are introduced to predict and study the effective properties of trabecular bone. Uniaxial Extension, Biaxial Extension, and Simple Shear are used to obtain the effective properties of trabecular bone by forming the periodic deformations.

5.4.1 Uniaxial extension (ε_{11}^0 applied)

E_b/E_m	σ_{11}	ε_{11}	Energy (W)	C_{1111}
10^{10}	14.0	1.00×10^{-2}	7.00×10^{-2}	1.40×10^{3}
10^{8}	14.0	1.00×10^{-2}	7.00×10^{-2}	1.40×10^{3}
10^{6}	14.0	1.00×10^{-2}	7.00×10^{-2}	1.40×10^{3}
10^{4}	14.0	1.00×10^{-2}	7.00×10^{-2}	1.40×10^{3}
10^{2}	15.5	1.00×10^{-2}	7.73×10^{-2}	1.55×10^{3}
10	28.3	1.00×10^{-2}	0.141	2.83×10^{3}
5	42.2	1.00×10^{-2}	0.211	4.22×10^{3}
1	1.42×10^{2}	1.00×10^{-2}	0.709	1.42×10^{4}

Table 5. 16 Uniaxial extension results for periodic boundary conditions

5.4.2 Biaxial extension ($\varepsilon_{11}^0 = \varepsilon_{22}^0$ applied)

E_b/E_m	σ_{11}	σ_{22}	ε_{11}	ε_{22}	Energy (W)	C_{1122}
10^{10}	14.6	14.6	0.01	0.01	0.146	60.0
10^{8}	14.6	14.6	0.01	0.01	0.146	60.0
10^{6}	14.6	14.6	0.01	0.01	0.146	60.0
10^{4}	14.6	14.6	0.01	0.01	0.146	60.0
10^{2}	16.8	16.8	0.01	0.01	0.173	1.80×10^{2}
10	34.0	34.0	0.01	0.01	0.360	7.70×10^{2}
5	52.8	52.8	0.01	0.01	0.568	1.46×10^{3}
1	1.85×10^{2}	1.85×10^{2}	0.01	0.01	1.85	4.30×10^{3}

Table 5. 17 Biaxial extension results for periodic boundary conditions

5.4.3 Simple shear strain (ε_{12}^0 applied)

E_b/E_m	σ_{12}	ε_{12}	Energy (W)	C_{1212}
10^{10}	8.70×10^{-2}	1.00×10^{-2}	4.36×10^{-4}	8.72
10^{8}	8.70×10^{-2}	1.00×10^{-2}	4.36×10^{-4}	8.72
10^{6}	8.70×10^{-2}	1.00×10^{-2}	4.36×10^{-4}	8.72
10^{4}	9.33×10^{-2}	1.00×10^{-2}	4.67×10^{-4}	9.35
10^{2}	0.718	1.00×10^{-2}	3.60×10^{-3}	72.0
10	6.20	1.00×10^{-2}	3.10×10^{-2}	6.20×10^{2}
5	12.0	1.00×10^{-2}	6.00×10^{-2}	1.20×10^{3}
1	50.0	1.00×10^{-2}	0.250	5.00×10^{3}

Table 5. 18 Simple shear strain results for periodic boundary conditions

5.4.4 Results and discussion

Comparison of results from displacement (D), and traction (T), and periodic (P) boundary conditions $E_b/E_m=10^6$, are shown in Table 5.19.

Window Size	C_{1111}			C_{1122}			C_{1212}		
	D	T	P	D	T	P	D	T	P
1	1.53×10^{3}	2.45×10^{-2}	1.40×10^{3}	60.0	6.89×10^{-3}	60.0	78.0	1.35×10^{-2}	8.72
2	1.52×10^{3}	4.86×10^{-2}	1.40×10^{3}	70.0	6.94×10^{-3}	60.0	44.4	2.22×10^{-2}	8.72
6	1.49×10^{3}	0.147	1.40×10^{3}	70.0	7.54×10^{-3}	60.0	19.4	5.95×10^{-2}	8.72

Table 5. 19 Comparison of bounds and periodic boundary conditions results

We make the following observations about these results:

1. The moduli under periodic boundary condition are independent of the sample window size, as expected.

2. Periodic boundary conditions give the effective properties of trabecular bone.

5.5 Mixed boundary conditions results

In this section we investigate the effect of mixed boundary conditions on elastic moduli C_{ijkl} . The mixed boundary conditions are involving both traction and displacement boundary conditions applied on the boundary of the sample material (Section 4.2.4). Mixed boundary conditions are used in experiments to obtain the Young's modulus of bone samples. Thus, they simulate the realistic materials testing conditions. We found that the moduli under mixed boundary conditions are very close to those of periodic boundary conditions.

5.5.1 Mixed uniaxial extension ($u_1 = \varepsilon_{11}^0 x_1, t_2 = 0$ on n_1 faces; $t_1 = 0, u_2 = 0$ on n_2 faces)

E_b/E_m	σ_{11}	ε_{11}	Energy (W)	C_{1111}
10^{10}	14.3	10^{-2}	7.14×10^{-2}	1.43×10^{3}
10^{8}	14.3	10^{-2}	7.14×10^{-2}	1.43×10^{3}
10^{6}	14.3	10^{-2}	7.14×10^{-2}	1.43×10^{3}
10^{4}	14.3	10^{-2}	7.14×10^{-2}	1.43×10^{3}
10^{2}	15.6	10^{-2}	7.80×10^{-2}	1.56×10^{3}
10	27.3	10^{-2}	0.136	2.73×10^{3}
5	39.8	10^{-2}	0.199	3.98×10^{3}
1	1.30×10^{2}	10^{-2}	0.650	1.30×10^{4}

Table 5. 20 Mixed uniaxial extension results of mixed boundary conditions

5.5.2 Biaxial extension ($u_1 = \varepsilon_{11}^0 x_1, t_2 = 0$ on n_1 faces; $t_1 = 0, u_2 = \varepsilon_{22}{}^o x_2$ on n_2 faces)

E_b/E_m	σ_{11}	σ_{22}	ε_{11}	ε_{22}	Energy (W)	C_{1122}
10^{10}	15.0	15.0	0.01	0.01	0.150	70.0
10^{8}	15.0	15.0	0.01	0.01	0.150	70.0
10^{6}	15.0	15.0	0.01	0.01	0.150	70.0
10^{4}	15.0	15.0	0.01	0.01	0.150	70.0
10^{2}	17.0	17.0	0.01	0.01	0.170	1.40×10^{2}
10	34.5	34.5	0.01	0.01	0.345	7.20×10^{2}
5	53.3	53.3	0.01	0.01	0.533	1.35×10^{3}
1	1.86×10^{2}	1.86×10^{2}	0.01	0.01	1.86	4.30×10^{3}

Table 5. 21 Biaxial extension results of mixed boundary conditions

5.5.3 Simple shear strain ($u_1 = \varepsilon_{12}^0 x_2, t_2 = 0$ on n_1 faces; $t_1 = 0, u_2 = \varepsilon_{21}{}^o x_1$ on n_2 faces)

E_b/E_m	σ_{12}	ε_{12}	Energy (W)	C_{1212}
10^{10}	8.70×10^{-2}	10^{-2}	4.36×10^{-4}	8.72
10^{8}	8.70×10^{-2}	10^{-2}	4.36×10^{-4}	8.72
10^{6}	8.70×10^{-2}	10^{-2}	4.36×10^{-4}	8.72
10^{4}	9.33×10^{-2}	10^{-2}	4.67×10^{-4}	9.35
10^{2}	0.718	10^{-2}	3.60×10^{-3}	72.0
10	6.20	10^{-2}	3.10×10^{-2}	6.20×10^{2}
5	12.0	10^{-2}	6.00×10^{-2}	1.20×10^{3}
1	50.0	10^{-2}	0.250	5.00×10^{3}

Table 5. 22 Simple shear strain results of mixed boundary conditions

5.5.4 Results and discussion

When we take $E_b/E_m=10^6$, the comparison among results from displacement (D), and traction(T), and mixed (M) boundary conditions is given in Table 5.23.

Window Size	C_{1111}			C_{1122}			C_{1212}		
	D	T	M	D	T	M	D	T	M
1	1.53×10^{3}	2.45×10^{-2}	1.43×10^{3}	60.0	6.89×10^{-3}	70.0	78.0	1.35×10^{-2}	8.72
2	1.52×10^{3}	4.86×10^{-2}	1.43×10^{3}	70.0	6.94×10^{-3}	70.0	44.4	2.22×10^{-2}	8.72
6	1.49×10^{3}	0.147	1.43×10^{3}	70.0	7.54×10^{-3}	70.0	19.4	5.95×10^{-2}	8.72

Table 5. 23 Comparisons of bounds and mixed boundary conditions results

1. The moduli under mixed boundary condition are independent of the sample window size.

2. The moduli under mixed boundary conditions are very close to those obtained under periodic boundary conditions (Fig. 5.7).

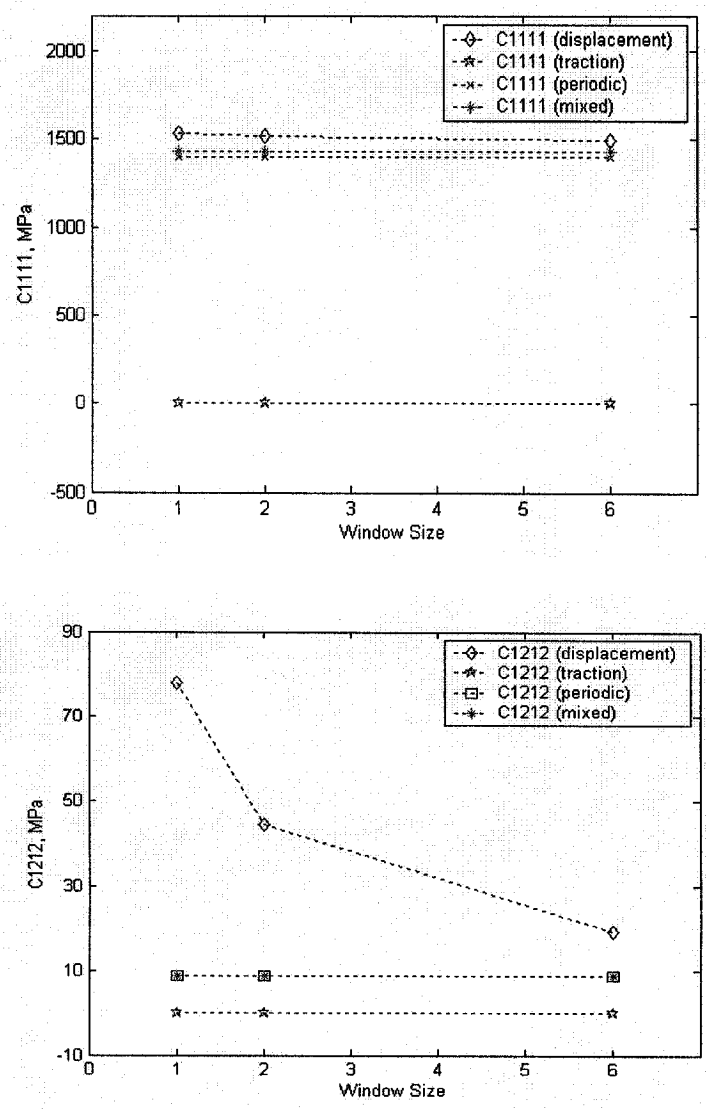

Figure 5. 7 Comparisons of periodic and mixed boundary conditions results

Fig. 5.7 showed that the elastic moduli obtained using periodic and mixed boundary conditions are independent of window size, and the results obtained using mixed boundary conditions are close to those obtained using periodic boundary conditions. C^{d}_{1111} is closer to C^{eff}_{1111} than C^{t}_{1111}, while C^{t}_{1212} is closer to C^{eff}_{1212} than C^{d}_{1212}

5.6 Comparisons of two unit cells results

For our periodic model, there are two ways to take the unit cell to examine the elastic properties of trabecular bone (as shown in Fig. 4.2 and Fig. 4.3). The first way is

that the cross bone structure is in the center of unit cell; this model was used in sections above. The second method to predict material behavior is to use the unit cell 2 in which a half squared bone is around outside of unit cell. The results of unit cell 2 will be shown in this section.

5.6.1 C^{d}_{1111} under displacement boundary conditions (ε^{0}_{11} applied)

No. of δ_0	1	2	6
E_b/E_m	C^{d}_{1111}	C^{d}_{1111}	C^{d}_{1111}
10^{10}	1.42×10^{3}	1.42×10^{3}	1.41×10^{3}
10^{8}	1.42×10^{3}	1.42×10^{3}	1.41×10^{3}
10^{6}	1.42×10^{3}	1.42×10^{3}	1.41×10^{3}
10^{4}	1.43×10^{3}	1.42×10^{3}	1.41×10^{3}
10^{2}	1.57×10^{3}	1.56×10^{3}	1.55×10^{3}
10	2.86×10^{3}	2.86×10^{3}	2.84×10^{3}
5	4.26×10^{3}	4.26×10^{3}	4.24×10^{3}
1	1.43×10^{4}	1.43×10^{4}	1.43×10^{4}

Table 5. 24 Displacement boundary conditions results (C^{d}_{1111}) of Unit Cell 2

5.6.2 C^{t}_{1111} under traction boundary conditions (σ^{0}_{11} applied)

No. of δ_0	1	2	6
E_b/E_m	C^{t}_{1111}	C^{t}_{1111}	C^{t}_{1111}
10^{10}	46.9	1.06×10^{2}	3.07×10^{2}
10^{8}	46.9	1.06×10^{2}	3.07×10^{2}
10^{6}	46.9	1.06×10^{2}	3.07×10^{2}
10^{4}	49.7	1.09×10^{2}	3.28×10^{2}
10^{2}	3.17×10^{2}	4.91×10^{2}	$9.19E\times10^{2}$
10	2.14×10^{3}	2.42×10^{3}	2.69×10^{3}
5	3.81×10^{3}	4.01×10^{3}	4.18×10^{3}
1	1.43×10^{4}	1.43×10^{4}	1.43×10^{4}

Table 5. 25 Traction boundary conditions results (C^{t}_{1111}) of Unit Cell 2

5.6.3 Bounds (C_{1111}^{app}) and comparison with Unit Cell1

Results are given for $E_b/E_m=10^6$.

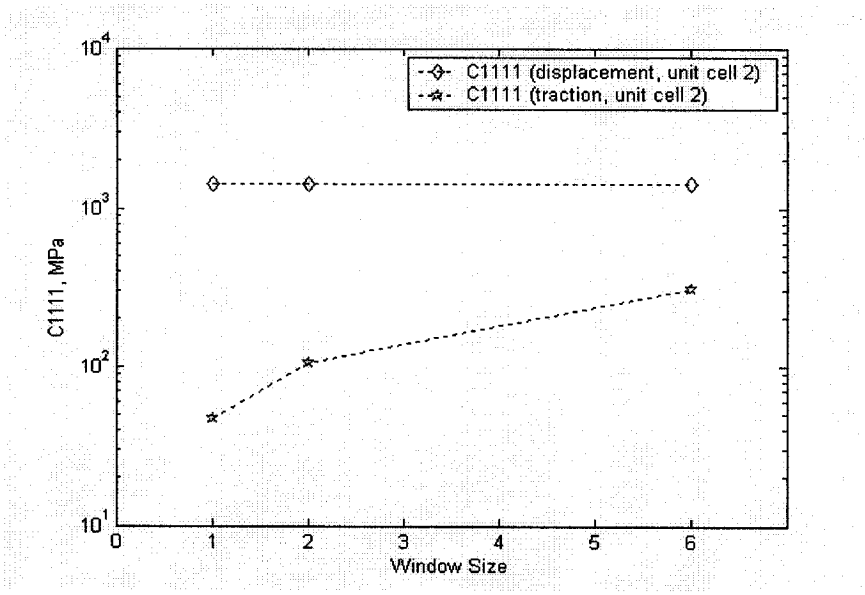

Figure 5. 8 Bounds C_{1111}^{app} obtained using Unit Cell 2

Fig. 5.8 shows that C_{1111}^{app} for Unit Cell 2 are becoming closer to each other with increasing window size.

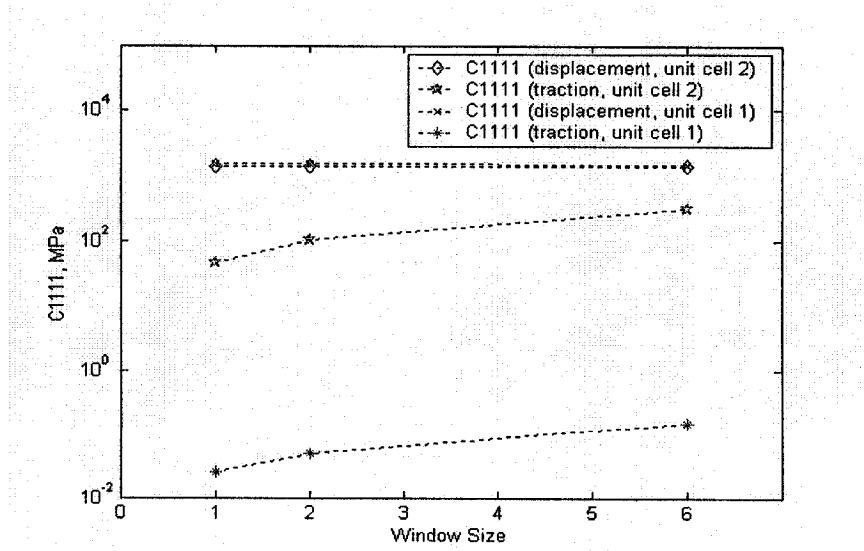

Figure 5. 9 Comparisons of bounds on C_{1111} for Unit Cells 1 and 2

Fig. 5.9 shows that the bounds C_{1111} for Unit Cells 2 are closer to each other than those obtained using Unit Cell 1.

5.6.4 C^{d}_{1122} under the displacement boundary conditions ($\varepsilon^{0}_{11}=\varepsilon^{0}_{22}$ applied)

No. of δ_0	1	2	6
E_b/E_m	C^{d}_{1122}	C^{d}_{1122}	C^{d}_{1122}
10^{10}	80.0	80.0	80.0
10^{8}	80.0	80.0	80.0
10^{6}	80.0	80.0	80.0
10^{4}	80.0	80.0	80.0
10^{2}	1.30×10^{2}	1.20×10^{2}	1.20×10^{2}
10	5.90×10^{2}	5.70×10^{2}	5.80×10^{2}
5	1.07×10^{3}	1.05×10^{3}	1.06×10^{3}
1	4.30×10^{3}	4.30×10^{3}	4.30×10^{3}

Table 5. 26 Displacement boundary conditions results (C^{d}_{1122}) using Unit Cell 2

5.6.5 C^{t}_{1122} obtained using traction boundary conditions ($\sigma^{0}_{11}=\sigma^{0}_{22}$ applied)

No. of δ_0	1	2	6
E_b/E_m	C^{t}_{1122}	C^{t}_{1122}	C^{t}_{1122}
10^{10}	34.4	41.5	63.2
10^{8}	34.4	41.5	63.2
10^{6}	34.4	41.5	63.2
10^{4}	35.7	42.4	71.8
10^{2}	1.59×10^{2}	1.34×10^{2}	97.8
10	7.76×10^{2}	6.57×10^{2}	5.79×10^{2}
5	1.24×10^{3}	1.11×10^{3}	1.06×10^{3}
1	4.30×10^{3}	4.30×10^{3}	4.30×10^{3}

Table 5. 27 Traction boundary conditions results (C^{t}_{1122}) using Unit Cell 2

5.6.6 C^{d}_{1212} obtained using displacement boundary conditions (ε^{0}_{12} applied)

No. of δ_0	1	2	6
E_b/E_m	C^{d}_{1212}	C^{d}_{1212}	C^{d}_{1212}
10^{10}	1.18×10^{2}	40.0	20.0
10^{8}	1.18×10^{2}	40.0	20.0
10^{6}	1.18×10^{2}	40.0	20.0
10^{4}	1.18×10^{2}	40.0	22.0
10^{2}	1.80×10^{2}	1.04×10^{2}	84.0
10	7.16×10^{2}	6.54×10^{2}	6.34×10^{2}
5	1.28×10^{3}	1.23×10^{3}	1.21×10^{3}
1	5.00×10^{3}	5.00×10^{3}	5.00×10^{3}

Table 5. 28 Displacement boundary conditions results (C^{d}_{1212}) using Unit Cell 2

5.6.7 C^{t}_{1212} obtained using traction boundary conditions (σ^{0}_{12} applied)

No. of δ_0	1	2	6
E_b/E_m	C^{t}_{1212}	C^{t}_{1212}	C^{t}_{1212}
10^{10}	2.70	4.50	6.71
10^{8}	2.70	4.50	6.71
10^{6}	2.70	4.50	6.71
10^{4}	3.33	5.18	7.41
10^{2}	65.8	68.5	70.4
10	6.13×10^{2}	6.17×10^{2}	6.17×10^{2}
5	1.19×10^{3}	1.19×10^{3}	1.20×10^{3}
1	5.00×10^{3}	5.00×10^{3}	5.00×10^{3}

Table 5. 29 Traction boundary conditions results (C^{t}_{1212}) using Unit Cell 2

5.6.8 Bounds (C^{app}_{1212}) and comparison with Unit Cell1

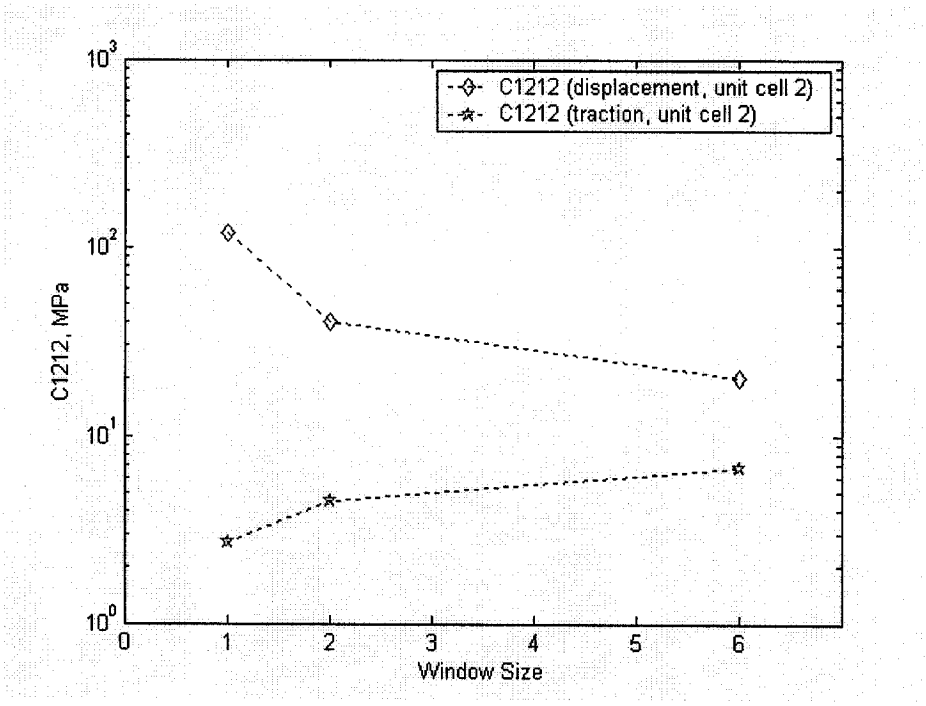

Figure 5. 10 Bounds C_{1212}^{app} obtained using Unit Cell 2

Fig.5.10 shows that C_{1212}^{app} are becoming closer to each other with increasing window size.

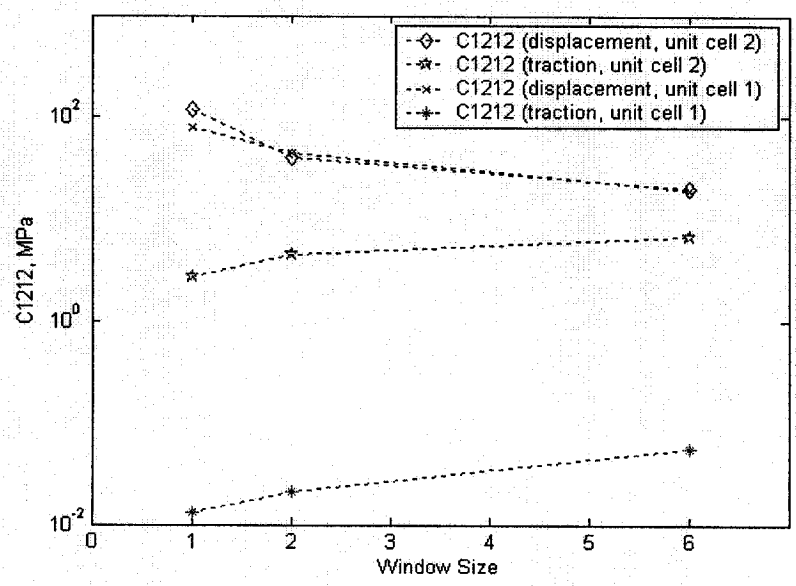

Figure 5. 11 Comparisons of bounds C_{1212}^{app} for Unit Cells 1 and 2

Fig. 5.11 shows that the bounds C_{1212}^{app} obtained using the Unit Cell 2 are closer to each other than those obtained using the Unit Cell 1.

5.6.9 Discussion

The results obtained using the Unit Cell 2 show the same trend as for the Unit Cell 1 under displacement boundary conditions for C_{1111}^{d} and C_{1212}^{d}. But, the results using the Unit cell 2 under traction boundary conditions are different than those obtained from Unit Cell 1. The Unit Cell 2 gives the closer bounds than the Unit Cell 1 because of its stiff edges. This restrains deformation under traction boundary conditions.

5.7 Effects of sharp-corners in idealized trabecular bone models

The experiments have shown that failure of the trabecular bone occurs mostly at the bone-corner interface. Therefore, the effects of sharp-corners versus rounded-corners are studied in this section. The volume fraction of the new model (with rounded corner) is same as in the earlier model (20%); bone size is changing to 0.5 and corner radius is 0.5.

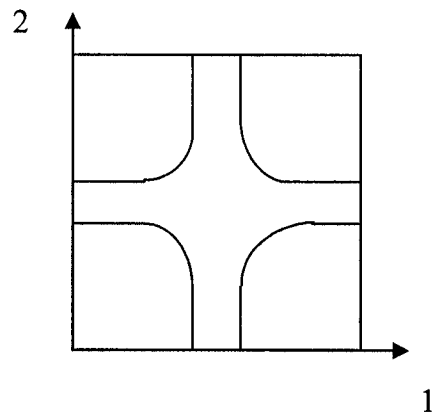

Figure 5. 12 The model of trabecular bone without sharp corners

5.7.1 Displacement boundary conditions results

Model	M6	M5	M6	M5	M6	M5
E_b/E_m	C^d_{1111}	C^d_{1111}	C^d_{1122}	C^d_{1122}	C^d_{1212}	C^d_{1212}
10^{10}	1.53×10^3	1.46×10^3	50.0	60.0	78.0	82.0
10^8	1.53×10^3	1.46×10^3	50.0	60.0	78.0	82.0
10^6	1.53×10^3	1.46×10^3	50.0	60.0	78.0	82.0
10^4	1.53×10^3	1.46×10^3	50.0	60.0	78.6	82.0
10^2	1.67×10^3	1.60×10^3	1.00×10^2	1.10×10^2	1.43×10^2	1.46×10^2
10	2.96×10^3	2.88×10^3	5.40×10^2	5.60×10^2	6.98×10^2	7.02×10^2
5	4.34×10^3	4.28×10^3	1.03×10^3	1.08×10^3	1.27×10^3	1.28×10^3
1	1.43×10^4	1.43×10^4	4.30×10^3	4.30×10^3	5.00×10^3	5.00×10^3

Table 5. 30 Displacement boundary conditions results for models with and without sharp corners

5.7.2 Traction boundary conditions results

Model	M6	M5	M6	M5	M6	M5
E_b/E_m	C^t_{1111}	C^t_{1111}	C^t_{1122}	C^t_{1122}	C^t_{1212}	C^t_{1212}
10^{10}	2.45×10^{-6}	2.39×10^{-6}	6.89×10^{-7}	6.75×10^{-7}	1.35×10^{-6}	1.33×10^{-6}
10^8	2.45×10^{-4}	2.39×10^{-4}	6.89×10^{-5}	6.75×10^{-5}	1.35×10^{-4}	1.33×10^{-4}
10^6	2.45×10^{-2}	2.39×10^{-2}	6.89×10^{-2}	6.75×10^{-3}	1.35×10^{-2}	1.33×10^{-2}
10^4	2.45	2.39	0.689	0.675	1.30	1.28
10^2	2.37×10^2	2.36×10^2	67.4	66.8	1.03×10^2	73.5
10	2.06×10^3	2.05×10^3	5.76×10^2	5.76×10^2	6.25×10^2	6.21×10^2
5	3.75×10^3	3.75×10^3	1.08×10^3	1.06×10^3	1.21×10^3	1.20×10^3
1	1.43×10^4	1.43×10^4	4.30×10^3	4.29×10^3	5.00×10^3	5.00×10^3

Table 5. 31 Traction boundary conditions results for models with and without sharp corners

5.7.3 Analysis of contour of nodal solutions

Data is given for uniaxial traction boundary condition and $E_b/E_m=10^6$.

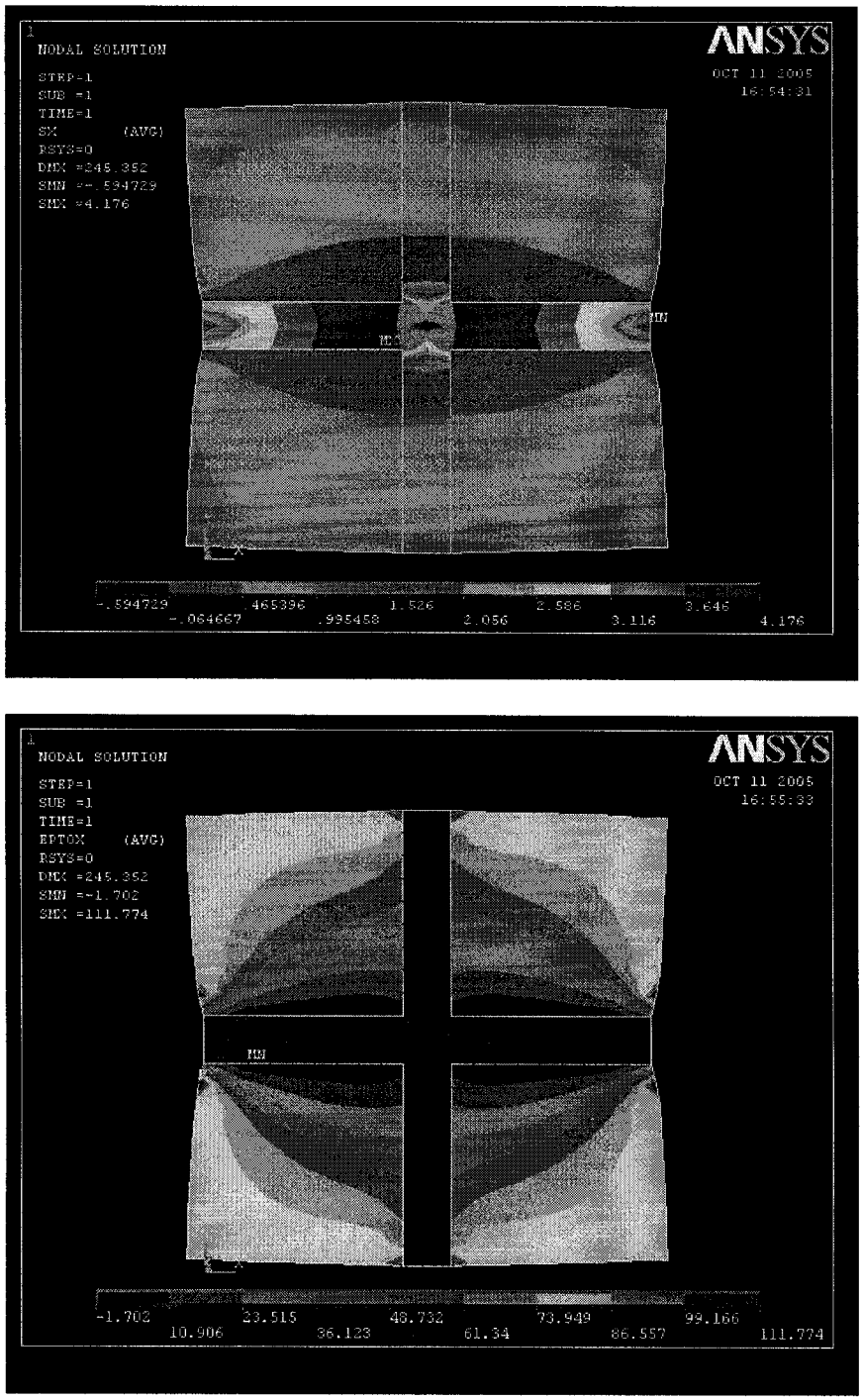

Figure 5. 13 Contour plot of normal stress σ_{xx} for model 6

Figure 5. 14 Contour plot of normal stress σ_{xx} for model 5

5.7.4 Discussion

Results from our finite element models show that there is no significant difference (only 2~5% differences) between the elastic moduli obtained using Model 6 and Model 5 for the volume fraction of 20%. However, stress in the bone tissue is reduced slightly in Model 5 as observed from Figures 5.13 and 5.14 due to rounded corners.

5.8 Effects of bone volume fractions

Volume fraction, the basic parameter in describing trabecular microstructure, can easily be calculated from three-dimensional reconstructions of micro-CT images. Because measurement of volume fraction is of primary importance for the evaluation of trabecular microstructure, several volume fractions of bone have been examined in this section. Two volume fraction ranges are used in this thesis. One is 5~20% (lower density area); another is 30~40% (high density area).

When modeling using 2D FEM models, the following assumptions are made.

- Unit cell δ_0 and $2\delta_0$ for lower and higher density areas
- Bone structure is represented as a cellular network with square cross sections
- Bone volume fraction of 5% - 20% and 30~40%
- Bone Young's modulus of 13.0 GPa
- Bone marrow Young's modulus of 13.0 Pa
- The Poisson's ratio for both phases is 0.3

5.8.1 Lower volume fractions

The stiffness matrix is computed and the C_{1111}, C_{1122}, and C_{1212} components are discussed in this section. The model ($2\delta_0$) used for determining the changes of moduli by varying the bone volume fractions is shown below.

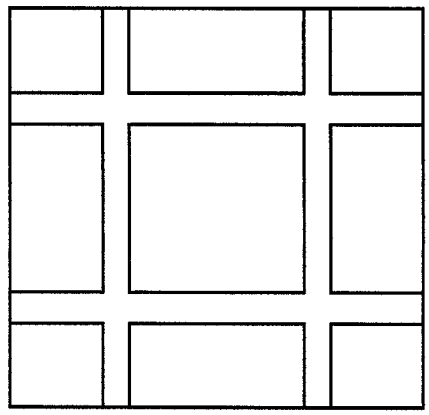

20%

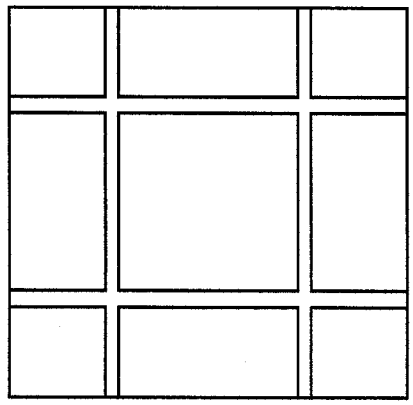

10%

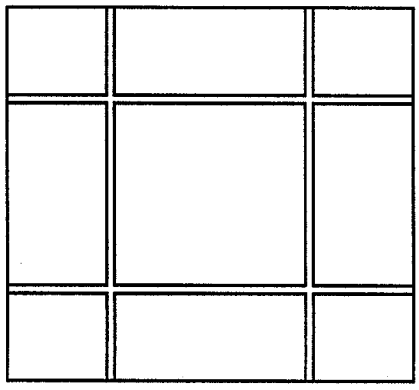

5%

Figure 5. 15 Changes of bone volume fraction from 5% to 20%

1. Uniaxial extension

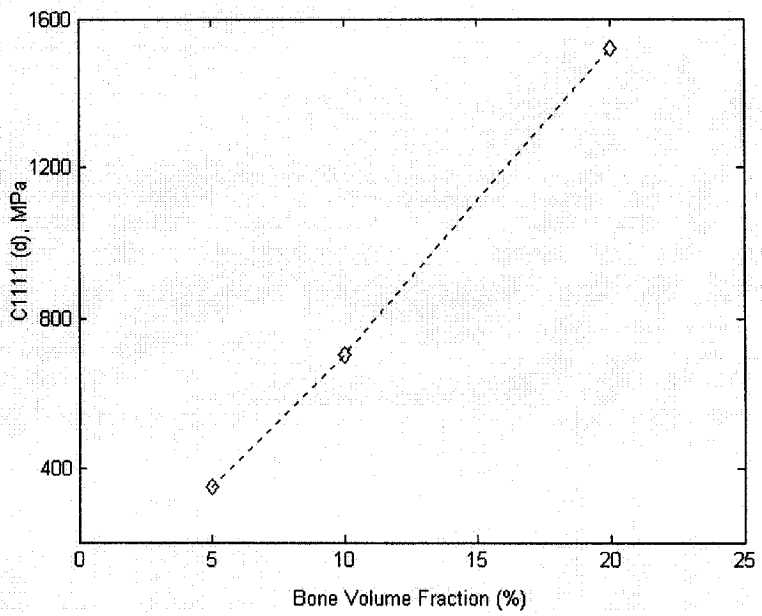

Figure 5. 16 C^d_{1111} as a function of bone volume fractions

2. Biaxial extension

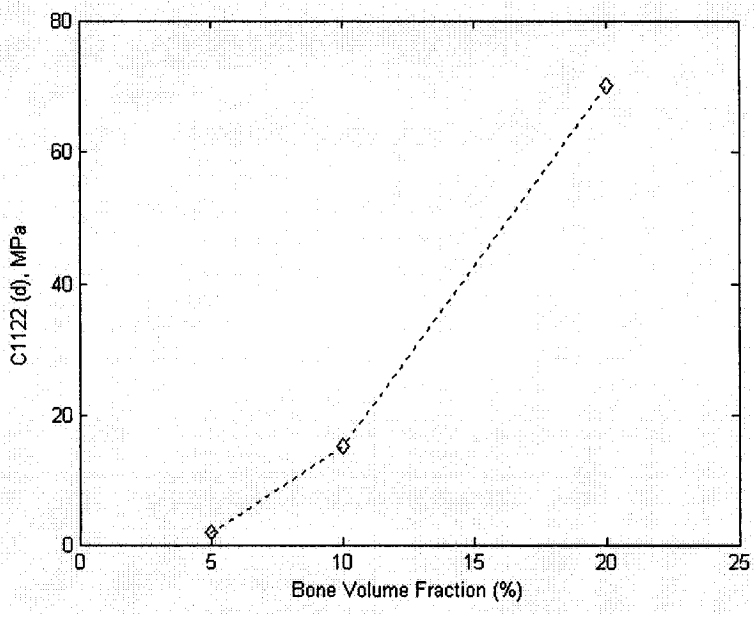

Figure 5. 17 C^d_{1122} as a function of bone volume fractions

3. Simple shear strain

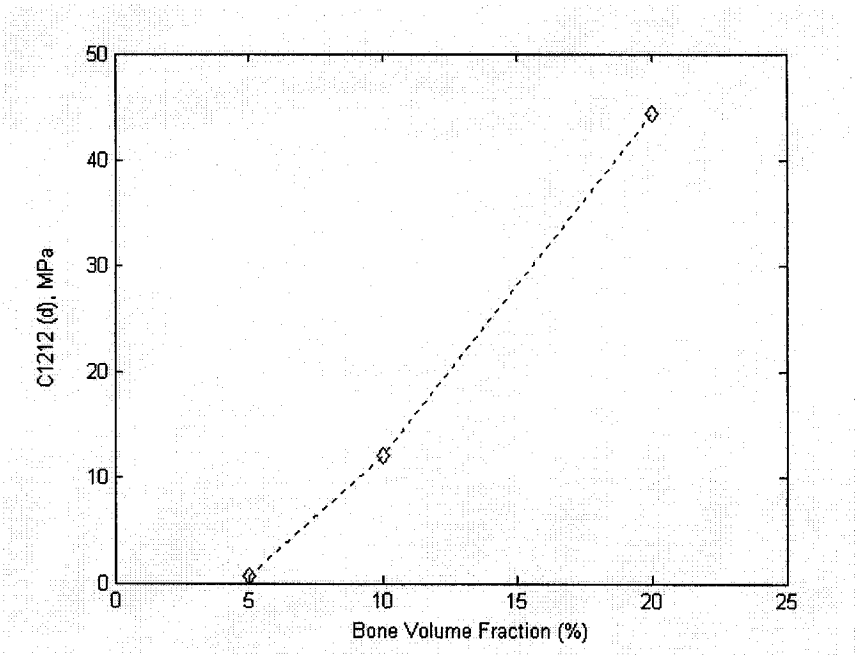

Figure 5. 18 C^d_{1212} as a function of bone volume fractions

4. Uniaxial tension

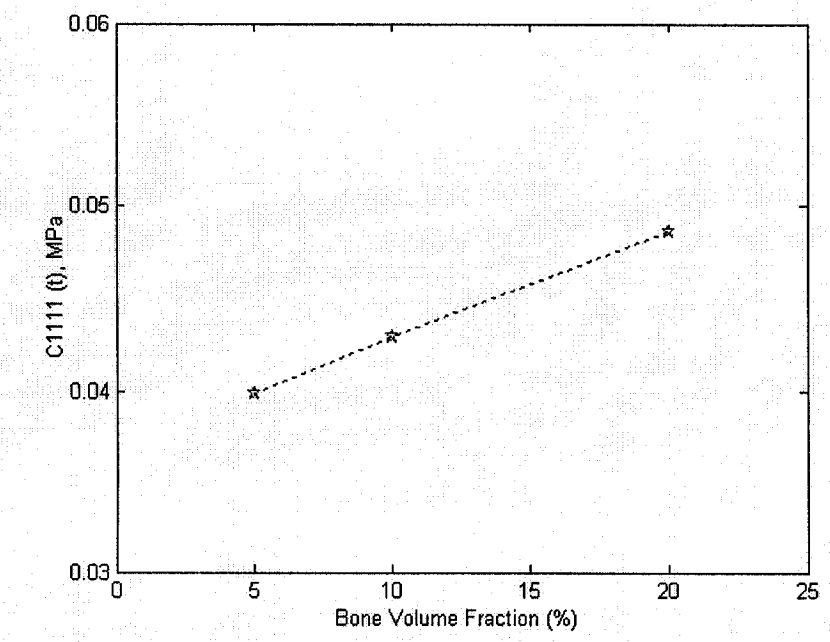

Figure 5. 19 C^t_{1111} as a function of bone volume fractions

5. Biaxial tension

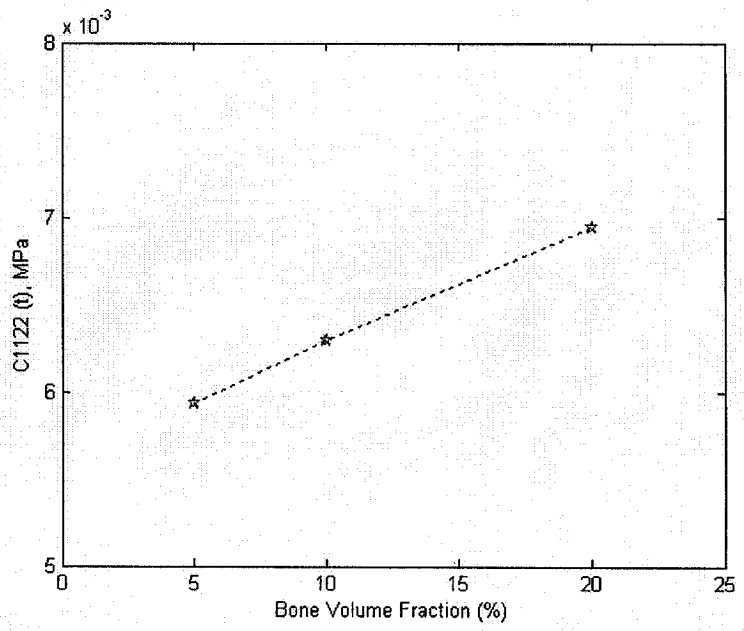

Figure 5. 20 C^t_{1122} as a function of bone volume fractions

6. Simple shear traction

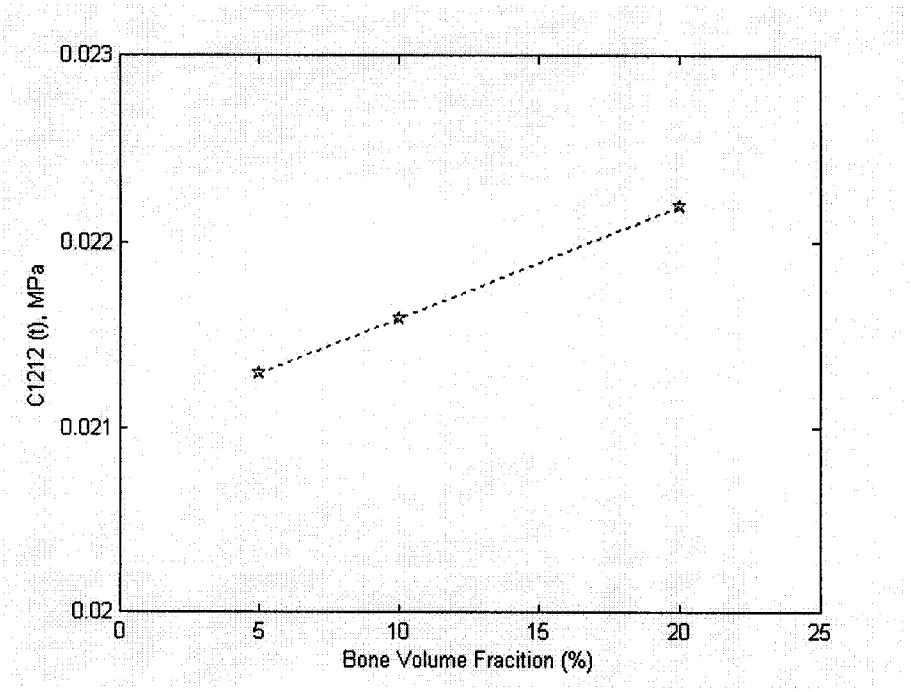

Figure 5. 21 C^t_{1212} as a function of bone volume fractions

7. Stiffness matrix

The stiffness tensors obtained directly from the displacement boundary conditions are given in their full form for the periodic model with bone volume fractions of 5%, 10% and 20%. (unit: MPa)

$$C_{ijkl}^{(20)d} = \begin{bmatrix} 1.52E+03 & 7.00E+01 & 0 \\ 7.00E+01 & 1.52E+03 & 0 \\ 0 & 0 & 4.44E+01 \end{bmatrix}$$

$$C_{ijkl}^{(10)d} = \begin{bmatrix} 7.06E+02 & 1.54E+01 & 0 \\ 1.54E+01 & 7.06E+02 & 0 \\ 0 & 0 & 1.20E+01 \end{bmatrix}$$

$$C_{ijkl}^{(5)d} = \begin{bmatrix} 3.48E+02 & 2.00E+00 & 0 \\ 2.00E+00 & 3.48E+02 & 0 \\ 0 & 0 & 5.90E-01 \end{bmatrix}$$

The stiffness tensors obtained directly from the traction boundary conditions are given in their full form for the periodic model with bone volume fractions of 5%, 10% and 20%. (unit: MPa)

$$C_{ijkl}^{(20)t} = \begin{bmatrix} 4.86E-02 & 6.94E-03 & 0 \\ 6.94E-03 & 4.86E-02 & 0 \\ 0 & 0 & 2.22E-02 \end{bmatrix}$$

$$C_{ijkl}^{(10)t} = \begin{bmatrix} 4.29E-02 & 6.29E-03 & 0 \\ 6.29E-03 & 4.29E-02 & 0 \\ 0 & 0 & 2.16E-02 \end{bmatrix}$$

$$C_{ijkl}^{(5)t} = \begin{bmatrix} 3.99E-02 & 5.93E-03 & 0 \\ 5.93E-03 & 3.99E-02 & 0 \\ 0 & 0 & 2.13E-02 \end{bmatrix}$$

8. Analysis

The following observations can be made about the C_{1111}, C_{1122} and C_{1212} stiffness components. These components decrease as the bone volume fraction decreases from 20% to 5%. Furthermore, we found that there are some differences between results from the displacement and traction boundary conditions. The changes in moduli of trabecular bone under displacement boundary conditions are larger than those in moduli under traction boundary conditions; the change of moduli under shear strain is larger than those of moduli under shear traction.

5.8.2 Higher volume fraction

1. Model 1 with 40% volume fraction

Mesh size is 0.264/0.264; sample size is 5x5x0.1 with holes (bone marrow). Data is calculated using $E_b/E_m=10^6$.

E_b/E_m	C^t_{1111}	C^d_{1111}	C^t_{1122}	C^d_{1122}	C^t_{1212}	C^d_{1212}
1.00×10^6	1.27×10^3	3.18×10^3	1.23×10^3	5.90×10^2	76.9	1.12×10^3

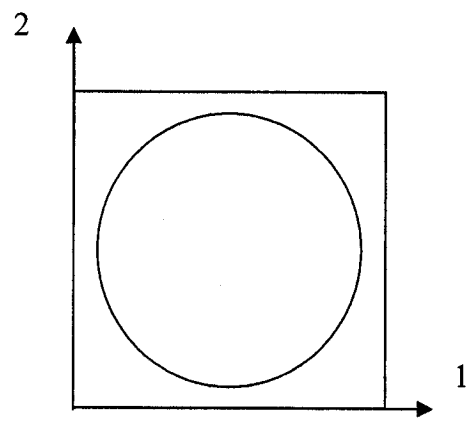

Figure 5. 22 Model 1 with 40% volume fraction

2. Model 2 with 40% volume fraction

Mesh size is 0.264/0.264; sample size is 5x5x0.1 with the stiff phase (bone) in the center. Data is calculated using $E_b/E_m=10^6$.

E_b/E_m	C^t_{1111}	C^d_{1111}	C^t_{1122}	C^d_{1122}	C^t_{1212}	C^d_{1212}
1.00×10^6	2.85×10^{-2}	2.94×10^3	9.60×10^{-3}	3.71×10^2	1.55×10^{-2}	5.08×10^2

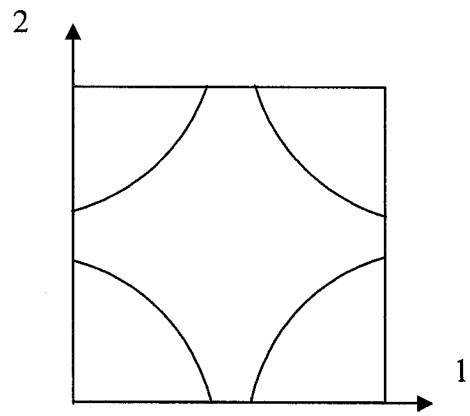

Figure 5. 23 Model 2 with 40% volume fraction

3. Model 3 with 40% volume fraction

Mesh size is 0.264/0.264; sample size is 5x5x0.1. Data is calculated using $E_b/E_m=10^6$.

E_b/E_m	C^t_{1111}	C^d_{1111}	C^t_{1122}	C^d_{1122}	C^t_{1212}	C^d_{1212}
1.00×10^6	3.23×10^{-2}	3.28×10^3	9.10×10^{-3}	3.90×10^2	1.84×10^{-2}	6.08×10^2

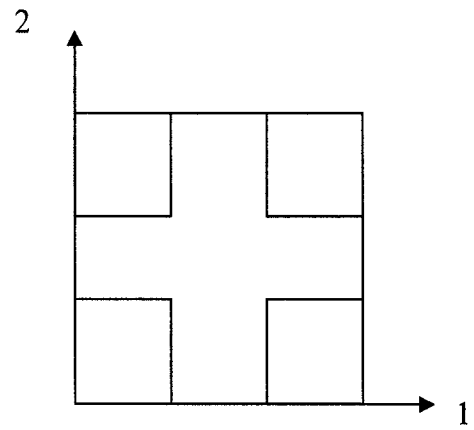

Figure 5. 24 Model 3 with 40% volume fraction

5.8.3 Discussion

Data is calculated using $E_b/E_m=10^6$.

Model	V_f of Bone (%)	C^d_{1111}	C^t_{1111}	$C^d_{1111} - C^t_{1111}$
1	40	1.27×10^3	3.18×10^3	1.91×10^3
2	40	2.85×10^{-2}	2.94×10^3	2.94×10^3
3	40	3.23×10^{-2}	3.28×10^3	3.28×10^3
4	20	46.9	1.42×10^3	1.37×10^3
5	20	2.39×10^{-2}	1.46×10^3	1.46×10^3
6	20	2.45×10^{-2}	1.53×10^3	1.53×10^3

Table 5. 32 Bounds C_{1111} of all models

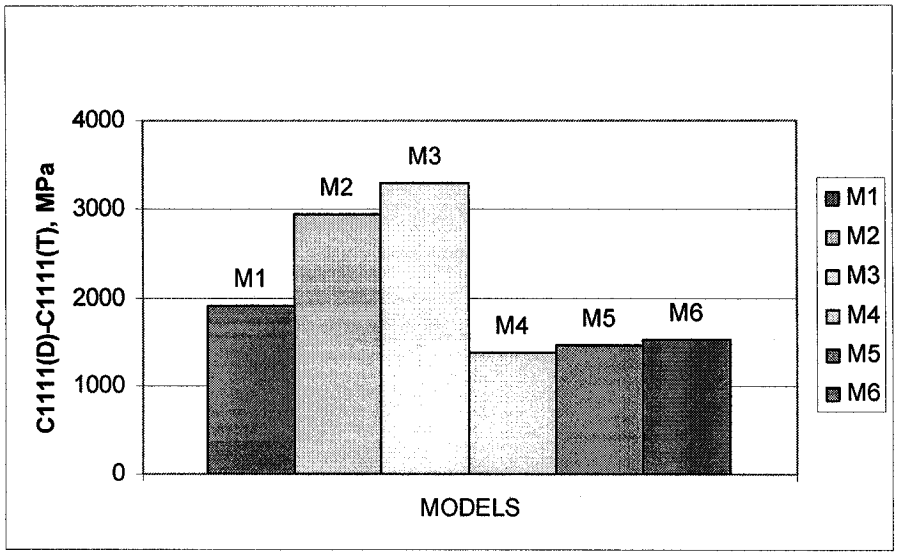

Figure 5. 25 Difference of upper and lower bounds C_{1111} of all models

1. The models with higher volume fraction (40%) of bone have higher stiffness C_{1111} than those with lower bone volume fraction (20%), as expected.
2. The models with stiff outer edges (M1 and M4) have the closest bounds.
3. The stiffness components C_{1111} of the models with rounded corners (M2 and M5) are little lower than those with sharp corners. This is due to the fact that stresses are locally lower near rounded corners.

Model	V_f of Bone (%)	C^d_{1212}	C^t_{1212}	C^d_{1212}-C^t_{1212}
M1	40	1.12×10^3	76.9	1.04×10^3
M2	40	5.08×10^2	1.55×10^{-2}	5.08×10^2
M3	40	6.08×10^2	1.84×10^{-2}	6.08×10^2
M4	20	1.18×10^2	2.70	1.18×10^2
M5	20	82.0	1.33×10^{-2}	82.0
M6	20	78.0	1.35×10^{-2}	78.0

Table 5. 33 Bounds C_{1212} of all models

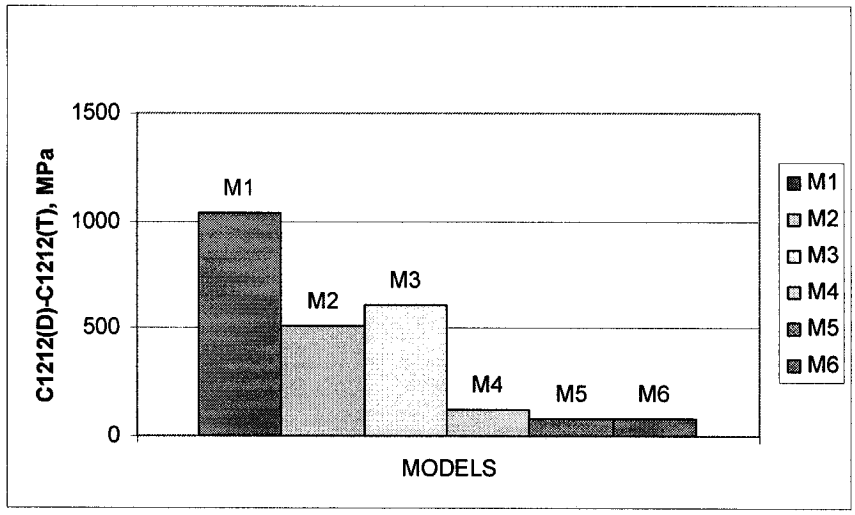

Figure 5. 26 Difference of upper and lower bounds C_{1212} of all models

4. The stiffness components C_{1111} and C_{1212} of the higher bone volume fraction are higher than those for lower bone volume fraction, as expected.
5. The effects of corner on C_{1212} are not as large as those to C_{1111}.
6. The models with higher bone volume fraction have wider bounds on C_{1212}.

5.9 The Hill condition, average stress, and average strain

So far we discussed apparent elastic stiffness components as a function of $\frac{E_b}{E_m}$, V_f, and geometry. Now we focus on more fundament issues such as the satisfactions of the average stress theorem, average strain theorem, and the Hill condition. Table 5.34 shows the component volume averages for uniform boundary conditions.

Applied BC's	Displacement boundary conditions					
	$\varepsilon^o_{xx} = 0.01$		$\varepsilon^o_{xx} = \varepsilon^o_{yy} = 0.01$		$\varepsilon^o_{xy} = 0.01$	
	$\bar{\varepsilon}_{ij}$	$\bar{\sigma}_{ij}$	$\bar{\varepsilon}_{ij}$	$\bar{\sigma}_{ij}$	$\bar{\varepsilon}_{ij}$	$\bar{\sigma}_{ij}$
XX	0.01	14.6	0.01	15.6	-6.67×10^{-8}	-5.96×10^{-4}
YY	1.88×10^{-7}	0.992	0.01	15.6	4.85×10^{-8}	-5.55×10^{-4}
XY	-1.43×10^{-7}	-7.17×10^{-4}	-1.16×10^{-7}	1.40×10^{-3}	0.01	0.816
$\bar{\sigma}_{ij}\bar{\varepsilon}_{ij}$	0.146		0.312		8.16×10^{-3}	
2W	0.146		0.311		8.20×10^{-3}	
Applied BC's	Traction boundary conditions					
	$\sigma^o_{xx} = 1$		$\sigma^o_{xx} = \sigma^o_{yy} = 1$		$\sigma^o_{xy} = 1$	
XX	45.4	1.00	32.6	1.00	-4.53×10^{-4}	-4.27×10^{-4}
YY	-12.8	2.15×10^{-5}	32.6	1.00	2.61×10^{-4}	-4.75×10^{-4}
XY	-3.53×10^{-4}	-8.29×10^{-6}	-2.39×10^{-4}	-1.81×10^{-5}	74.0	1.00
$\bar{\sigma}_{ij}\bar{\varepsilon}_{ij}$	45.4		65.2		74.0	
2W	45.4		65.2		75.1	

Table 5. 34 Average stress/strain and the Hill conditions for uniform boundary conditions

In contrast, if we apply a nonuniform boundary condition, for example, bending, the average stress, average strain, and the Hill condition will not be satisfied. Table 5.35 gives the component volume averages for the nonuniform boundary conditions.

Applied BC's	$\kappa_{xy}^{o} = 1$	
	$\overline{\varepsilon_{ij}}$	$\overline{\sigma_{ij}}$
XX	0.91	9.91×10^{-4}
YY	-3.24×10^{-9}	-1.25×10^{-5}
XY	-6.7110^{-10}	2.33×10^{-5}
$\overline{\sigma_{ij}}\,\overline{\varepsilon_{ij}}$	9.02×10^{-4}	
2W	4.44×10^{3}	
Applied BC's	$\mu_{xy}^{0} = 0.01$	
XX	2.50×10^{-2}	3.53×10^{7}
YY	2.20×10^{-3}	1.40×10^{6}
XY	7.90×10^{-3}	7.44×10^{5}
$\overline{\sigma_{ij}}\,\overline{\varepsilon_{ij}}$	8.91×10^{5}	
2W	9.88×10^{5}	

Table 5. 35 The Hill condition not satisfied for non-uniform boundary conditions

Also, periodic and mixed boundary conditions calculated and the results show that the Hill condition and the average strain theorem are satisfied for periodic and mixed boundary conditions. Table 5.36 and Table 5.37 give the component volume averages for the periodic and mixed boundary conditions.

Applied BC's	Periodic boundary conditions					
	$\varepsilon^o_{xx} = 0.01$		$\varepsilon^o_{xx} = \varepsilon^o_{yy} = 0.01$		$\varepsilon^o_{xy} = 0.01$	
	$\bar{\varepsilon}_{ij}$	$\bar{\sigma}_{ij}$	$\bar{\varepsilon}_{ij}$	$\bar{\sigma}_{ij}$	$\bar{\varepsilon}_{ij}$	$\bar{\sigma}_{ij}$
XX	0.01	14	0.01	14.6	-5.33 $\times 10^{-8}$	-5.72 $\times 10^{-4}$
YY	1.98 $\times 10^{-7}$	0.962	0.01	14.6	4.05 $\times 10^{-8}$	-5.23 $\times 10^{-4}$
XY	-1.38 $\times 10^{-7}$	-8.35 $\times 10^{-4}$	-1.09 $\times 10^{-7}$	1.34 $\times 10^{-3}$	0.01	8.70 $\times 10^{-2}$
$\bar{\sigma}_{ij}\bar{\varepsilon}_{ij}$	0.14		0.292		8.70×10^{-4}	
2W	0.14		0.292		8.72×10^{-4}	

Table 5. 36 Average stress/strain and the Hill conditions for periodic boundary conditions

Applied BC's	Mixed boundary conditions					
	$\varepsilon^o_{xx} = 0.01$, $t_{ij}=0$		$\varepsilon^o_{xx} = \varepsilon^o_{yy} = 0.01$, $t_{ij}=0$		$\varepsilon^o_{xy} = 0.01$, $t_{ij}=0$	
	$\bar{\varepsilon}_{ij}$	$\bar{\sigma}_{ij}$	$\bar{\varepsilon}_{ij}$	$\bar{\sigma}_{ij}$	$\bar{\varepsilon}_{ij}$	$\bar{\sigma}_{ij}$
XX	0.01	14.3	0.01	15	-5.57 $\times 10^{-8}$	-5.63 $\times 10^{-4}$
YY	2.27 $\times 10^{-7}$	0.845	0.01	15	4.29 $\times 10^{-8}$	-5.17 $\times 10^{-4}$
XY	-1.67 $\times 10^{-7}$	-9.66 $\times 10^{-4}$	-1.37 $\times 10^{-7}$	1.18 $\times 10^{-3}$	0.01	8.70 $\times 10^{-2}$
$\bar{\sigma}_{ij}\bar{\varepsilon}_{ij}$	0.143		0.3		8.70×10^{-4}	
2W	0.143		0.3		8.72×10^{-4}	

Table 5. 37 Average stress/strain and the Hill conditions for mixed boundary conditions

5.10 Comparison of 2D and 3D models with the same bone volume fraction

Although the full understanding of the mechanical behavior of a composite material requires a three-dimensional (3D) analysis, it is more difficult to numerically analyze due to larger computational resources required. 3D geometries can be approximated by planar problems: planar stress and strain analyses.

In this section we introduce the 3D model and compare the results with those obtained using our 2D model with the same bone volume fraction (20%), same mechanical properties of constituents and similar structural features (Fig. 5.27).

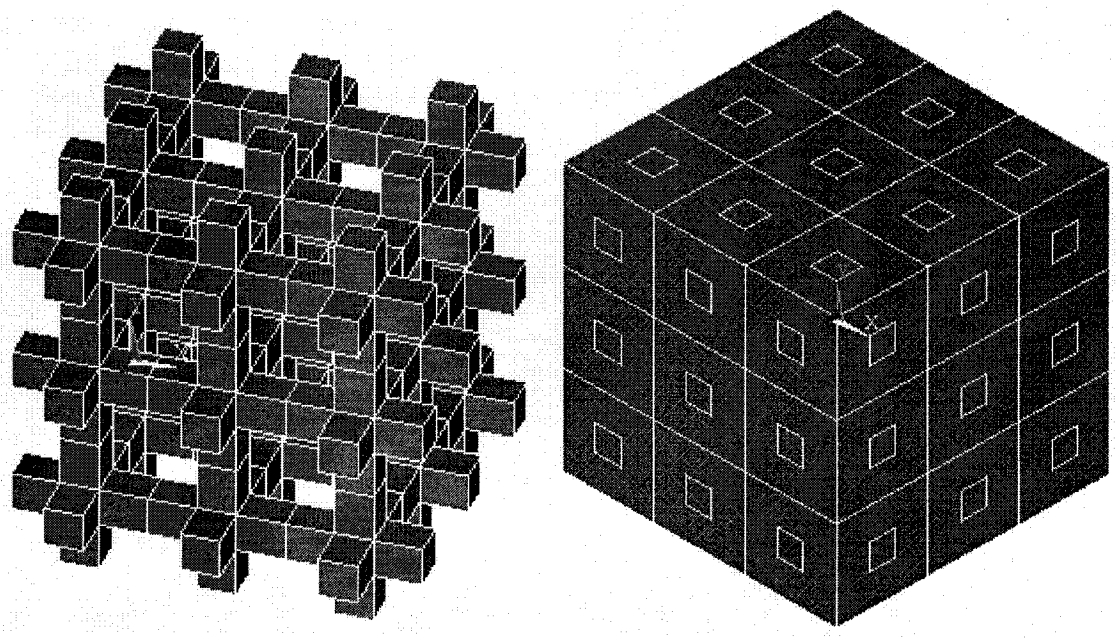

Figure 5. 27 The 3D model with δ_o = 3 unit cells with 20% bone volume fraction

We have also applied the displacement and traction boundary conditions. The results compared with those of 2D model as follows,

Window Size	3D		2D		3D		2D	
	C^t_{1111}	C^d_{1111}	C^t_{1111}	C^d_{1111}	C^t_{1212}	C^d_{1212}	C^t_{1212}	C^d_{1212}
1	2.30×10^{-2}	1.32×10^{3}	2.45×10^{-2}	1.53×10^{3}	9.17×10^{-3}	3.74×10^{2}	1.35×10^{-2}	78
2	5.00×10^{-2}	1.32×10^{3}	4.86×10^{-2}	1.52×10^{3}	1.80×10^{-2}	2.20×10^{2}	2.22×10^{-2}	44.4
3	7.31×10^{-2}	1.31×10^{3}	7.26×10^{-2}	1.50×10^{3}	2.70×10^{-2}	1.72×10^{2}	3.14×10^{-2}	32

Table 5. 38 Comparison of bounds for 2D and 3D models

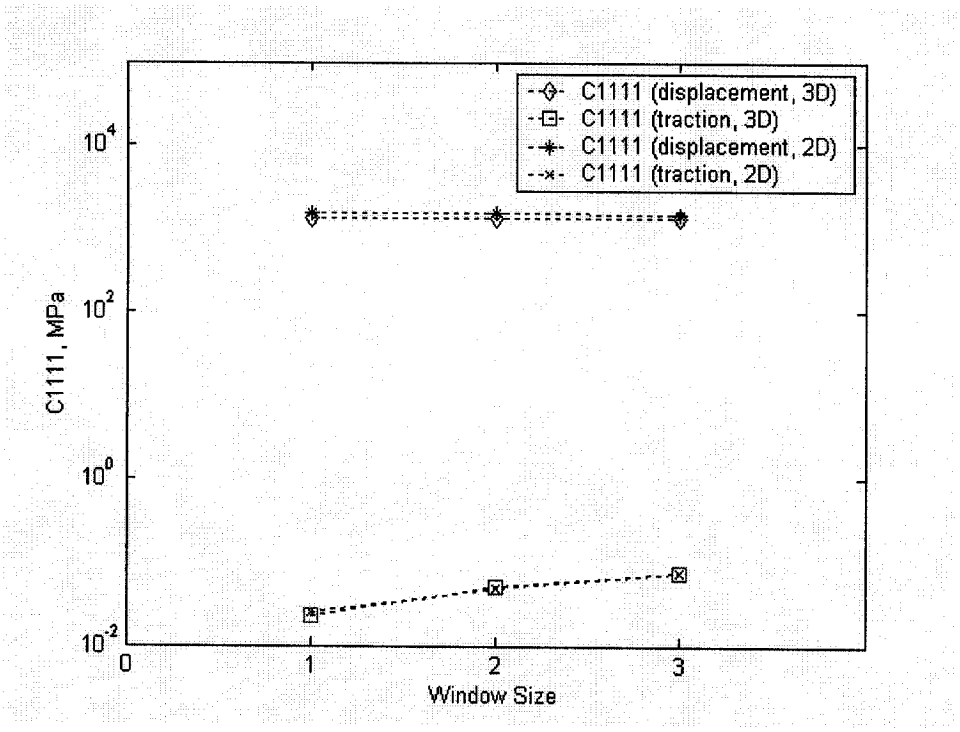

Figure 5. 28 Comparison of bounds C_{1111} between 2D and 3D

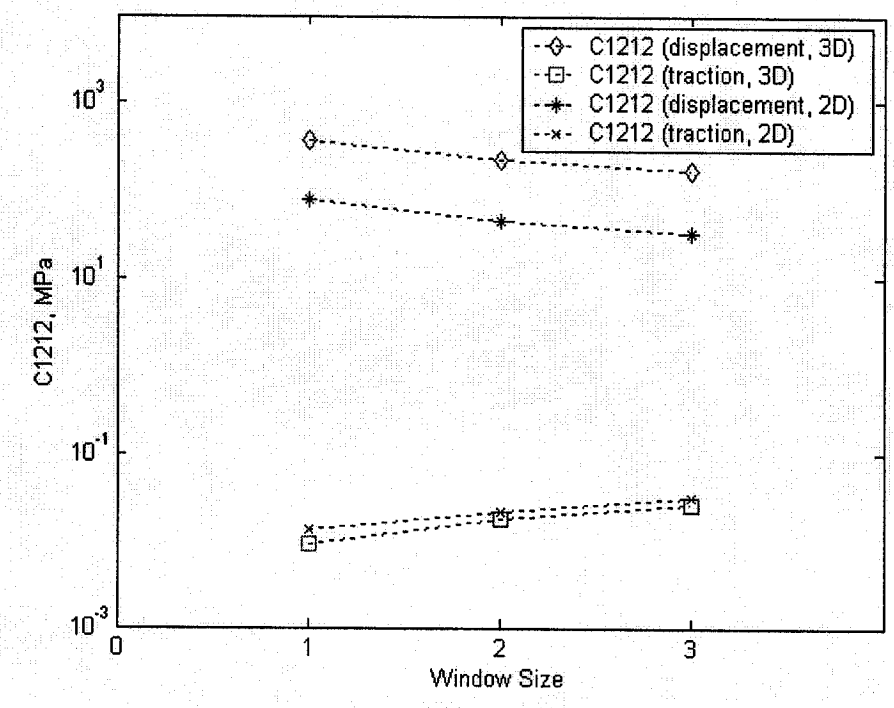

Figure 5. 29 Comparison of bounds C_{1212} between 2D and 3D

From the results obtained above, we can conclude that the analysis of 2D model can represent the one of 3D model because they have same trend by increasing the window size (No. of unit cells), and almost same values for bounds C_{1111} and closer bounds C_{1212} for 2D model. Thus, the 2D model studied in this thesis approximates well the elastic moduli of trabecular bone.

5.11 Periodic model discussion

Effects of mesh size, the first step of analyzing the periodic models, are discussed in section 1. To begin with, same mesh size, different mesh size of bone marrow, and different mesh size of bone tissue were studied to determine which mesh size is used to predict the elastic moduli of trabecular bone using ANSYS. We found that the same mesh size used for bone and bone marrow is more accurate with less element numbers than the models with different mesh sizes for bone tissue and bone marrow. Elastic strain energy is more sensitive to the change of mesh size of bone marrow; on the contrary, it does not change with the change of mesh size of bone. Then, the effects of mesh size on different loads are observed. Elastic strain energy is changing with the same trend under different boundary conditions; however, it is more sensitive to the mesh size under displacement boundary condition, especially under simple shear strain. Relatively crude mesh size (0.264) was picked up to mesh 2D models due to its sufficient accuracy (5%) as compared with a very fine mesh.

Effects of the ratio of moduli of bone tissue and bone marrow were considered in section 2. For displacement bc's, the elastic moduli results asymptote very quickly for lower mismatches and they are independent after the ratio of 1.00E+04. The moduli under traction boundary condition are depended on the changes of the ratio of bone and

marrow in the linear way. Thus, in most of our calculations we chose the ratio of bone and bone marrow as 1.00E+06 to represent the properties of trabecular bone.

Effects of sample window size are shown in section 3. The apparent stiffness components C_{1111} and C_{1212} are becoming closer to each other as window sizes increase. However, the bounds are still wide open when window size goes to 6 and it is impossible to further increase the window size due to the limitation of the version of ANSYS.

Periodic boundary conditions results in section 4 have shown that the moduli under periodic boundary condition are independent on the sample window size, as expected. Thus, periodic boundary conditions give the effective properties of trabecular bone, as expected.

Mixed boundary conditions results in Section 5 have demonstrated that the moduli under mixed boundary condition are also independent on the sample window size like periodic boundary conditions. The moduli under mixed boundary conditions are very close to those obtained using periodic boundary conditions.

The comparisons of two unit cells chosen from same model are given in Section 6. The Unit Cell 2 has shown the same trend as the Unit Cell 1 under displacement boundary conditions. But, it gives the difference when compared with the Unit Cell1 under the traction boundary conditions. After the ratio of 10, it follows an asymptotic line not in linear way like unit cell 1. Also, the unit cell 2 gives closer bounds than the unit cell 1 because of its stiff edges.

The effects of sharp-corner of trabecular bone are examined in Section 7. Results from our finite element models show that there is no significant difference (only 2~5% differences) between models with rounded versus sharp corners for the volume fraction

of 20%. As a result, we conclude that the shape of corners has a small effect on the moduli of trabecular bone. However, the stress of bone without sharp corners is reduced as observed from Figure 5.14 and Figure 5.15.

The effects of bone volume fractions in section 8 have shown that C_{1111}, C_{1122} and C_{1212} stiffness components go down with the changes of bone volume fractions from higher volume fraction to lower volume fraction in the linear way. Thus, the moduli of trabecular bone are affected by varying the bone volume fractions. Some special geometries are tested in this section.

The Hill condition, average stress, and average strain are shown (Table 5.33) to hold for the three uniform loadings involving displacement and traction boundary conditions. The results have shown that average stress, average strain, and the Hill condition are satisfied for uniform boundary conditions. Also, it should be noted that the traction shear boundary condition has a larger Hill Condition discrepancy because the model must be constrained from rigid body motion by applying displacement boundary conditions to several nodes. Conversely, Table 5.34 gives an example of nonuniform boundary conditions to show average stress, average strain, and the Hill condition are not satisfied for nonuniform boundary conditions.

The comparisons of 2D and 3D are investigated in Section 10 by applying displacement and traction boundary conditions. We found that the 2D model can represent 3D model to predict the elastic moduli of trabecular bone because of the close results for 2D and 3D cases.

CHAPTER 6

CONCLUSIONS

The purpose of this research was to examine the effects of scale and boundary conditions on the moduli of trabecular bone using numerical methods, specifically the finite element software package ANSYS Version 8.1. The analysis of the moduli of trabecular bone was performed using numerical simulations based on the concepts of effective and apparent properties. The relevant mechanical background was presented in Chapter 2, and the specific methodology employed in this thesis was presented in Chapter 4 and Chapter 5. During the course of studying the moduli of trabecular bone, the apparent and effective properties of trabecular bone were evaluated using the theoretical framework presented in Chapters 2 and 4. In Chapter 5 results to were presented and discussed. The effected of different factors on elastic moduli was discussed in this Chapter. This thesis also briefly summarizes the theoretical background on periodic models and methodology for obtaining the effective properties of trabecular bone in the 2D models, as well as 3D model (Chapters 2 and 3).

As three-dimensional materials are harder to study numerically a simplification of the fully three-dimensional case was proposed involving planar elasticity. We find that our 2D and 3D results are very close to each other. This analysis be found in Chapter 5.

In this research, FEM was used to examine moduli of trabecular bone, and the results of this work were presented in Chapter 5. Several models of different bone structures were studied in comparison with the effects of scale and boundary conditions. These models were modeled by the crossing rods or struts with or without sharp corners,

open or closed cells, and center square or spherical models. Techniques for implementing the displacement, traction, mixed, and periodic boundary conditions were also presented.

The moduli of trabecular bone were fully characterized using both displacement and traction boundary conditions. The elastic bounds for the classical elasticity tensor were found for several material window sizes and compared to the effective properties obtained by using periodic boundary conditions. These results calculated using periodic boundary conditions were compared to the elastic modulus applied by the mixed boundary conditions. The closed cell was found to have the closer bounds on the apparent stiffness than the open cell. A large difference for determining the apparent modulus of trabecular bone by changing its volume fraction was also found. The effect of sharp corner had shown that it seems no significantly different between models with or without sharp corners; however, the stress of bone, to a certain extent, is reduced. Finally, the comparison of 2D and 3D models was presented.

The Hill condition, and average stress and average strain theorems were satisfied for uniform boundary conditions within computational error as well as periodic and mixed boundary conditions. Conversely, the Hill condition was not satisfied for nonuniform loadings. Meanwhile, for satisfying the Hill condition, the bone marrow had to have a certain amount of modulus to represent voids for uniform boundary conditions. The uniform displacement boundary condition results were not affected by the mechanical properties of bone marrow due to the fact that the elastic strain energy resided solely in the stiff phase. The uniform traction boundary condition results were affected by the mechanical properties of bone marrow and they were necessary in calculating the compliance terms because the applied traction produced a small non-negligible amount of

elastic strain energy when compared to the even smaller elastic strain energy residing in the stiff phase.

Finally, we can conclude the following

1. The apparent elastic moduli of trabecular are affected by the window sizes, the boundary conditions, the different unit cell choices, and the mesh sizes.

- Effects of mesh size

  The moduli are not changing after certain mesh size under different loads.

- Effects of the boundary conditions

  The moduli under traction boundary conditions are depended on the changes of bone and bone marrow in the linear way. For displacement boundary conditions, they are independent after the ratio of 1.00E+04.

- Effects of the window sizes

  Although the apparent moduli are still wide open in 6 unit cells case (δ_o = 6), the trend that they will go close to each other is clear.

- Effects of the different unit cells

  The unit cell 2 gives the closer bounds than the unit cell 1 because of its stiff edges.

2. The moduli under periodic boundary condition are independent on the sample window sizes.

- They are more close to the moduli under uniform extension boundary conditions for cellular network. On the other hand, they are more close to the moduli under shear traction boundary conditions.

- The moduli under mixed boundary conditions are very close to those of periodic boundary conditions.

3. Effects of sharp-corner
   - There is no significant difference (only 2~5% differences) between Model 1 and Model 2.
   - However, the stress in bone is reduced when structure had rounded corners.

4. Effects of bone volume fractions
   - The stiffness C decreases with the changes of bone volume fractions from 20% to 5% in a linear way.
   - The moduli of trabecular bone are affected by varying the bone volume fractions.

5. Comparison of 2D and 3D models
   - The analysis of 2D model can represent those of 3D model because they have same trend by increasing the window size (unit cell no.), and almost same amount for bounds C_{1111} and closer bounds C_{1212} for 2D model; as a result, it is feasible for the 2D model in this thesis to predict the elastic moduli of trabecular bone instead of the 3D model.

Future work should be focused on several aspects as follows. First, we will be interested in the models without fill (bone marrow) like foams. Then, the non uniform loadings and mechanical properties of trabecular bone will be studied. For example, to account for the bone soft tissue including fluids, bone poroelasticity could be considered. Also, the random periodic models have to be studied to account for the bone's complex

structure. Finally, it would be very helpful for clinical applications if we would accumulate data about the structure-property relations in trabecular bone.

In conclusion, the numerical modeling of trabecular bone is a useful tool to predict the apparent and effective properties of trabecular bone, and it makes it possible to better understand the results from the experiments. As we know, the pure displacement and traction conditions are very difficult to load in the laboratory, so the investigation of boundary condition effects can be done most efficiently numerically. There results can give insight to researchers involved in computational modeling of materials and in experimental testing of mechanical properties of bone and other cellular materials.

The challenges in testing bone (and other cellular materials) involve the fact that we may not have a sufficient amount of bone tissue to use for testing, because only a limited amount is available in skeleton and its properties are changing spatially. If the specimen is smaller than the RVE, the results from experimental testing will depend on size of the specimen and applied boundary conditions and will represent apparent, not effective, properties. The present study addresses the issue of the size of the specimen and the nature of boundary conditions to be applied so the measured or calculated results give effective properties.

REFERENCES

Aboudi, J., 1991. Mechanics of Composite Materials – A Unified Micromechanical Approach, Elsevier.

Adachi, T., Tomita, Y. and Tanaka, M., 1998. " Computational Simulation of Deformation Behavior of 2D-Lattice Continuum", Int. J. Mech. Sci. 40, 857-866.

ANSYS, Version 8.1, ANSYS Inc., Canonsburg, PA USA.

Ashby, M. F., 1983. "The mechanical properties of cellular solids", Metallurgical Transactions A 14A, 1755-1769.

Ashman, Richard B. and Rho, Jae Young, 1988. "Elastic modulus of trabecular bone material", J. Biomechanics 21, 177-181.

ASBMR (American Society for Bone and Mineral Research), 2001. http://depts.washington.edu/bonebio/bonAbout/structure.html.

Beaupre, G. S. and Hayes, W. C., 1985. "Finite element analysis of a three-dimensional open-celled model for trabecular bone", J. Biomechanical Eng. 107, 249-256.

Bourne, Benjamin C., van der Meulen, Marjolein C.H., 2004. "Finite element models predict cancellous apparent modulus when tissue modulus is scaled from specimen CT-attenuation", J. Biomechanics 37, 613–621.

Bouyge, F., 2000. "A multiscale model of cancellous bone", M.S. Thesis, Georgia Institute of Technology.

Bouyge, F., Jasiuk, I., and Ostoja-Starzewski, M., 2001. "A micromechanically based couple-stress model of an elastic two-phase composite", Inter. J. Solids and Struc. 38, 1721-1735.

Carter, D.R. and Hayes, W.C., 1977. "The compressive behavior of bone as a two-phase porous structure", J. Bone Jt Surg. 59A, 954-962.

Christensen, R. M., 1986. "Mechanics of Low Density Materials", J. Mech. Phys. Solids 34, 563-578.

Ding, M., Odgaard, A., and Hvid, I., 1999. "Accuracy of cancellous bone volume fraction measured by micro-CT scanning", J. Biomechanics 32, 323-326.

Drugan, WJ, and Willis, JR, "A Micromechanics-Based Nonlocal Constitutive Equation and Estimates of Representative Volume Element Size for Elastic Composites", Journal of the Mechanics and Physics of Solids, Vol. 44, pp. 497-524, 1996.

Ford, C. and Gibson, L. J., 1998. "Uniaxial strength asymmetry in cellular materials: an analytical model", Int. J. Mech. Sci. 40, 521-531.

Fyhrie, D. P.; Kimura, J. H., 1999. "Cancellous bone biomechanics", J. Biomechanics 32, 1139-48.

Gibson, L. J., 1985. "The mechanical behaviour of cancellous bone", J. Biomechanics 18, 317-328.

Gibson, L.J. and Ashby, M.F.,1988. Cellular Solids Structure and Properties. Pergamon Press, Oxford, England.

Guo, X-D. E., McMahon, T. A., Keaveny, T. M., Hayes, W. C., and Gibson, L. J., 1994, "Finite element modeling of damage accumulation in trabecular bone under cyclic loading", J. Biomechanics 27, 145-155.

Guo, X. E., and Kim, C. H., 1999. "Effects of age-related bone loss: a 3D microstructural simulation", Proc. 1999 Bioengineering Conference ASME BED-Vol. 42, 327-328.

Harrigan, Timothy P., Jasty, Murali, Mann, Robert W. and Harris, William H., 1988. "Limitations of the continuum assumption in cancellous bone", J. Biomechanics 21, 269-275.

Hashin Z. 1964. "The Elastic Moduli of Heterogeneous Materials" J. Applied Mechanics, 29, 143-150.

Hill, R., 1963. "Elastic Properties of Reinforced Solids: Some Theoretical Principles", J. Mech. Phy. Solids, 11, 357-372.

Hollister, S. J., Brennan, J.M., and Kikuchi, N., 1994. "A homogenization sampling procedure for calculating trabecular bone effective stiffness and tissue level stress", J. Biomechanics 27, 433-444.

Hollister, S.J., Fyhrie, D. P., Jepsen, K. J. and Goldstein, S. A., 1991. "Application of homogenization theory to the study of trabecular bone mechanics", J. Biomechanics 24, 825-839.

Huet, C., 1990. "Application of Variational Concepts to Size Effects in Elastic Heterogeneous Bodies", J. Mech. and Phy. Solids 38, 813-841.

Jacobs, C. R., Davis, B.R., Rieger, C.J., Francis, J.J., Saad, M., Fyhrie, D.P., 1999. "The impact of boundary conditions and mesh size on the accuracy of cancellous bone tissue modulus determination using large-scale finite-element modeling", J. Biomechanics 32. 1159-1164.

Jian, Tan, Saltzman, W. Mark, 2004. "Biomaterials with hierarchically defined micro- and nanoscale structure", J. Biomaterials, 25, 3593-3601.

Jiang, M., 2000. "Scale and boundary condition effects in fiber-reinforced composites", Ph.D. Thesis, Georgia Institute of Technology.

Jiang, M., Jasiuk, I., and Ostoja-Starzewski, M., 2002. "Apparent elastic and elastoplastic behavior of periodic composites", Inter. J. Solids Struct. 39, 199-212.

Kuhn, J.L., Goldstein, S.A., Feldkamp, L.A., Goulet, R.W., and Jesion, F., 1990. "Evaluation of a microcomputed tomography system to study trabecular bone structure", J.Ortho. Res. 8, 833-842.

Najarian, S., Biomechanics,1995. Notes of Introduction to Biomedical Engineering

Ostoja-Starzewski, M., Boccara, S., and Jasiuk, I., 1999. "Couple-stress moduli and characteristic length of a two-phase composite", Mech. Res. Comm. 26, 387-396.

Pecullan, S, Gibiansky, LV, and Torquato, S, 1999. "Scale Effects on the Elastic Behavior of Periodic and Hierarchical Two-Dimensional Composites", Journal of Mechanics and Physics of Solids, Vol. 47, pp. 1509-1542.

Reuss, A., 1929. 'Berechnung der Fließgrenze Mischkristallen auf Grung der Plastizitätsbedingung für Einkristalle", ZAMM 9, 49-58.

Pindera, Marek-Jerzy, Aboudi, Jacob, Arnold, Steven M., 1995. "Limitations of the uncoupled, RVE-based micromechanical approach in the analysis of functionally graded composites", J. Mechanics of Materials 20, 77-94.

Pugh, J. W., Rose, R. M. and Radin, E. L., 1973. "A structural model for the mechanical behaviour of bone" J. Biomechanics 6, 657-670.

Rho, Jae Young, Ashman, Richard B. and Turner, Charles H., 1993. "Young's modulus of trabecular and cortical bone material: Ultrasonic and microtensile measurements", J. Biomechanics 26, 111-119

Silva, M. J., and Gibson, L. J., 1997."Modeling the mechanical behavior of vertebral trabecular bone: effects of age-related changes in microstructure", Bone 21, 191-199.

Silva, M. J., Hayes, W. C. and Gibson, L. J., 1995. "The effects of non-periodic microstructure on the elastic properties of two-dimensional cellular solids", Int. J. Mech. Sci. 37, 1161-1177.

Stone, J. L., Beaupre, G. S. and Hayes, W. C., 1983. "Multiaxial characteristics of trabecular bone", J. Biomechanics 16, 743-752.

Turner, C.H. and Burr, D.B., 1993. "Basic biomechanical measurements of bone: a tutorial", Bone 14, 595-608.

Ulrich, D., Rietbergen, B., Weinands, H., and Rüegsegger, P., 1998. "Finite element analysis of trabecular bone structure: a comparison of image-based meshing techniques", J. Biomechanics 31, 1187-1192.

Van Rietbergen, B., Odgaard, A., Kabel, J., and Huiskes, R., 1996. "Direct mechanics assessment of elastic symmetries and properties of trabecular bone architecture", J. Biomechanics 29, 1653-1657.

Van Rietbergen, B., Weinanas, H., Huiskes, R., and Odgaard, A., 1995. "A new method to determine trabecular bone elastic properties and loading using micromechanical finite-element models", J. Biomechanics 28, 68-81.

Voigt, W, 1910. "Lehrbuch der Kristallphysik," BG Teubner.

Wagner, H. D. and Weiner, S., 1992. "On the relationship between the microstructure of bone and its mechanical stiffness", J. Biomechanics 25, 1311-1320.

Werner, H. J., Matin, H., Behrend, D., Schmitz, K. P., and Schober, H. C., 1996. "The loss of stiffness as osteoporosis progresses", Med. Eng. Phys. 18, 601-606.

Zysset, Philippe K., Guo, X. Edward, Hoffler, C. Edward, Moore, Kristin E., Goldstein, Steven A., 1999. "Elastic modulus and hardness of cortical and trabecular bone lamellae measured by nanoindentation in the human femur" J. Biomechanics 32 1005 -1012

APPENDIX A

Finite Element Analysis (FEA)

Finite Element Analysis is a way to simulate loading conditions on a design and determine the design's response to those conditions.

The design is modeled using discrete building blocks called elements. Each element has exact equations that describe how it responds to a certain load. The sum of the response of all elements in the model gives the total response of the design. The elements have a finite number of unknowns, hence the name finite elements.

The finite element model, which has a finite number of unknowns, can only approximate the response of the physical system, which has infinite unknowns.

The advantages of FEA are to reduce the amount of prototype testing and to simulate designs that are not suitable for prototype testing.

APPENDIX B

ANSYS SOFTWARE

ANSYS is a complete FEA software package used by engineers worldwide in virtually all fields of engineering. Partial listing of the capabilities:

1. Structural
    - Linear
    - Nonlinear
        - Material, Geometric, Contact
    - Dynamics
        - Model, Harmonic, Transient Dynamic, Spectrum, Random Vibration
        - Explicit Dynamics with ANSYS LS-DYNA
2. Thermal
    - Steady State and Transient
3. Fluid (CFD, Acoustics, and other fluid analyses)
4. Low- and High-Frequency Electromagnetics
5. Coupled Field